

# OMEN-SED 1.0: A new, numerically efficient sediment module for the coupling to Earth System Models

Dominik Hülse<sup>1</sup>, Sandra Arndt<sup>1,2</sup>, Stuart Daines<sup>3</sup>, Pierre Regnier<sup>2</sup>, and Andy Ridgwell<sup>1,4</sup>

<sup>1</sup>School of Geographical Sciences, University of Bristol, Clifton, Bristol BS8 1SS, UK

<sup>2</sup>Department of Earth and Environmental Sciences, Université Libre de Bruxelles, Brussels, Belgium

<sup>3</sup>Earth System Science, University of Exeter, North Park Road, Exeter EX4 4QE, UK

<sup>4</sup>Department of Earth Sciences, University of California, Riverside, CA 92521, USA

*Correspondence to:* Dominik Hülse (Dominik.Huelse@bristol.ac.uk)

**Abstract.** Here we describe the first version of a new, analytical early diagenetic model resolving organic matter cycling and associated biogeochemical dynamics in marine sediments called OMEN-SED (Organic Matter ENabled SEDiment model). Most biogeochemical cycles and reactions in the surface sediments can be related either directly or indirectly to the degradation of organic matter.

- Despite its fundamental importance, an appropriate Earth system model of the coupled atmosphere-ocean-sediment system which is able to model all relevant processes and feedbacks over geological time-scales currently does not exist. The major problem is the high computational cost of simulating the essential redox reactions in marine sediments which are important to calculate burial of organic matter and benthic recycling fluxes of chemical compounds. In most Earth system models sediment-water dynamics are either neglected or treated in a very simplistic way. To provide a more realistic description of organic matter degradation and nutrient cycles in marine sediments we have developed OMEN-SED, a new, one-dimensional, numerically efficient reactive transport model. OMEN-SED is the first analytical model to explicitly describe organic matter cycling as well as associated dynamics of the most important terminal electron acceptors (i.e. O<sub>2</sub>, NO<sub>3</sub>, SO<sub>4</sub>), related reduced substances (NH<sub>4</sub>, H<sub>2</sub>S), the full suite of secondary-redox reactions, macronutrients (PO<sub>4</sub>) and associated pore water quantities (ALK, DIC). To represent a redox-dependent sedimentary P cycle we consider the formation and burial of Fe-bound P and authigenic Ca-P minerals. Thus, OMEN-SED captures most of the features of a complex, numerical diagenetic model, however, its computational efficiency allows the coupling to global Earth System models and therefore the investigation of coupled global biogeochemical dynamics over different timescales. This paper provides a detailed description of

the new sediment model, **tested with observations, SA and global observations** and describes it's coupling to the Earth System model cGENIE.

## Contents

|       |  |           |
|-------|--|-----------|
| 1     | <b>Introduction</b>  | <b>4</b>  |
| 25    | <b>2 Model Description</b>   | <b>9</b>  |
| 2.1   | General Model Approach . . . . .   | 10        |
| 2.2   | Conservation Equations and Analytical Solution . . . . .                     | 13        |
| 2.2.1 | Organic matter or Particulate Organic Carbon (POC) . . . . .                 | 13        |
| 2.2.2 | Oxygen . . . . .   | 14        |
| 30    | 2.2.3 Nitrate and Ammonium . . . . .   | 17        |
| 2.2.4 | Sulfate and Sulfide . . . . .  | 18        |
| 2.2.5 | Phosphate . . . . .  | 19        |
| 2.2.6 | Dissolved Inorganic Carbon (DIC) . . . . .                                   | 23        |
| 2.2.7 | Alkalinity . . . . .   | 23        |
| 35    | 2.3 Determination of Integration Constants . . . . .                         | 25        |
| 2.3.1 | Generic Boundary Condition Matching (GBCM) . . . . .                         | 25        |
| 2.3.2 | Abstracting out the bioturbation boundary . . . . .                          | 27        |
| 2.4   | Model Parameters . . . . .   | 28        |
| 2.4.1 | Transport Parameters . . . . .   | 28        |
| 40    | 2.4.2 Stoichiometries and reaction parameters . . . . .                      | 31        |
| 3     | <b>Stand-alone sensitivity analysis and case studies</b>                     | <b>31</b> |
| 3.1   | Sensitivity Analysis . . . . .   | 31        |
| 3.1.1 | Methodology . . . . .  | 31        |
| 3.1.2 | Results . . . . .  | 35        |
| 45    | 3.2 Case study: Simulations of sediment cores . . . . .                      | 37        |
| 3.2.1 | Methodology . . . . .  | 37        |
| 3.2.2 | Results . . . . .  | 38        |
| 3.3   | Case study: Stand-alone simulations of global ocean transect . . . . .       | 40        |
| 3.3.1 | Methodology . . . . .  | 40        |
| 50    | 3.3.2 Results . . . . .  | 42        |
| 4     | <b>Coupled pre-industrial Earth system model simulations</b>                 | <b>44</b> |
| 4.1   | Coupling to the cGENIE Earth system model . . . . .                          | 44        |
| 4.2   | Parameterising the OM degradation rate constants in a global model . . . . . | 46        |
| 4.2.1 | Methodology . . . . .  | 47        |

|          |  |           |
|----------|--|-----------|
| 55       | 4.2.2 Results . . . . .                                    | 49        |
|          | 4.3 Modelled fluxes and sediment characteristics . . . . . | 52        |
| <b>5</b> | <b>Scope of applicability and model limitations</b>        | <b>55</b> |
| <b>6</b> | <b>Conclusions</b>   | <b>56</b> |
| <b>7</b> | <b>Code Availability</b>                                   | <b>57</b> |
| 60       | <b>A Reaction Network</b>                                  | <b>57</b> |
|          | <b>B Sensitivity Analysis</b>                              | <b>57</b> |
|          | B1 . . . . .   | 57        |

## 1 Introduction

Dominik: Introduction needs polishing, this is my first draft

65

DH: Will delete the  
sub-headings!

### Role of marine sediments for climate and global biogeochemical cycles:

Marine surface sediments are key components in the Earth system. They host the largest carbon reservoir within the surficial Earth system, provide the only long term sink for atmospheric CO<sub>2</sub>, recycle nutrients and represent the most important geochemical archive used for deciphering past changes in biogeochemical cycles and climate (e.g. Berner, 1991; Archer and Maier-Reimer, 1994; Ridgwell and Zeebe, 2005; Arndt et al., 2013). Physical and chemical processes in sediments (i.e. diagenetic processes) depend on the water column and vice versa: Diagenesis is controlled by the external supply of solid material (e.g. organic matter, calcium carbonate, opal) from the water column and is affected by overlying bottom water concentrations of solutes. At the same time, sediments impact the water column directly either by short- and long-term storage of deposited material or diagenetic processing of deposited material and diffusion of some of the resulting products (e.g. nutrients, DIC) to the overlying bottom waters. This so-called benthic-pelagic coupling is essential for understanding global biogeochemical cycles and climate (e.g. Archer and Maier-Reimer, 1994; Archer et al., 2000; Soetaert et al., 2000; Mackenzie, 2005).

80 Biological primary production of organic matter (OM, CH<sub>2</sub>O in equation R1) and the reverse process of degradation can be written in a greatly simplified reaction as:



On geological timescales production of OM is generally greater than degradation which results in some organic matter being buried in marine sediments and oxygen accumulating in the atmosphere.

85 Thus burial of OM leads to net oxygen input to, and CO<sub>2</sub> removal from the atmosphere (Berner, 2004). On shorter timescales, the upper few meters of the sediments where early diagenesis occurs are specifically important as this zone controls whether a substance is recycled to the water column or buried for a longer period of time in the deeper sediments (Hensen et al., 2006). Most biogeochemical cycles and reactions in this part of marine sediments can be related either directly or 90 indirectly to the degradation of organic matter (Arndt et al., 2013). Oxygen and nitrate for instance, the most powerful electron acceptors, are consumed in the course of the degradation of organic matter, resulting in the release of ammonium and phosphorus to the pore water. As such, degradation of OM in the sediments can profoundly affect the oxygen and nutrient inventory of the ocean and thus primary productivity (Van Cappellen and Ingall, 1994; Lenton and Watson, 2000). Furthermore, 95 organic matter degradation releases metabolic CO<sub>2</sub> to the pore water, causing it to have a lower pH and provoking the dissolution of calcium carbonate CaCO<sub>3</sub> (Emerson and Bender, 1981).

Nutrient recycling from marine sediments has been suggested to play a key role for climate and ocean biogeochemistry for different events during Earth history. For example, feedbacks between

phosphorus storage and erosion from shelf sediments and marine productivity have been hypothesised to play an important role for glacial/interglacial atmospheric CO<sub>2</sub> changes (Broecker, 1982; Ruttenberg, 1993). Furthermore, nutrient recycling from anoxic sediments has been invoked to explain the occurrence of more extreme events in Earth history, for instance Oceanic Anoxic Events (OAEs, e.g. Mort et al., 2007; Tsandev and Slomp, 2009). OAEs represent severe disturbances of the global carbon, oxygen and nutrient cycles of the ocean and are usually characterized by widespread bottom water anoxia and photic zone euxinia (Jenkyns, 2010). One way to explain the genesis and persistence of OAEs is increased oxygen demand due to enhanced primary productivity. Increased nutrient inputs to fuel primary productivity may have come from marine sediments as the burial efficiency of phosphorus declines when bottom waters become anoxic (Ingall and Jahnke, 1994; Van Cappellen and Ingall, 1994). The recovery from OAE like conditions is thought to involve the permanent removal of excess CO<sub>2</sub> from the atmosphere and ocean by burying carbon in the form of organic matter in marine sediments (e.g. Arthur et al., 1988; Jarvis et al., 2011), which is consistent with the geological record of widespread black shale formation (Stein et al., 1986). However, the overall amount, exact timing and the rate of organic matter burial remain a topic of an ongoing debate. Therefore, globally quantifying the burial and degradation of organic matter in marine sediments and related biogeochemical dynamics is important for understanding climate and the cycling of many chemical elements on various timescales.

#### **Diagenetic Models:**

Quantifications of diagenetic processes are possible through the application of idealised mathematical representations of diagenesis, or so-called diagenetic models (see e.g. Berner, 1980; Boudreau, 1997). The number of research questions that can be addressed with diagenetic models is infinite and a plethora of different approaches have been developed, mainly following two distinct directions (Arndt et al., 2013). First, state-of-the art vertically resolved numerical models simulating the entire suite of essential coupled redox and equilibrium reactions within marine sediments (e.g. BRNS, Aguilera et al., 2005; CANDI, Boudreau, 1996; MEDIA, Meysman et al., 2003; STEADYSED, Van Cappellen and Wang, 1996). These “complete”, non-steady-state models, thus resolve the resulting characteristic redox-zonation of marine sediments through explicitly including oxic OM degradation, denitrification, oxidation by manganese and iron (hydr)oxides, sulfate reduction and methanogenesis as well as the reoxidation of reduced byproducts (i.e. NH<sub>4</sub>, Mn<sup>2+</sup>, Fe<sup>2+</sup>, H<sub>2</sub>S, CH<sub>4</sub>, see e.g. Regnier et al., 2011; Arndt et al., 2013). Furthermore, they incorporate various mineral dissolution and precipitation reactions, as well as fast equilibrium sorption processes for example of NH<sub>4</sub>, PO<sub>4</sub> and metal ions (i.e. Mn<sup>2+</sup>, Fe<sup>2+</sup> and Mg<sup>2+</sup>, compare Van Cappellen and Wang, 1996; Meysman et al., 2003). Modelled, depth-dependent, transport processes usually comprise advection, diffusion, bioturbation and bio-irrigation. This group of diagenetic models generally uses a so-called multi-G approach (Jørgensen, 1978; Berner, 1980), thus dividing the bulk organic matter pool into a number of compound classes that are characterised by different degradabilities  $k_i$ , which are gen-

erally dependent on the type and concentration of the specific terminal electron acceptor (TEA). Alternative approaches, in particular reactive continuum models (Boudreau and Ruddick, 1991), assume a continuous distribution of reactive types but are much less often used. These complex, “complete” models have a great potential for quantifying OM degradation dynamics for sites where  
140 enough observations are available to constrain its model parameters (see e.g. Boudreau et al., 1998; Wang and Van Cappellen, 1996; Thullner et al., 2009, for applications). However, due to the high degree of coupled processes and depth-varying parameters the diagenetic equation needs to be solved numerically, thus resulting in a very high computational demand and consequently rendering their application in an Earth system model (ESM) framework prohibitive. Additionally, their global applicability is limited by the restricted transferability of model parameters from one site to the global scale (Arndt et al., 2013).

The second group of models solves the diagenetic equation analytically or semi-analytically, thus providing an alternative and computational more efficient approach. However, finding an analytical solution, especially when complex reaction networks are to be considered, is not straightforward and  
150 generally requires the assumption of steady state. The complexity of the reaction network can be reduced by dividing the sediment column into distinct zones and accounting for the most pertinent biogeochemical processes within each zone, thus increasing the likelihood of finding an analytical solution. In general, analytical diagenetic models are less sophisticated and comprehensive than numerical models and are used for the coupling to global ESMs (e.g. HAMOCC and NorESM use  
155 the model of Heinze et al. (1999)) or box models (e.g. DCESS, Shaffer et al., 2008 or MBM using MEDUSA, Munhoven, 2007). These analytic or semi-analytical models account for the most important transport processes (i.e advection, bioturbation and molecular diffusion) through basic parametrizations and include fewer biogeochemical reactions which are generally restricted to the upper, bioturbated 10 cm of the sediments. They assume that the sedimentary organic matter pool  
160 is composed of just a single compound class which is either degraded with a globally invariant degradation rate constant (Munhoven, 2007) or a fixed rate constant depending on local oxygen concentrations (Shaffer et al., 2008; Palastanga et al., 2011). Pore water tracers explicitly represented in DCESS (Shaffer et al., 2008) and the HAMOCC model of Heinze et al. (1999) and Palastanga et al.  
165 (2011) are restricted to DIC, TA, PO<sub>4</sub> and O<sub>2</sub>. The MEDUSA model (Munhoven, 2007) considers CO<sub>2</sub>, HCO<sub>3</sub><sup>-</sup>, CO<sub>3</sub><sup>2-</sup> and O<sub>2</sub>. Other species produced or consumed during OM degradation are neglected. Thus, with oxygen being the only TEA explicitly modelled the influence of reduced species  
170 is only implicitly included in the boundary conditions for O<sub>2</sub>. A newer versions of the HAMOCC model, being a notable exception, as Ilyina et al. (2013) include NO<sub>3</sub> and denitrification explicitly. Furthermore, the version of Palastanga et al. (2011) represents an redox-dependent explicit sedimentary phosphorus cycle. Yet, reoxidation of reduced byproducts, so-called secondary redox-reactions, or sorption processes are not included in any of the discussed models.

### **How are sediments resolved in Earth system models:**

Earth system models generally track the biogeochemical dynamics of organic and inorganic carbon, essential nutrients (nitrogen, phosphorus) and oxygen with the aim of investigating the evolution of  
175 the ocean's redox structure and carbonate system and its feedbacks on global climate. This general aim thus defines a minimum set of state variables and reaction processes that need to be resolved for an efficient representation of the benthic-pelagic coupling in Earth system models. A suitable sediment model has to provide a robust quantification of organic (and inorganic) carbon burial fluxes, as well as benthic uptake/return fluxes of oxygen, growth-limiting nutrients and reduced species. As  
180 a consequence, the reaction network must account for the most important primary and secondary redox reactions, equilibrium reactions, mineral precipitation/dissolution and adsorption/desorption, resulting in a complex set of coupled reaction-transport equations.

Even though there are more appropriate sediment representations, in most current ESMs sediment-water dynamics are either neglected or treated in a very simplistic way (Soetaert et al., 2000; Hülse  
185 et al., 2017). Most Earth system Models of Intermediate Complexity (EMICs) and also some of the higher resolution global carbon cycle models represent the sediment-water interface either as a reflective or a conservative/semi-reflective boundary (Hülse et al., 2017). Thus, all particulate material deposited on the seafloor is either instantaneously consumed (reflective boundary), or a fixed fraction is buried in the sediments (conservative/semi-reflective boundary). Both highly simplified  
190 approaches furthermore completely neglect the exchange of solute species through the sediment-water interface and, therefore, cannot resolve the complex benthic-pelagic coupling. However, due to their computational efficiency, both representations are often used in global biogeochemical models (e.g. Najjar et al., 2007; Ridgwell et al., 2007; Goosse et al., 2010). A superior approach is the vertically integrated dynamic model, which represents the whole sediment column as a single  
195 box (Hülse et al., 2017). Here, OM deposited on the seafloor is added to the sediment box where it gets degraded and dissolved species diffuse through the sediment-water interface in accordance with these transformations. This approach thus ignores the vertical extent of the sediments and the temporary storage of dissolved species (Soetaert et al., 2000). Yet, it is computationally efficient and allows differentiating between various fractions of organic matter. Most EMICs incorporate a  
200 vertically integrated dynamic model for particulate inorganic carbon only (i.e. mainly  $\text{CaCO}_3$ ) and just a few consider oxic-only sediment degradation of organic matter (Hülse et al., 2017).

The most complex description of diagenetic organic matter degradation in Earth system models is the second group of vertically resolved diagenetic models as discussed above (e.g. Heinze et al.,  
1999; Munhoven, 2007; Shaffer et al., 2008). These models solve the one-dimensional reaction-  
205 transport equation for a number of solid and dissolved species for the upper, bioturbated 10 cm of the sediments. Examples of global ESMs employing a vertically resolved diagenetic model are NorESM (Tjiputra et al., 2013) and HAMOCC (Palastanga et al., 2011; Ilyina et al., 2013), both using a version of Heinze et al. (1999). None of the EMICs reviewed by Hülse et al. (2017) use such a

sediment representation. DCESS (Shaffer et al., 2008) and MBM (Munhoven, 2007) are box models  
210 employing a vertically resolved diagenetic model. However, in general oxygen is the only TEA explicitly modelled and secondary redox reactions and reduced species are completely neglected in these approaches. Furthermore, all models represent the bulk OM pool as a single fraction with a fixed degradation rate constant.

**Problem with that:**

215 Obviously, such a simplification of the OM pool can neither account for the observed vast structural complexity in natural organic matter and its resulting different degradation rates nor for the rapid decrease in OM degradability in the uppermost centimetres of the sediments (Arndt et al., 2013). It has been suggested that at least a 3G approach is necessary to accurately represent organic matter dynamics in this part of the sediments where most OM is degraded (e.g. Soetaert et al., 1996). Even  
220 more restrictive is the use of O<sub>2</sub> as the only TEA and the complete absence of reduced substances and related secondary redox reactions. Even though for the majority of the modern sediments (i.e. in the deep-ocean) O<sub>2</sub> is the primary electron acceptor and Archer et al. (2002) suggested that aerobic degradation accounts for 66% of total organic matter respiration more recent model and data studies have reported that sulfate reduction is the dominant degradation pathway on a global average (with  
225 contributions of 55-76% Canfield et al., 2005; Jørgensen and Kasten, 2006; Thullner et al., 2009). Oxygen becomes progressively less important as TEA with decreasing seafloor depth and sulfate reduction has been shown to account for 83% of OM degradation in coastal sediments (Krumins et al., 2013). In these environments most O<sub>2</sub> is used to reoxidise reduced substances produced during anaerobic degradation (Canfield et al., 2005; Thullner et al., 2009). Thus, the in situ production of  
230 e.g. NO<sub>3</sub> and SO<sub>4</sub> through oxidation of NH<sub>4</sub> and H<sub>2</sub>S forms an important sink for O<sub>2</sub> which is entirely neglected in current sediment representations in global models. In addition, due to the lack of an appropriate sedimentary P cycle (with the exception of the HAMOCC version of Palastanga et al. (2011), no current global ESM is able to model the redox dependent P release from marine sediments and its implications for primary productivity, global biogeochemical cycles and climate.

235 **Solution presented here:**

Analytical approaches with distinct biogeochemical zones were implemented and used in the seventies and eighties to describe observed pore water profiles (e.g. Vanderborght and Billen, 1975; Vanderborght et al., 1977; Billen, 1982; Goloway and Bender, 1982) and later for inclusion into 1-D ecosystem models (e.g. Ruardij and Van Raaphorst, 1995) and global Earth system models (Tromp  
240 et al., 1995). However, alongside the oxic zone these models only describe one anoxic zone explicitly, either a denitrification (Vanderborght and Billen, 1975; Vanderborght et al., 1977; Billen, 1982; Goloway and Bender, 1982; Ruardij and Van Raaphorst, 1995) or a sulfate reduction zone (Tromp et al., 1995). Furthermore, the approaches of Vanderborght and Billen (1975), Goloway and Bender (1982) and Tromp et al. (1995) do not explicitly model the produced reduced species (i.e.  
245 NH<sub>4</sub> and H<sub>2</sub>S, respectively). In addition, the model of Tromp et al. (1995) ignores reoxidation of

H<sub>2</sub>S produced during sulfate reduction. In order to provide a more realistic description of organic matter degradation and nutrient cycles in marine sediments we have developed the OrganicMatter ENabled SEDiment model (OMEN-SED), a new, one-dimensional, numerically efficient reactive transport model. OMEN-SED is the first analytical model to explicitly describe OM cycling as well  
250 as associated dynamics of the most important TEAs (i.e. O<sub>2</sub>, NO<sub>3</sub>, SO<sub>4</sub>), related reduced substances (NH<sub>4</sub>, H<sub>2</sub>S), the full suite of secondary-redox reactions, macronutrients (PO<sub>4</sub>) and associated pore water quantities (ALK, DIC). To represent a redox-dependent sedimentary P cycle we consider the formation and burial of Fe-bound P and authigenic Ca-P minerals. Thus, OMEN-SED captures most  
255 of the features of a complex, numerical diagenetic model, however, its computational efficiency allows the coupling to global Earth system models and therefore the investigation of coupled global biogeochemical dynamics over different timescales. Here, the model is presented as a 2G-approach, however, a third, non-degradable OM fraction can easily be added and OMEN-SED can be further extended to a Multi-G approach.

The first part of the paper provides a detailed description of OMEN-SED (Section 2). This includes descriptions of the general model approach (Section 2.1), of the conservation equations for all explicitly represented biogeochemical tracers (Section 2.2), as well as a summary of global relationships used to constrain reaction and transport parameters in OMEN-SED (Section 2.4). In addition, a generic algorithm is described which is used to match internal boundary conditions and to determine the integration constants for the analytical solutions (Section 2.3). In order to validate  
265 the stand-alone version of OMEN-SED the second part of the paper performs an extensive sensitivity analysis for the most important model parameters and resulting sediment-water interface fluxes are compared with a global database (Section 3.1). In addition, results of the stand-alone model are compared with observed pore water profiles from different ocean depths (Section 3.2) and OMEN-SED simulations of TEA-fluxes along a typical ocean transect are compared with observations and results  
270 from a complete, numerical diagenetic model (Section 3.3). Thereafter, the coupling of OMEN-SED to the carbon-centric version of the “GENIE” Earth system model (cGENIE, Ridgwell et al., 2007) is described (Section 4.1). Sensitivity studies are carried out using this coupled model and modelled organic matter concentrations in the surface sediments are compared to a global database (Seiter et al., 2004, Section 4.2). Finally, potential applicabilities of OMEN-SED are suggested and model  
275 limitations are critically analyzed (Section 5).

## 2 Model Description

OMEN-SED is a new, one-dimensional, computationally efficient reaction-transport model designed for the coupling to regional/global biogeochemical and Earth system models. OMEN-SED is implemented as a Fortran version that can be easily coupled to a pelagic model via the coupling  
280 routine **OMEN\_SED\_main**. In addition, OMEN-SED exists as a stand-alone version implemented

in MATLAB and the entire model can be executed on a standard personal computer in less than 0.1 seconds. The source code of both, the Fortran and the MATLAB stand-alone version, as well as instructions for executing OMEN-SED and for plotting model results are available as a supplement to this paper. The following section provides a detailed description of OMEN-SED and the fundamental equations underlying the model are highlighted. Tables 1 and 15 summarise the biogeochemical reaction network and Tables 9 and 10 provide a glossary of model parameters along with their respective units.

**SA:** maybe include some examples and test figures in supplement?

## 2.1 General Model Approach

In OMEN-SED, the calculation of benthic uptake, recycling and burial fluxes is generally based on the vertically resolved conservation equation for solid and dissolved species in porous media (e.g. Berner, 1980; Boudreau, 1997):

$$\frac{\partial \xi C_i}{\partial t} = -\frac{\partial}{\partial z} \left( -\xi D_i \frac{\partial C_i}{\partial z} + \xi w C_i \right) + \xi \sum_j R_i^j \quad (1)$$

where  $C_i$  is the concentration of biogeochemical species  $i$ ,  $\xi$  equals the porosity  $\phi$  for solute species and  $(1 - \phi)$  for solid species. The term  $z$  is the sediment depth,  $t$  denotes the time,  $D_i$  is the apparent diffusion coefficient of species  $i$  ( $D_i = D_{i,0} + D_{\text{bio}} = D_{\text{mol},i} \cdot f_{ir} + D_{\text{bio}}$  for dissolved species and  $D_i = D_{\text{bio}}$  for solid species),  $w$  is the burial rate and  $\sum_j R_i^j$  represents the sum of all biogeochemical rates  $j$  affecting species  $i$ .

OMEN-SED accounts for both the advective, as well as the diffusive transport of dissolved and solid species. Solid and dissolved species are buried in the sediment according to a constant burial rate  $w$ , thus neglecting the effect of sediment compaction (i.e.  $\frac{\partial \phi}{\partial z} = 0$ ) due to mathematical constraints. The molecular diffusion of dissolved species is described by Fick's law applying a species-specific apparent diffusion coefficient,  $D_{\text{mol},i}$ . In addition, the activity of infaunal organisms in the bioturbated zone is simulated using a diffusive term (e.g. Boudreau, 1986), with a constant bioturbation coefficient  $D_{\text{bio}}$  in the bioturbated zone, while  $D_{\text{bio}}$  is set to zero below the maximum bioturbation depth,  $z_{\text{bio}}$ . The pumping activity by burrow-dwelling animals and the resulting ventilation of tubes, the so-called bioirrigation, is encapsulated in a factor  $f_{ir}$  that enhances the molecular diffusion coefficient (hence,  $D_{i,0} = D_{\text{mol},i} \cdot f_{ir}$ , Soetaert et al., 1996). The reaction network of OMEN-SED accounts for the most important primary and secondary redox reactions, equilibrium reactions, mineral dissolution and precipitation, as well as adsorption and desorption processes that affect the dissolved and solid species explicitly resolved in OMEN-SED. Tables 1 and 15 provide a summary of the reactions and biogeochemical tracers considered in OMEN-SED together with their respective reaction stoichiometries.

All parameters in Eq. (1) may vary with depth and many reaction rate expressions depend on the concentration of other species. Expressing Eq. (1) for a set of chemical species thus results in a non-linear, coupled set of equations that can only be solved numerically. However, OMEN-SED

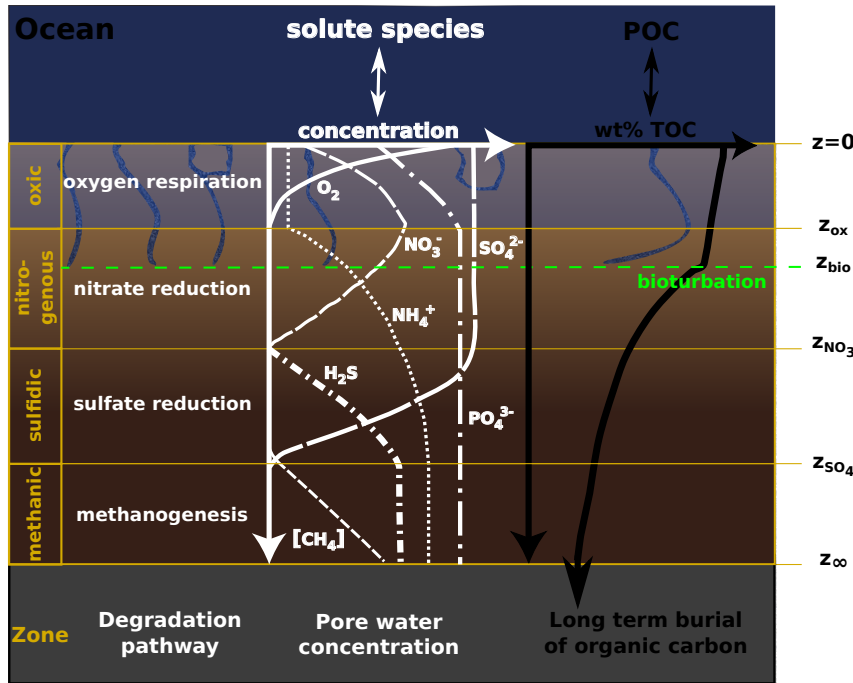


**Figure 1.** Schematic of the different modelled species and zones in OMEN-SED. Here showing the case  $z_{\text{ox}} < z_{\text{bio}} < z_{\text{NO}_3} < z_{\text{SO}_4}$ .

**Table 1.** Reactions and biogeochemical tracers implemented in the reaction network of OMEN-SED. The primary and secondary redox reactions are listed in the sequence they occur with increasing sediment depth.

|                           | Description   |
|---------------------------|---|
| Primary redox reactions   | Degradation of organic matter via aerobic degradation, denitrification, sulfate reduction, methanogenesis (implicit)  |
| Secondary redox reactions | Oxidation of ammonium and sulfide by oxygen, anaerobic oxidation of methane by sulfate                                |
| Adsorption/Desorption     | Ad-/Desorption of P on/from Fe(OH) <sub>3</sub> , NH <sub>4</sub> adsorption, PO <sub>4</sub> adsorption              |
| Mineral precipitation     | Formation of authigenic P   |
| Biogeochemical tracers    | Organic matter (2-G), oxygen, nitrate, ammonium, sulfate, sulfide (hydrogen sulfide), phosphate, Fe-bound P, DIC, ALK |

is designed for the coupling to Earth system models and, therefore, cannot afford a computationally expensive numerical solution. Yet, a computationally efficient analytical solution of Eq. (1) can be derived by 1) assuming steady state conditions (i.e.  $\frac{\partial C_i}{\partial t} = 0$ ) and 2) reducing the vertical variability in parameters and reaction rate expressions by dividing the sediment column into a number of functional biogeochemical zones (Fig. 1, compare e.g. Billen, 1982; Goloway and Bender, 1982; Tromp et al., 1995; Gypens et al., 2008, for similar solutions). More specifically, OMEN-SED divides the sediment column into: I) a bioturbated and II) a non-bioturbated zone defined by an imposed, constant bioturbation depth  $z_{\text{bio}}$  (Fig. 1). Furthermore, it resolves the dynamic redox stratification of marine sediments by dividing the sediment into 1) an oxic zone delineated by the oxygen penetration depth  $z_{\text{ox}}$ ; 2) a denitrification (or nitrogenous) zone situated between  $z_{\text{ox}}$  and the nitrate penetration depth  $z_{\text{NO}_3}$ ; 3) a sulfate reduction zone situated between  $z_{\text{NO}_3}$  and the sulfate penetration depth  $z_{\text{SO}_4}$ ; and 4) a methanogenic zone situated below  $z_{\text{SO}_4}$  (Fig. 1). In each of these zones Eq. (1) is applied with depth invariant parameters. Yet, parameter values may differ across zones. The biogeochemical zones are linked by stating continuity in both concentrations and fluxes at the dynamic, internal boundaries ( $z_b \in \{z_{\text{bio}}, z_{\text{ox}}, z_{\text{NO}_3}, z_{\text{SO}_4}\}$ , compare e.g. Billen, 1982; Ruardij and Van Raaphorst, 1995). These boundaries are dynamic because their depth varies in response to changing ocean boundary conditions and forcings (see Section 2.3.1 for details). Furthermore, the maximum bioturbation depth is not restricted to a specific biogeochemical zone, hence OMEN-SED allows bioturbation to occur in the anoxic zones of the sediment (here all zones  $z > z_{\text{ox}}$  combined).

In addition, the formulation of the reaction term in Eq. (1) varies between zones and encapsulates the most pertinent reaction processes within the respective zone (see Section 2.2), thus simplifying the mathematical description of the reaction network while retaining most of its biogeochemical complexity.

All consumption or production processes of dissolved species related to the degradation of organic matter are a function of the organic matter concentration and, because first-order decay is assumed in the kinetic expression, can be expressed as a series of exponential terms ( $\sum_j \alpha_j \exp(-\beta_j z)$ , see Eq. (2)). In addition, slow adsorption/desorption and mineral precipitation processes can be expressed as zero or first order (reversible) reaction ( $Q$  or  $k \cdot (C_i - \tilde{C})$ , in Eq. (2)). Fast adsorption is described as an instantaneous equilibrium reaction using a constant adsorption coefficient  $K_i$ . The reoxidation of reduced substances is accounted for implicitly by adding a (consumption/production) flux to the internal boundary conditions (see Sections 2.2.2, 2.2.3 and 2.2.4 **SA: make reference to the section where this is explained in detail**). This simplification has been used previously by Gypens et al. (2008) for nitrate and ammonium and can be justified as it has been shown that the reoxidation mainly occurs within a thin layer at the oxic/anoxic interface (Soetaert et al., 1996). The general

**DH:** Do you mean these sections? Not discussed in further details anywhere else

350 reaction-transport equation of OMEN-SED is thus given by:

$$\frac{\partial C_i}{\partial t} = 0 = \frac{D_i}{1+K_i} \frac{\partial^2 C_i}{\partial z^2} - w \frac{\partial C_i}{\partial z} - \frac{1}{1+K_i} \left( \sum_j \alpha_j \exp(-\beta_j z) + \sum_l k_l \cdot C_i - \sum_m Q_m \right) \quad (2)$$

where  $1/\beta_j$  can be interpreted as the length scale and  $\alpha_j$  as the relative importance (or the magnitude at  $z=0$ ) of reaction  $j$  (Boudreau, 1997),  $k_l$  are generic first order reaction rate constants and  $Q_m$  are zeroth-order (or constant) reaction rates.

355 The analytical solution of Eq. (2) is of the general form:

$$C_i(z) = A \exp(az) + B \exp(bz) + \sum_j \frac{\alpha_j}{D\beta_j^2 - w\beta_j - \sum_l k_l} \cdot \exp(-\beta_j z) + \frac{\sum_m Q_m}{\sum_l k_l} \quad (3)$$

with

$$a = \frac{w - \sqrt{w^2 + 4 \cdot D \cdot \sum_l k_l}}{2 \cdot D}, \quad b = \frac{w + \sqrt{w^2 + 4 \cdot D \cdot \sum_l k_l}}{2 \cdot D} \quad (4)$$

360 where  $A$  and  $B$  are integration constants that can be determined by applying a set of internal boundary conditions (see Section 2.3).

Based on Eq. (2) and its analytical solution Eq. (3), OMEN-SED returns the fraction of particulate organic carbon (POC) buried in the sediment,  $f_{\text{POC}}$ , as well as the benthic uptake/return fluxes  $F_{C_i}$  of dissolved species  $C_i$  (in mol cm<sup>-2</sup> year<sup>-1</sup>) in response to changing boundary conditions and  
365 forcings:

$$f_{\text{POC}} = \frac{\text{POC}(z_\infty)}{\text{POC}(0)} \quad (5)$$

$$F_{C_i} = \phi(0) \left( D_i \frac{\partial C_i(z)}{\partial z} \Big|_{z=0} - w \cdot C_i(0) \right) \quad (6)$$

where  $w$  is the deposition rate,  $D_i$  is the diffusion coefficient and  $\text{POC}(0)$ ,  $\text{POC}(z_\infty)$ ,  $C_i(0)$  denotes  
370 the concentration of POC and dissolved species  $i$  at the SWI and at the lower sediment boundary, respectively.

## 2.2 Conservation Equations and Analytical Solution

### 2.2.1 Organic matter or Particulate Organic Carbon (POC)

In marine sediments, particulate organic carbon (POC) is degraded by heterotrophic activity coupled to the sequential utilisation of terminal electron acceptors according to the free energy gain of the half-reaction ( $\text{O}_2 > \text{NO}_3^- > \text{MnO}_2 > \text{Fe(OH)}_3 > \text{SO}_4^{2-}$ , e.g. Stumm and Morgan, 2012). Here, organic matter degradation is described via a multi G-model approach (Arndt et al., 2013,

**Table 2.** OM Boundary conditions applied in OMEN-SED. For the boundaries we define:  $z_{\text{bio}}^- := \lim_{h \rightarrow 0} (z_{\text{bio}} - h)$  and  $z_{\text{bio}}^+ := \lim_{h \rightarrow 0} (z_{\text{bio}} + h)$ .

| Boundary             | Condition           |  |
|----------------------|---------------------|--|
| $z = 0$              | known concentration | 1) $\text{POC}_i(0) = \text{POC}_{0i}$   |
| $z = z_{\text{bio}}$ | continuity          | 2) $\text{POC}_i(z_{\text{bio}}^-) = \text{POC}_i(z_{\text{bio}}^+)$<br>3) $-D_{\text{bio}} \cdot \frac{\partial \text{POC}_i}{\partial z} \Big _{z_{\text{bio}}^-} = 0$ |

and references therein), dividing the bulk OM into a number  $i$  of discrete compound classes  $\text{POC}_i$  characterised by class-specific first-order degradation rate constants  $k_i$ . The conservation equation  
380 for organic matter dynamics is thus given by:

$$\frac{\partial \text{POC}_i}{\partial t} = 0 = D_{\text{POC}_i} \frac{\partial^2 \text{POC}_i}{\partial z^2} - w \frac{\partial \text{POC}_i}{\partial z} - k_i \cdot \text{POC}_i \quad (7)$$

with  $D_{\text{POC}_i} = D_{\text{bio}}$  for  $z \leq z_{\text{bio}}$  and  $D_{\text{POC}_i} = 0$  for  $z > z_{\text{bio}}$ . Integration of equations (7) yields the following general solutions:

385 I. Bioturbated zone ( $z \leq z_{\text{bio}}$ )

$$\text{POC}_i^I(z) = A_{1i} \cdot \exp(a_{1i}z) + B_{1i} \cdot \exp(b_{1i}z)$$

which using the boundary condition at  $z = 0$  can be rewritten as:

$$390 \quad \text{POC}_i^I(z) \stackrel{\text{BC1}}{=} A_{1i} \cdot [\exp(a_{1i}z) - \exp(b_{1i}z)] + \text{POC}_{0i} \cdot \exp(b_{1i}z) \quad (8)$$

II. Non-bioturbated zone ( $z_{\text{bio}} < z$ )

$$390 \quad \text{POC}_i^{II}(z) = A_{2i} \cdot \exp(a_{2i}z) \quad (9)$$

where

$$395 \quad a_{1i} = \frac{w - \sqrt{w^2 + 4 \cdot D_{\text{POC}_i} \cdot k_i}}{2 \cdot D_{\text{POC}_i}}, \quad b_{1i} = \frac{w + \sqrt{w^2 + 4 \cdot D_{\text{POC}_i} \cdot k_i}}{2 \cdot D_{\text{POC}_i}}, \quad a_{2i} = -\frac{k_i}{w} \quad (10)$$

Determining the integration constants ( $A_{1,i}$ ,  $B_{1,i}$ ,  $A_{2,i}$ ) requires the definition of a set of boundary conditions (Table 2). For organic matter, OMEN-SED applies a known concentration/flux at the sediment-water interface and assumes continuity across the bottom of the bioturbated zone,  $z_{\text{bio}}$ . See Section 2.3.1 for further details on how to find the analytical solution.

## 400 2.2.2 Oxygen

OMEN-SED explicitly accounts for oxygen consumption by the aerobic degradation of organic matter within the oxic zone, as well as the oxidation of reduced species (i.e.  $\text{NH}_4$ ,  $\text{H}_2\text{S}$ ) produced in the anoxic zones of the sediment. In the oxic zone ( $z < z_{\text{ox}}$ ), the aerobic degradation consumes oxygen

with a fixed O<sub>2</sub> : C ratio (O<sub>2</sub>C, Tab. 10). A predefined fraction,  $\gamma_{\text{NH}_4}$ , of the ammonium produced  
 405 during the aerobic degradation of OM is nitrified to nitrate, consuming two moles of oxygen per mole  
 of ammonium produced. In addition, OMEN-SED implicitly accounts for the oxygen consumption  
 due to oxidation of reduced species (NH<sub>4</sub>, H<sub>2</sub>S) produced below the oxic zone through the flux  
 boundary condition at the dynamically calculated (see section 2.4.2 for details) oxygen penetration  
 depth  $z_{\text{ox}}$ . All oxygen consumption processes can thus be formulated as a function of organic matter  
 410 degradation. The conservation equation for oxygen is given by: **SA: I'd show the POC substitution  
 in the equations below:**

$$\frac{\partial \text{O}_2}{\partial t} = 0 = D_{\text{O}_2} \frac{\partial^2 \text{O}_2}{\partial z^2} - w \frac{\partial \text{O}_2}{\partial z} - \frac{1-\phi}{\phi} \sum_i k_i \cdot [\text{O}_2 \text{C} + 2\gamma_{\text{NH}_4} \text{NC}_i] \cdot \text{POC}_i(z) \quad (11)$$

415 which, using Eq. (8) and (9) for the depth-distribution of POC<sub>i</sub>(z), can be written as:

**DH:** you mean the way I did it or in the solution?  
 I think it's easier to understand (also how to get the solution) if it's done in the ODE

I Bioturbated zone ( $z \leq z_{\text{bio}}$ )

$$\begin{aligned} \frac{\partial \text{O}_2^I}{\partial t} = 0 &\stackrel{8}{=} D_{\text{O}_2}^I \frac{\partial^2 \text{O}_2}{\partial z^2} - w \frac{\partial \text{O}_2}{\partial z} \\ &- \frac{1-\phi}{\phi} \sum_i k_i \cdot [\text{O}_2 \text{C} + 2\gamma_{\text{NH}_4} \text{NC}_i] \cdot \left( A_{1i} \cdot [\exp(a_{1i}z) - \exp(b_{1i}z)] + \text{POC}_{0i} \cdot \exp(b_{1i}z) \right) \end{aligned}$$

420 II Non-bioturbated zone ( $z_{\text{bio}} < z < z_{\text{ox}}$ )

$$\frac{\partial \text{O}_2^{II}}{\partial t} = 0 \stackrel{9}{=} D_{\text{O}_2}^{II} \frac{\partial^2 \text{O}_2}{\partial z^2} - w \frac{\partial \text{O}_2}{\partial z} - \frac{1-\phi}{\phi} \sum_i k_i \cdot [\text{O}_2 \text{C} + 2\gamma_{\text{NH}_4} \text{NC}_i] \cdot \left( A_{2i} \cdot \exp(a_{2i}z) \right)$$

where  $D_{\text{O}_2}^I$  and  $D_{\text{O}_2}^{II}$  denote the O<sub>2</sub> diffusion coefficient for the bioturbated and non-bioturbated  
 425 zone, respectively. The term  $\frac{1-\phi}{\phi}$  accounts for the volume conversion from solid to dissolved phase  
 and NC<sub>i</sub> is the nitrogen to carbon ratio in OM. Integration yields the following analytical solution  
 for each zone:

I Bioturbated zone ( $z \leq z_{\text{bio}}$ ):

$$\text{O}_2^I(z) = A_{\text{O}_2}^1 + B_{\text{O}_2}^1 \cdot \exp(b_{\text{O}_2}^1 z) + \sum_i \Phi_{1,i}^I \cdot \exp(a_{1i}z) + \sum_i \Phi_{1,i}^{II} \cdot \exp(b_{1i}z) + \sum_i \Phi_{1,i}^{III} \cdot \exp(b_{1i}z) \quad (12)$$

II Non-bioturbated zone ( $z_{\text{bio}} < z < z_{\text{ox}}$ )

$$\text{O}_2^{II}(z) = A_{\text{O}_2}^2 + B_{\text{O}_2}^2 \cdot \exp(b_{\text{O}_2}^2 z) + \sum_i \Phi_{i,2}^I \cdot \exp(a_{2i}z) \quad (13)$$

**Table 3.** Boundary conditions for oxygen. For the boundaries we define:  $z_{\text{bio}}^- := \lim_{h \rightarrow 0} (z_{\text{bio}} - h)$  and  $z_{\text{bio}}^+ := \lim_{h \rightarrow 0} (z_{\text{bio}} + h)$ .

| Boundary             | Condition   |  |
|----------------------|---|--|
| $z = 0$              | known concentration                                 | 1) $O_2(0) = O_{20}$   |
| $z = z_{\text{bio}}$ | continuity  | 2) $O_2(z_{\text{bio}}^-) = O_2(z_{\text{bio}}^+)$   |
| $z = z_{\text{ox}}$  | $O_2$ consumption<br>( $z_{\text{ox}} = z_\infty$ ) | 3) $-(D_{O_2,0} + D_{\text{bio}}) \cdot \frac{\partial O_2}{\partial z} \Big _{z_{\text{bio}}^-} = -D_{O_2,0} \cdot \frac{\partial O_2}{\partial z} \Big _{z_{\text{bio}}^+}$  |
|                      | $(z_{\text{ox}} < z_\infty)$                        | 4) <b>IF</b> ( $O_2(z_\infty) > 0$ )   |
|                      | with  | 4.1) $\frac{\partial O_2}{\partial z} \Big _{z_{\text{ox}}} = 0$<br><b>ELSE</b>  |
|                      |   | 4.2) $O_2(z_{\text{ox}}) = 0$ and $-D_{O_2} \cdot \frac{\partial O_2}{\partial z} \Big _{z_{\text{ox}}} = F_{\text{red}}(z_{\text{ox}})$<br>$F_{\text{red}}(z_{\text{ox}}) = \frac{1-\phi}{\phi} \cdot \int_{\tilde{z}_{\text{NO}_3}}^{\infty} \sum_i (2\gamma_{\text{NH}_4} \text{NC}_i + 2\gamma_{\text{H}_2\text{S}} \text{SO}_4 \text{C}) k_i \text{POC}_i dz$ |

Note:  $\tilde{z}_{\text{NO}_3} = z_{\text{ox}}$  as upper boundary here, as  $z_{\text{NO}_3}$  is not known at this point.

435 with

$$\begin{aligned}
 b_{O_2}^1 &= \frac{w}{D_{O_2}^I}, \quad b_{O_2}^2 = \frac{w}{D_{O_2}^{II}} \\
 \Phi_{1,i}^I &= \frac{1-\phi}{\phi} \cdot \frac{k_i \cdot (O_2 \text{C} + 2\gamma_{\text{NH}_4} \text{NC}_i) \cdot A_{1i}}{D_{O_2}^I (-a_{1i})^2 - w \cdot (-a_{1i})}, \quad \Phi_{1,i}^{II} = -\frac{1-\phi}{\phi} \cdot \frac{k_i \cdot (O_2 \text{C} + 2\gamma_{\text{NH}_4} \text{NC}_i) \cdot A_{1i}}{D_{O_2}^I (-b_{1i})^2 - w \cdot (-b_{1i})} \\
 \Phi_{1,i}^{III} &= \frac{1-\phi}{\phi} \cdot \frac{k_i \cdot (O_2 \text{C} + 2\gamma_{\text{NH}_4} \text{NC}_i) \cdot \text{POC}_{0i}}{D_{O_2}^I (-b_{1i})^2 - w \cdot (-b_{1i})} \\
 \Phi_{i,2}^I &:= \frac{1-\phi}{\phi} \cdot \frac{k_i \cdot (O_2 \text{C} + 2\gamma_{\text{NH}_4} \text{NC}_i) \cdot A_{2i}}{D_{O_2}^{II} (-a_{2i})^2 - w \cdot (-a_{2i})}
 \end{aligned}$$

440 Determining the four integration constants ( $A_{O_2}^1, B_{O_2}^1, A_{O_2}^2, B_{O_2}^2$ , see Section 2.3 for details), as well as the *a priori* unknown oxygen penetration depth requires the definition of five boundary conditions (see Table 3). At the sediment-water interface, OMEN-SED applies a Dirichlet condition (i.e. known concentration) and assumes concentration and flux continuity across the bottom of the bioturbated zone,  $z_{\text{bio}}$ . The oxygen penetration depth  $z_{\text{ox}}$  marks the lower boundary and is dynamically calculated as the depth at which  $O_2(z) = 0$ . Therefore, OMEN-SED applies a Dirichlet boundary condition  $O_2(z_{\text{ox}}) = 0$ . In addition, a flux boundary is applied that implicitly accounts for the oxygen consumption by the partial oxidation of  $\text{NH}_4$  and  $\text{H}_2\text{S}$  diffusing into the oxic zone from below (BC 4.2, Table 3). It is assumed that respective fractions ( $\gamma_{\text{NH}_4}$  and  $\gamma_{\text{H}_2\text{S}}$ ) are directly reoxidised at the oxic/anoxic interface and the remaining fraction escapes reoxidation. OMEN-SED iteratively solves for  $z_{\text{ox}}$  by first testing if there is oxygen left at  $z_\infty$  (i.e.  $O_2(z_\infty) > 0$ ) and, otherwise, by finding the root for the flux boundary condition 4.2 (Table 3). If  $z_{\text{ox}} = z_\infty$ , a zero diffusive flux boundary condition is applied as lower boundary condition.

**DH:** Edited explanation of finding  $z_{\text{ox}}$

### 2.2.3 Nitrate and Ammonium

455 Nitrogen dynamics in OMEN-SED are controlled by the metabolic production of ammonium, nitrification, denitrification as well as ammonium adsorption. Ammonium is produced by organic matter degradation in both the oxic and anoxic zones, while denitrification consumes nitrate in the denitrification zone with a fixed  $\text{NO}_3 : \text{C}$  ratio ( $\text{NO}_3\text{C}$ , Tab. 10) **SA: need explanation**. The adsorption of ammonium to sediment particles is formulated as an equilibrium process with constant equilibrium  
 460 adsorption coefficient  $K_{\text{NH}_4}$ , thus assuming that the adsorption is fast compared with the characteristic time scales of transport processes (Wang and Van Cappellen, 1996). In addition, a defined fraction,  $\gamma_{\text{NH}_4}$ , of metabolically produced ammonium is directly nitrified to nitrate in the oxic zone, while the nitrification of upward diffusing ammonium produced in the sulfidic and methanic zones is implicitly accounted for in the boundary conditions. The conservation equations for ammonium  
 465 and nitrate are thus given by:

**DH:** explanation sufficient?

#### 1. Oxic zone ( $z \leq z_{\text{ox}}$ )

$$\frac{\partial \text{NO}_3^I}{\partial t} = 0 = D_{\text{NO}_3} \frac{\partial^2 \text{NO}_3^I}{\partial z^2} - w \frac{\partial \text{NO}_3^I}{\partial z} + \gamma_{\text{NH}_4} \frac{1-\phi}{\phi} \cdot \sum_i \text{NC}_i \cdot k_i \cdot \text{POC}_i(z) \quad (14)$$

$$\frac{\partial \text{NH}_4^I}{\partial t} = 0 = \frac{D_{\text{NH}_4}}{1+K_{\text{NH}_4}} \frac{\partial^2 \text{NH}_4^I}{\partial z^2} - w \frac{\partial \text{NH}_4^I}{\partial z} + \frac{1-\gamma_{\text{NH}_4}}{1+K_{\text{NH}_4}} \cdot \frac{1-\phi}{\phi} \cdot \sum_i \text{NC}_i \cdot k_i \cdot \text{POC}_i(z) \quad (15)$$

470

#### 2. Denitrification (or nitrogenous) zone ( $z_{\text{ox}} < z \leq z_{\text{NO}_3}$ )

$$\frac{\partial \text{NO}_3^{II}}{\partial t} = 0 = D_{\text{NO}_3} \frac{\partial^2 \text{NO}_3^{II}}{\partial z^2} - w \frac{\partial \text{NO}_3^{II}}{\partial z} - \frac{1-\phi}{\phi} \text{NO}_3\text{C} \cdot \sum_i k_i \cdot \text{POC}_i(z) \quad (16)$$

475

$$\frac{\partial \text{NH}_4^{II}}{\partial t} = 0 = \frac{D_{\text{NH}_4}}{1+K_{\text{NH}_4}} \frac{\partial^2 \text{NH}_4^{II}}{\partial z^2} - w \frac{\partial \text{NH}_4^{II}}{\partial z} \quad (17)$$

#### 3. Sulfidic and methanic zone ( $z_{\text{NO}_3} < z \leq z_{\infty}$ )

$$\frac{\partial \text{NH}_4^{III}}{\partial t} = 0 = \frac{D_{\text{NH}_4}}{1+K_{\text{NH}_4}} \frac{\partial^2 \text{NH}_4^{III}}{\partial z^2} - w \frac{\partial \text{NH}_4^{III}}{\partial z} + \frac{1}{1+K_{\text{NH}_4}} \cdot \frac{1-\phi}{\phi} \cdot \sum_i \text{NC}_i \cdot k_i \cdot \text{POC}_i(z) \quad (18)$$

where  $D_{\text{NO}_3}$  and  $D_{\text{NH}_4}$  denote the diffusion coefficients for  $\text{NO}_3$  and  $\text{NH}_4$  which depend on  
 480 the bioturbation status of the respective geochemical zone (compare Section 2.3.1). Integration of Eq. (14) - (18) yields the analytical solutions, which are not further developed here but follow the procedure outlined in Section 2.2.2 for oxygen (also see Section 2.3.1 for more details on how to find the analytical solution). Table 4 summarises the boundary conditions applied in OMEN-SED to solve Eq. (14) - (18) and to find the *a priori* unknown nitrate penetration depth,  $z_{\text{NO}_3}$ . The model  
 485 assumes known bottom water concentrations for both  $\text{NO}_3$  and  $\text{NH}_4$ , the complete consumption of

**Table 4.** Boundary conditions for nitrate and ammonium. For the boundaries we define:  $z_-^- := \lim_{h \rightarrow 0} (z_- - h)$  and  $z_+^+ := \lim_{h \rightarrow 0} (z_- + h)$ .

| Boundary              | Condition   |   |
|-----------------------|---|---|
| $z = 0$               | known concentration   | 1) $\text{NO}_3(0) = \text{NO}_{30}$  |
| $z = z_{\text{bio}}$  | continuity  | 2) $\text{NO}_3(z_{\text{bio}}^-) = \text{NO}_3(z_{\text{bio}}^+)$  |
| $z = z_{\text{ox}}$   | continuity  | 3) $-(D_{\text{NO}_3,0} + D_{\text{bio}}) \cdot \frac{\partial \text{NO}_3}{\partial z}  _{z_{\text{bio}}^-} = -D_{\text{NO}_3,0} \cdot \frac{\partial \text{NO}_3}{\partial z}  _{z_{\text{bio}}^+}$   |
|                       | where:  | 4) $\text{NO}_3(z_{\text{ox}}^-) = \text{NO}_3(z_{\text{ox}}^+)$  |
| $z = z_{\text{NO}_3}$ | $\text{NO}_3$ consumption<br>( $z_{\text{NO}_3} = z_\infty$ ) | 5) $-D_{\text{NO}_3} \cdot \frac{\partial \text{NO}_3}{\partial z}  _{z_{\text{ox}}^-} + \gamma_{\text{NH}_4} \cdot F_{\text{NH}_4}(z_{\text{ox}}) = -D_{\text{NO}_3} \cdot \frac{\partial \text{NO}_3}{\partial z}  _{z_{\text{ox}}^+}$<br>$F_{\text{NH}_4}(z_{\text{ox}}) = \frac{1}{1+K_{\text{NH}_4}} \cdot \frac{1-\phi}{\phi} \cdot \int_{z_{\text{NO}_3}}^\infty \sum_i \text{NC}_i \cdot k_i \cdot \text{POC}_i dz$   |
|                       |   | 6) <b>IF</b> ( $\text{NO}_3(z_\infty) > 0$ )  |
|                       |   | 6.1) $\frac{\partial \text{NO}_3}{\partial z}  _{z_{\text{NO}_3}} = 0$  |
|                       |   | <b>ELSE</b>   |
|                       |   | 6.2) $\text{NO}_3(z_{\text{NO}_3}) = 0 \quad \text{and} \quad \frac{\partial \text{NO}_3}{\partial z}  _{z_{\text{NO}_3}} = 0$  |
| $z = 0$               | known concentration   | 1) $\text{NH}_4(0) = \text{NH}_{40}$  |
| $z = z_{\text{bio}}$  | continuity  | 2) $\text{NH}_4(z_{\text{bio}}^-) = \text{NH}_4(z_{\text{bio}}^+)$  |
| $z = z_{\text{ox}}$   | continuity  | 3) $-\frac{D_{\text{NH}_4,0} + D_{\text{bio}}}{1+K_{\text{NH}_4}} \cdot \frac{\partial \text{NH}_4}{\partial z}  _{z_{\text{bio}}^-} = -\frac{D_{\text{NH}_4,0}}{1+K_{\text{NH}_4}} \cdot \frac{\partial \text{NH}_4}{\partial z}  _{z_{\text{bio}}^+}$   |
|                       | where:  | 4) $\text{NH}_4(z_{\text{ox}}^-) = \text{NH}_4(z_{\text{ox}}^+)$  |
| $z = z_{\text{NO}_3}$ | continuity<br>flux  | 5) $-\frac{D_{\text{NH}_4}}{1+K_{\text{NH}_4}} \cdot \frac{\partial \text{NH}_4}{\partial z}  _{z_{\text{ox}}^-} - \gamma_{\text{NH}_4} \cdot F_{\text{NH}_4}(z_{\text{ox}}) = -\frac{D_{\text{NH}_4}}{1+K_{\text{NH}_4}} \cdot \frac{\partial \text{NH}_4}{\partial z}  _{z_{\text{ox}}^+}$<br>$F_{\text{NH}_4}(z_{\text{ox}}) = \frac{1}{1+K_{\text{NH}_4}} \cdot \frac{1-\phi}{\phi} \cdot \int_{z_{\text{NO}_3}}^\infty \sum_i \text{NC}_i \cdot k_i \cdot \text{POC}_i dz$ |
| $z = z_\infty$        | zero $\text{NH}_4$ flux                                       | 6) $\text{NH}_4(z_{\text{NO}_3}^-) = \text{NH}_4(z_{\text{NO}_3}^+)$  |
|                       |   | 7) $-\frac{D_{\text{NH}_4}}{1+K_{\text{NH}_4}} \cdot \frac{\partial \text{NH}_4}{\partial z}  _{z_{\text{NO}_3}^-} = -\frac{D_{\text{NH}_4}}{1+K_{\text{NH}_4}} \cdot \frac{\partial \text{NH}_4}{\partial z}  _{z_{\text{NO}_3}^+}$  |
|                       |   | 8) $\frac{\partial \text{NH}_4}{\partial z}  _{z_\infty} = 0$   |

nitrate at the nitrate penetration depth (in case  $z_{\text{NO}_3} < z_\infty$ ) and no change in ammonium flux at  $z_\infty$ . In addition, concentration and diffusive flux continuity across  $z_{\text{bio}}$  and  $z_{\text{ox}}$  is considered for  $\text{NO}_3$  and  $\text{NH}_4$ . Furthermore, the reoxidation of upward-diffusing reduced ammonium is accounted for in the oxic-anoxic boundary condition for nitrate and ammonium. OMEN-SED iteratively solves for  $z_{\text{NO}_3}$  by first testing if there is nitrate left at  $z_\infty$  (i.e.  $\text{NO}_3(z_\infty) > 0$ ) and, otherwise, by finding the root for the flux boundary condition 6.2 (Table 4).

## 2.2.4 Sulfate and Sulfide

Below the denitrification zone ( $z > z_{\text{NO}_3}$ ), organic matter degradation is coupled to sulfate reduction, consuming sulfate and producing hydrogen sulfide with a fixed  $\text{SO}_4 : \text{C}$  ratio ( $\text{SO}_4\text{C}$ , Tab. 10). In addition, the anaerobic oxidation of upward diffusing methane (AOM) produced below the sulfate penetration and the associated consumption of sulfate and production of sulfide; as well as the production of sulfate and consumption of sulfide through sulfide oxidation are implicitly accounted

for through the boundary conditions (Table 5). The conservation equations for sulfate and sulfide are thus given by:

500

1. Oxic and nitrogenous zone ( $z \leq z_{\text{NO}_3}$ )

$$\frac{\partial \text{SO}_4^I}{\partial t} = 0 = D_{\text{SO}_4} \frac{\partial^2 \text{SO}_4^I}{\partial z^2} - w \frac{\partial \text{SO}_4^I}{\partial z} \quad (19)$$

$$505 \quad \frac{\partial \text{H}_2\text{S}^I}{\partial t} = 0 = D_{\text{H}_2\text{S}} \frac{\partial^2 \text{H}_2\text{S}^I}{\partial z^2} - w \frac{\partial \text{H}_2\text{S}^I}{\partial z} \quad (20)$$

2. Sulfidic zone ( $z_{\text{NO}_3} < z \leq z_{\text{SO}_4}$ )

$$\frac{\partial \text{SO}_4^{II}}{\partial t} = 0 = D_{\text{SO}_4} \frac{\partial^2 \text{SO}_4^{II}}{\partial z^2} - w \frac{\partial \text{SO}_4^{II}}{\partial z} - \frac{1-\phi}{\phi} \cdot \sum_i \text{SO}_4 \text{C} \cdot k_i \cdot \text{POC}_i(z) \quad (21)$$

$$\frac{\partial \text{H}_2\text{S}^{II}}{\partial t} = 0 = D_{\text{H}_2\text{S}} \frac{\partial^2 \text{H}_2\text{S}^{II}}{\partial z^2} - w \frac{\partial \text{H}_2\text{S}^{II}}{\partial z} + \frac{1-\phi}{\phi} \cdot \sum_i \text{SO}_4 \text{C} \cdot k_i \cdot \text{POC}_i(z) \quad (22)$$

510 3. Methanic zone ( $z_{\text{SO}_4} < z \leq z_\infty$ )

$$\frac{\partial \text{H}_2\text{S}^{III}}{\partial t} = 0 = D_{\text{H}_2\text{S}} \frac{\partial^2 \text{H}_2\text{S}^{III}}{\partial z^2} - w \frac{\partial \text{H}_2\text{S}^{III}}{\partial z} \quad (23)$$

where  $D_{\text{SO}_4}$  and  $D_{\text{H}_2\text{S}}$  denote the diffusion coefficients for  $\text{SO}_4$  and  $\text{H}_2\text{S}$  which depend on the bioturbation status of the respective geochemical zone (compare Section 2.3.1). Integration of Eq. 515 (19) - (23) yields the analytical solution and Table 5 summarises the boundary conditions applied. OMEN-SED assumes known concentrations at the sediment-water interface and continuity across the bioturbation depth and the nitrate penetration depth. The reoxidation of reduced  $\text{H}_2\text{S}$  to  $\text{SO}_4$  is accounted for implicitly via the oxic-anoxic boundary condition for both species, while reduction of  $\text{SO}_4$  and the associated production of  $\text{H}_2\text{S}$  via AOM is accounted for through the respective 520 boundary conditions at  $z_{\text{SO}_4}$ . In case  $z_{\text{SO}_4} < z_\infty$ , OMEN-SED assumes zero sulfate concentration at  $z_{\text{SO}_4}$  and its diffusive flux must equal the amount of methane produced below (with a methane to carbon ratio of MC); or, in case  $z_{\text{SO}_4} = z_\infty$ , a zero diffusive flux condition for sulfate is considered. OMEN-SED iteratively solves for  $z_{\text{SO}_4}$  by first testing if there is sulfate left at  $z_\infty$  (i.e.  $\text{SO}_4(z_\infty) > 0$ ) and, otherwise, by finding the root for the flux boundary condition 8.2 (Table 5). At the lower 525 boundary  $z_\infty$  zero diffusive flux of  $\text{H}_2\text{S}$  is considered.

## 2.2.5 Phosphate

The biogeochemical description of phosphorus (P) dynamics builds on the work of Slomp et al. (1996) and accounts for phosphorus recycling through organic matter degradation, adsorption onto sediments and iron(III) hydroxides (Fe-bound P), as well as carbonate fluorapatite (CFA or authigenic P) formation (see Figure 2 for a schematic overview of the sedimentary P cycle). In the oxic zone of the sediment,  $\text{PO}_4$  liberated through organic matter degradation can adsorb to iron(III) hydroxides forming Fe-bound P (or FeP, Slomp et al., 1998). Below the oxic zone,  $\text{PO}_4$  is not only

**Table 5.** Boundary conditions for sulfate and sulfide. For the boundaries we define:  $z_-^- := \lim_{h \rightarrow 0} (z_- - h)$  and  $z_-^+ := \lim_{h \rightarrow 0} (z_- + h)$ .

| Boundary              | Condition   |   |
|-----------------------|---|---|
| $z = 0$               | known concentration   | 1) $\text{SO}_4(0) = \text{SO}_{40}$  |
| $z = z_{\text{bio}}$  | continuity  | 2) $\text{SO}_4(z_{\text{bio}}^-) = \text{SO}_4(z_{\text{bio}}^+)$  |
|                       | flux  | 3) $-(D_{\text{SO}_4,0} + D_{\text{bio}}) \cdot \frac{\partial \text{SO}_4}{\partial z} \Big _{z_{\text{bio}}^-} = -D_{\text{SO}_4,0} \cdot \frac{\partial \text{SO}_4}{\partial z} \Big _{z_{\text{bio}}^+}$   |
| $z = z_{\text{ox}}$   | continuity  | 4) $\text{SO}_4(z_{\text{ox}}^-) = \text{SO}_4(z_{\text{ox}}^+)$  |
|                       | flux  | 5) $-D_{\text{SO}_4} \cdot \frac{\partial \text{SO}_4}{\partial z} \Big _{z_{\text{ox}}^-} + \gamma_{\text{H}_2\text{S}} \cdot F_{\text{H}_2\text{S}}(z_{\text{ox}}) = -D_{\text{SO}_4} \cdot \frac{\partial \text{SO}_4}{\partial z} \Big _{z_{\text{ox}}^+}$  |
|                       | where:  | $F_{\text{H}_2\text{S}}(z_{\text{ox}}) = \frac{1-\phi}{\phi} \cdot \left( \int_{z_{\text{NO}_3}}^{\text{SO}_4} \sum_i \text{SO}_4 \cdot k_i \cdot \text{POC}_i dz + \gamma_{\text{CH}_4} \cdot \int_{z_{\text{SO}_4}}^{\infty} \sum_i \text{MC} \cdot k_i \cdot \text{POC}_i dz \right)$  |
| $z = z_{\text{NO}_3}$ | continuity  | 6) $\text{SO}_4(z_{\text{NO}_3}^-) = \text{SO}_4(z_{\text{NO}_3}^+)$  |
|                       | flux  | 7) $-D_{\text{SO}_4} \cdot \frac{\partial \text{SO}_4}{\partial z} \Big _{z_{\text{NO}_3}^-} = -D_{\text{SO}_4} \cdot \frac{\partial \text{SO}_4}{\partial z} \Big _{z_{\text{NO}_3}^+}$  |
| $z = z_{\text{SO}_4}$ | SO <sub>4</sub> consumption<br>( $z_{\text{SO}_4} = z_\infty$ ) | 8) <b>IF</b> ( $\text{SO}_4(z_\infty) > 0$ )<br>8.1) $\frac{\partial \text{SO}_4}{\partial z} \Big _{z_{\text{SO}_4}} = 0$<br><b>ELSE</b>   |
|                       | ( $z_{\text{SO}_4} < z_\infty$ )<br>with                        | 8.2) $\text{SO}_4(z_{\text{SO}_4}) = 0 \quad \text{and} \quad -D_{\text{SO}_4} \cdot \frac{\partial \text{SO}_4}{\partial z} \Big _{z_{\text{SO}_4}} = \gamma_{\text{CH}_4} \cdot F_{\text{CH}_4}(z_{\text{SO}_4})$<br>$F_{\text{CH}_4}(z_{\text{SO}_4}) = \frac{1-\phi}{\phi} \cdot \int_{z_{\text{SO}_4}}^{\infty} \sum_i \text{MC} \cdot k_i \cdot \text{POC}_i dz$  |
| $z = 0$               | known concentration   | 1) $\text{H}_2\text{S}(0) = \text{H}_2\text{S}_0$   |
| $z = z_{\text{bio}}$  | continuity  | 2) $\text{H}_2\text{S}(z_{\text{bio}}^-) = \text{H}_2\text{S}(z_{\text{bio}}^+)$  |
|                       | flux  | 3) $-(D_{\text{H}_2\text{S},0} + D_{\text{bio}}) \cdot \frac{\partial \text{H}_2\text{S}}{\partial z} \Big _{z_{\text{bio}}^-} = -D_{\text{H}_2\text{S},0} \cdot \frac{\partial \text{H}_2\text{S}}{\partial z} \Big _{z_{\text{bio}}^+}$   |
| $z = z_{\text{ox}}$   | continuity  | 4) $\text{H}_2\text{S}(z_{\text{ox}}^-) = \text{H}_2\text{S}(z_{\text{ox}}^+)$  |
|                       | flux  | 5) $-D_{\text{H}_2\text{S}} \cdot \frac{\partial \text{H}_2\text{S}}{\partial z} \Big _{z_{\text{ox}}^-} - \gamma_{\text{H}_2\text{S}} F_{\text{H}_2\text{S}}(z_{\text{ox}}) = -D_{\text{H}_2\text{S}} \cdot \frac{\partial \text{H}_2\text{S}}{\partial z} \Big _{z_{\text{ox}}^+}$  |
|                       | where:  | $F_{\text{H}_2\text{S}}(z_{\text{ox}}) = \frac{1-\phi}{\phi} \cdot \left( \int_{z_{\text{NO}_3}}^{\text{SO}_4} \sum_i \text{SO}_4 \cdot k_i \cdot \text{POC}_i dz + \gamma_{\text{CH}_4} \cdot \int_{z_{\text{SO}_4}}^{\infty} \sum_i \text{MC} \cdot k_i \cdot \text{POC}_i dz \right)$  |
| $z = z_{\text{NO}_3}$ | continuity  | 6) $\text{H}_2\text{S}(z_{\text{NO}_3}^-) = \text{H}_2\text{S}(z_{\text{NO}_3}^+)$  |
|                       | flux  | 7) $-D_{\text{H}_2\text{S}} \cdot \frac{\partial \text{H}_2\text{S}}{\partial z} \Big _{z_{\text{NO}_3}^-} = -D_{\text{H}_2\text{S}} \cdot \frac{\partial \text{H}_2\text{S}}{\partial z} \Big _{z_{\text{NO}_3}^+}$  |
| $z = z_{\text{SO}_4}$ | continuity<br>flux (with AOM)<br>where:                         | 8) $\text{H}_2\text{S}(z_{\text{SO}_4}^-) = \text{H}_2\text{S}(z_{\text{SO}_4}^+)$<br>9) $-D_{\text{H}_2\text{S}} \cdot \frac{\partial \text{H}_2\text{S}}{\partial z} \Big _{z_{\text{SO}_4}^-} + \gamma_{\text{CH}_4} \cdot F_{\text{CH}_4}(z_{\text{SO}_4}) = -D_{\text{H}_2\text{S}} \cdot \frac{\partial \text{H}_2\text{S}}{\partial z} \Big _{z_{\text{SO}_4}^+}$<br>$F_{\text{CH}_4}(z_{\text{SO}_4}) = \frac{1-\phi}{\phi} \cdot \int_{z_{\text{SO}_4}}^{\infty} \sum_i \text{MC} \cdot k_i \cdot \text{POC}_i dz$ |
| $z = z_\infty$        | zero H <sub>2</sub> S flux                                      | 10) $\frac{\partial \text{H}_2\text{S}}{\partial z} \Big _{z_\infty} = 0$   |

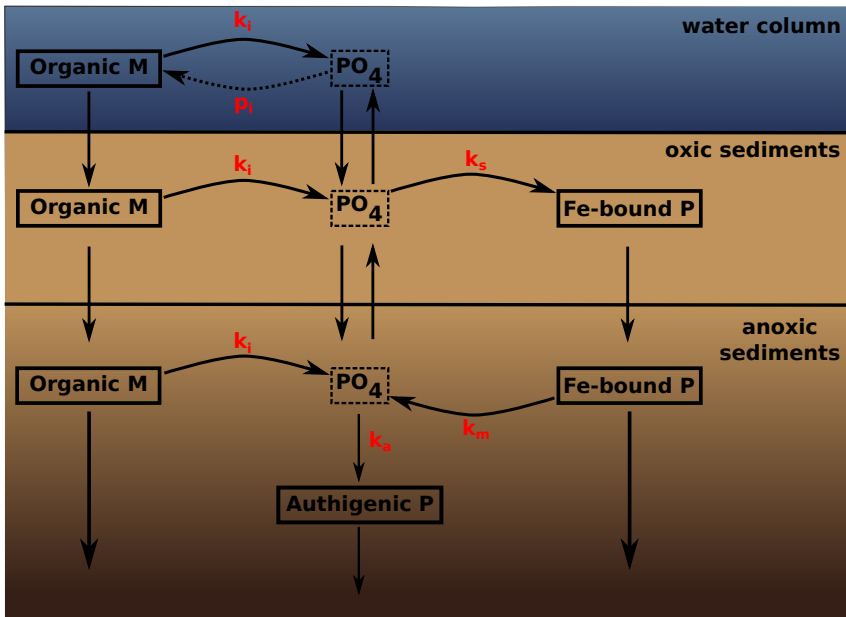


**Figure 2.** A schematic of the sedimentary P cycle in OMEN-SED. Red numbers represent kinetic rate constants for phosphorus dynamics (compare Table 10;  $p_i$  represents uptake rate of  $\text{PO}_4$  via primary production in shallow environments). Adapted from Slomp et al. (1996).

produced via organic matter degradation but can also be released from the Fe-bound P pool due to the reduction of iron(III) hydroxides under anoxic conditions. Furthermore, in these zones phosphate concentrations build up and pore waters can thus become supersaturated with respect to carbonate fluorapatite, thus triggering the authigenic formation of CFA (Van Cappellen and Berner, 1988). Phosphorus bound in these authigenic minerals represents a permanent sink for reactive phosphorus (Slomp et al., 1996). As for ammonium, the adsorption of P to the sediment matrix is treated as an equilibrium processes, parameterised with dimensionless adsorption coefficients for the oxic and anoxic zone, respectively ( $K_{\text{PO}_4}^{\text{ox}}$ ,  $K_{\text{PO}_4}^{\text{anox}}$  Slomp et al., 1998). The sorption and desorption of P to iron(III) hydroxides as well as the authigenic fluorapatite formation are described as first-order reactions with rate constants  $k_s$ ,  $k_m$  and  $k_a$ , respectively (Table 10). The rate of the respective process is calculated as the product of the rate constant and the difference between the current concentration (of  $\text{PO}_4$  and FeP) and an equilibrium or asymptotic concentration Slomp et al. (1996). The asymptotic Fe-bound P concentration is  $\text{FeP}^\infty$  and the equilibrium concentration for P sorption and authigenic fluorapatite formation are  $\text{PO}_4^s$  and  $\text{PO}_4^a$ , respectively (Table 10). The last term in Eq. (24) and (25) represents sorption of  $\text{PO}_4$  to FeP in the oxic zone, the last term in Eq. (26) and (27) is the release of  $\text{PO}_4$  from the FeP pool and the 4th term in Eq. (27) represents the permanent loss of  $\text{PO}_4$  to authigenic fluorapatite formation. The conservation equations for phosphate and Fe-bound P are thus given by:

**Table 6.** Boundary conditions for phosphate and Fe-bound P (FeP). For the boundaries we define:  $z_-^- := \lim_{h \rightarrow 0} (z_- - h)$  and  $z_+^+ := \lim_{h \rightarrow 0} (z_- + h)$ .

| Boundary             | Condition                |  |
|----------------------|--------------------------|--|
| $z = 0$              | known concentration      | 1) $\text{PO}_4(0) = \text{PO}_{40}$   |
| $z = z_{\text{bio}}$ | continuity               | 2) $\text{PO}_4(z_{\text{bio}}^-) = \text{PO}_4(z_{\text{bio}}^+)$   |
|                      | flux                     | 3) $(D_{\text{PO}_4,0} + D_{\text{bio}}) \cdot \frac{\partial \text{PO}_4}{\partial z}  _{z_{\text{bio}}^-} = D_{\text{PO}_4,0} \cdot \frac{\partial \text{PO}_4}{\partial z}  _{z_{\text{bio}}^+}$  |
| $z = z_{\text{ox}}$  | continuity               | 4) $\text{PO}_4(z_{\text{ox}}^-) = \text{PO}_4(z_{\text{ox}}^+)$   |
|                      | flux                     | 5) $-\frac{D_{\text{PO}_4}}{1+K_{\text{PO}_4}^{\text{ox}}} \cdot \frac{\partial \text{PO}_4}{\partial z}  _{z_{\text{ox}}^-} = -\frac{D_{\text{PO}_4}}{1+K_{\text{PO}_4}^{\text{anox}}} \cdot \frac{\partial \text{PO}_4}{\partial z}  _{z_{\text{ox}}^+}$ |
| $z = z_\infty$       | flux                     | 10) $\frac{\partial \text{PO}_4}{\partial z}  _{z_\infty} = 0$   |
| $z = 0$              | known concentration      | 1) $\text{FeP}(0) = \text{FeP}_0$  |
| $z = z_{\text{bio}}$ | continuity               | 2) $\text{FeP}(z_{\text{bio}}^-) = \text{FeP}(z_{\text{bio}}^+)$   |
|                      | flux                     | 3) $\frac{\partial \text{FeP}}{\partial z}  _{z_{\text{bio}}^-} = \frac{\partial \text{FeP}}{\partial z}  _{z_{\text{bio}}^+}$   |
| $z = z_{\text{ox}}$  | continuity               | 4) $\text{FeP}(z_{\text{ox}}^-) = \text{FeP}(z_{\text{ox}}^+)$   |
|                      | flux                     | 5) $\frac{\partial \text{FeP}}{\partial z}  _{z_{\text{ox}}^-} = \frac{\partial \text{FeP}}{\partial z}  _{z_{\text{ox}}^+}$   |
| $z = z_\infty$       | asymptotic concentration | 10) $\text{FeP}(z_\infty) = \text{FeP}_\infty$   |

### 1. Oxic zone ( $z \leq z_{\text{ox}}$ )

$$\frac{\partial \text{PO}_4^I}{\partial t} = \frac{D_{\text{PO}_4}}{1+K_{\text{PO}_4}^{\text{ox}}} \frac{\partial^2 \text{PO}_4^I}{\partial z^2} - w \frac{\partial \text{PO}_4^I}{\partial z} + \frac{1-\phi}{\phi} \frac{1}{1+K_{\text{PO}_4}^{\text{ox}}} \sum_i (\text{PC}_i \cdot k_i \cdot \text{POC}_i(z)) - \frac{k_s}{1+K_{\text{PO}_4}^{\text{ox}}} (\text{PO}_4^I - \text{PO}_4^s) \quad (24)$$

$$555 \quad \frac{\partial \text{FeP}^I}{\partial t} = D_{\text{FeP}} \frac{\partial^2 \text{FeP}^I}{\partial z^2} - w \frac{\partial \text{FeP}^I}{\partial z} + \frac{\phi}{1-\phi} k_s (\text{PO}_4^I - \text{PO}_4^s) \quad (25)$$

### 2. Anoxic zones ( $z_{\text{ox}} < z \leq z_\infty$ )

$$\frac{\partial \text{FeP}^{II}}{\partial t} = D_{\text{FeP}} \frac{\partial^2 \text{FeP}^{II}}{\partial z^2} - w \frac{\partial \text{FeP}^{II}}{\partial z} - k_m (\text{FeP}^{II} - \text{FeP}^\infty) \quad (26)$$

$$560 \quad \frac{\partial \text{PO}_4^{II}}{\partial t} = \frac{D_{\text{PO}_4}}{1+K_{\text{PO}_4}^{\text{anox}}} \frac{\partial^2 \text{PO}_4^{II}}{\partial z^2} - w \frac{\partial \text{PO}_4^{II}}{\partial z} + \frac{1-\phi}{\phi} \frac{1}{1+K_{\text{PO}_4}^{\text{anox}}} \sum_i (\text{PC}_i \cdot k_i \cdot \text{POC}_i(z)) - \frac{k_a}{1+K_{\text{PO}_4}^{\text{anox}}} (\text{PO}_4^{II} - \text{PO}_4^a) + \frac{(1-\phi)}{\phi} \frac{k_m}{1+K_{\text{PO}_4}^{\text{anox}}} (\text{FeP}^{II} - \text{FeP}^\infty) \quad (27)$$

where  $D_{\text{PO}_4}$  denotes the diffusion coefficient for  $\text{PO}_4$  which depends on the bioturbation status of the respective geochemical zone and  $D_{\text{FeP}} = D_{\text{bio}}$  for  $z \leq z_{\text{bio}}$  and  $D_{\text{FeP}} = 0$  for  $z > z_{\text{bio}}$  (compare Section 2.3.1). Integration of Eq. (24) - (27) yields the analytical solution and Table 6 summarises the boundary conditions applied in OMEN-SED. The model assumes known bottom water concentrations and equal concentrations and diffusive fluxes at  $z_{\text{bio}}$  and  $z_{\text{ox}}$  for both species. Additionally OMEN-SED considers no change in phosphate flux and an asymptotic Fe-bound P concentration at  $z_\infty$ .

**DH:** I think what I wrote before also applies: a asymptotic Fe-bound P concentration at  $z_\infty$  is assumed! (but is the same as “no flux condition” as it is now?’)

**Table 7.** Boundary conditions for DIC. For the boundaries we define:  $z_-^- := \lim_{h \rightarrow 0} (z_- - h)$  and  $z_-^+ := \lim_{h \rightarrow 0} (z_- + h)$ .

| Boundary              | Condition           |  |
|-----------------------|---------------------|--|
| $z = 0$               | known concentration | 1) $\text{DIC}(0) = \text{DIC}_0$  |
| $z = z_{\text{bio}}$  | continuity          | 2) $\text{DIC}(z_{\text{bio}}^-) = \text{DIC}(z_{\text{bio}}^+)$   |
|                       | flux                | 3) $-(D_{\text{DIC},0} + D_{\text{bio}}) \cdot \frac{\partial \text{DIC}}{\partial z}  _{z_{\text{bio}}^-} = -D_{\text{DIC},0} \cdot \frac{\partial \text{DIC}}{\partial z}  _{z_{\text{bio}}^+}$  |
| $z = z_{\text{SO}_4}$ | continuity          | 4) $\text{DIC}(z_{\text{SO}_4}^-) = \text{DIC}(z_{\text{SO}_4}^+)$   |
|                       | flux (with AOM)     | 5) $-D_{\text{DIC}} \cdot \frac{\partial \text{DIC}}{\partial z}  _{z_{\text{SO}_4}^-} + \gamma_{\text{CH}_4} \cdot F_{\text{CH}_4}(z_{\text{SO}_4}) = -D_{\text{DIC}} \cdot \frac{\partial \text{DIC}}{\partial z}  _{z_{\text{SO}_4}^+}$ |
|                       | where:              | $F_{\text{CH}_4}(z_{\text{SO}_4}) = \frac{1-\phi}{\phi} \cdot \int_{z_{\text{SO}_4}}^{\infty} \sum_i \text{MC} \cdot k_i \cdot \text{POC}_i dz$  |
| $z = z_\infty$        | zero DIC flux       | 6) $\frac{\partial \text{DIC}}{\partial z}  _{z_\infty} = 0$   |

## 2.2.6 Dissolved Inorganic Carbon (DIC)

- 570 OMEN-SED accounts for the production of dissolved inorganic carbon (DIC) through organic matter degradation, as well as methane oxidation. Organic matter degradation produces dissolved inorganic carbon with a stoichiometric DIC : C ratio of 1:2 in the methanic zone and 1:1 in the rest of the sediment column ( $\text{DIC}_{\text{CII}}$  and  $\text{DIC}_{\text{CI}}$  respectively). DIC production through methane oxidation is implicitly taken into account through the boundary condition at  $z_{\text{SO}_4}$ . A mechanistic description of  
 575 DIC production from  $\text{CaCO}_3$  dissolution would lead to significant mathematical problems and is therefore not included in the current version of OMEN-SED. The conservation equations for DIC are thus given by:

1. Oxic, nitrogenous and sulfidic zone ( $z \leq z_{\text{SO}_4}$ )

$$580 \frac{\partial \text{DIC}^I}{\partial t} = 0 = D_{\text{DIC}} \frac{\partial^2 \text{DIC}^I}{\partial z^2} - w \frac{\partial \text{DIC}^I}{\partial z} + \frac{1-\phi}{\phi} \cdot \sum_i \text{DIC}_{\text{C}^I} \cdot k_i \cdot \text{POC}_i(z) \quad (28)$$

2. Methanic zone ( $z_{\text{SO}_4} < z \leq z_\infty$ )

$$\frac{\partial \text{DIC}^{II}}{\partial t} = 0 = D_{\text{DIC}} \frac{\partial^2 \text{DIC}^{II}}{\partial z^2} - w \frac{\partial \text{DIC}^{II}}{\partial z} + \frac{1-\phi}{\phi} \cdot \sum_i \text{DIC}_{\text{C}^{II}} \cdot k_i \cdot \text{POC}_i(z) \quad (29)$$

- 585 where  $D_{\text{DIC}}$  denotes the diffusion coefficient for DIC which depends on the bioturbation status of the respective geochemical zone. Integration of Eq. (28) and (29) yields the analytical solution and Table 7 summarises the boundary conditions applied in OMEN-SED. A Dirichlet condition is applied at the sediment-water interface. In addition, the model assumes a zero diffusive flux through the lower boundary  $z_\infty$  and continuity across the bottom of the bioturbated zone, as well as the  
 590 sulfate penetration depth. An additional flux boundary condition at  $z_{\text{SO}_4}$ , implicitly accounts for DIC production through anaerobic oxidation of methane (Table 7 Eq. 5).

## 2.2.7 Alkalinity

SA: TODO: again need  
to mention carboantes

Organic matter degradation and secondary redox reactions exert a complex influence on alkalinity (e.g. Jourabchi et al., 2005; Wolf-Gladrow et al., 2007; Krumins et al., 2013). To model alkalinity, OMEN-SED divides the sediment column into four geochemical zones, where different equations describe the biogeochemical processes using variable stoichiometric coefficients (compare values in Table 10). Above  $z_{\text{ox}}$ , the combined effects of  $\text{NH}_4$  and P release due to aerobic OM degradation increases alkalinity according to  $\text{ALK}^{\text{OX}}$  whereas nitrification decreases alkalinity with stoichiometry  $\text{ALK}^{\text{NIT}}$ . In the remaining three zones anaerobic OM degradation generally results in an increase in alkalinity, with the exact magnitude depending on the nature of the terminal electron acceptor used (i.e.  $\text{ALK}^{\text{DEN}}$ ,  $\text{ALK}^{\text{SUL}}$ ,  $\text{ALK}^{\text{MET}}$ ). In addition, the effect of secondary redox reactions, such as nitrification, sulfide and methane oxidation are implicitly accounted for in the boundary conditions. Again, a mechanistic description of ALK production from  $\text{CaCO}_3$  dissolution would lead to significant mathematical problems and is therefore not included in the current version of OMEN-SED. In OMEN-SED, the conservation equations for alkalinity are thus given by:

1. Oxic zone ( $z \leq z_{\text{ox}}$ )

$$\frac{\partial \text{ALK}^I}{\partial t} = 0 = D_{\text{ALK}} \frac{\partial^2 \text{ALK}^I}{\partial z^2} - w \frac{\partial \text{ALK}^I}{\partial z} + \frac{1-\phi}{\phi} \cdot \sum_i \left( \text{ALK}^{\text{NIT}} \cdot \frac{\gamma_{\text{NH}_4}}{1+K_{\text{NH}_4}} \text{NC}_i + \text{ALK}^{\text{OX}} \right) \cdot k_i \cdot \text{POC}_i(z) \quad (30)$$

2. Denitrification or nitrogenous zone ( $z_{\text{ox}} < z \leq z_{\text{NO}_3}$ )

$$\frac{\partial \text{ALK}^{II}}{\partial t} = 0 = D_{\text{ALK}} \frac{\partial^2 \text{ALK}^{II}}{\partial z^2} - w \frac{\partial \text{ALK}^{II}}{\partial z} + \frac{1-\phi}{\phi} \cdot \sum_i \text{ALK}^{\text{DEN}} \cdot k_i \cdot \text{POC}_i(z) \quad (31)$$

3. Sulfidic zone ( $z_{\text{NO}_3} < z \leq z_{\text{SO}_4}$ )

$$\frac{\partial \text{ALK}^{III}}{\partial t} = 0 = D_{\text{ALK}} \frac{\partial^2 \text{ALK}^{III}}{\partial z^2} - w \frac{\partial \text{ALK}^{III}}{\partial z} + \frac{1-\phi}{\phi} \cdot \sum_i \text{ALK}^{\text{SUL}} \cdot k_i \cdot \text{POC}_i(z) \quad (32)$$

4. Methanic zone ( $z_{\text{SO}_4} < z \leq z_{\infty}$ )

$$\frac{\partial \text{ALK}^{IV}}{\partial t} = 0 = D_{\text{ALK}} \frac{\partial^2 \text{ALK}^{IV}}{\partial z^2} - w \frac{\partial \text{ALK}^{IV}}{\partial z} + \frac{1-\phi}{\phi} \cdot \sum_i \text{ALK}^{\text{MET}} \cdot k_i \cdot \text{POC}_i(z) \quad (33)$$

where  $D_{\text{ALK}}$  denotes the diffusion coefficient for alkalinity which depends on the bioturbation status of the respective geochemical zone. Integration of Eq. (30) - (33) yields the analytical solution and Table 8 summarises the boundary conditions applied in OMEN-SED. A Dirichlet boundary condition is applied at the sediment-water interface. The decrease of alkalinity due to oxidation of reduced species produced in the anoxic zones (with stoichiometry  $\text{ALK}^{\text{NIT}}$  and  $\text{ALK}^{\text{H}_2\text{S}}$ ) is implicitly taken into account through the flux boundary condition at  $z_{\text{ox}}$  (Table 8 Eq. 5). Furthermore, the oxidation of methane by sulfate reduction increases alkalinity with stoichiometry  $\text{ALK}^{\text{AOM}}$  which is accounted for through the flux boundary condition at  $z_{\text{SO}_4}$  (Table 8 Eq. 9). At the lower boundary  $z_{\infty}$  a zero diffusive flux condition is applied.

**Table 8.** Boundary conditions for alkalinity. For the boundaries we define:  $z_-^- := \lim_{h \rightarrow 0} (z_- - h)$  and  $z_-^+ := \lim_{h \rightarrow 0} (z_- + h)$ .

| Boundary              | Condition           |  |
|-----------------------|---------------------|--|
| $z = 0$               | known concentration | 1) $\text{ALK}(0) = \text{ALK}_0$  |
| $z = z_{\text{bio}}$  | continuity          | 2) $\text{ALK}(z_{\text{bio}}^-) = \text{ALK}(z_{\text{bio}}^+)$   |
|                       | flux                | 3) $-(D_{\text{ALK},0} + D_{\text{bio}}) \cdot \frac{\partial \text{ALK}}{\partial z}  _{z_{\text{bio}}^-} = -D_{\text{ALK},0} \cdot \frac{\partial \text{ALK}}{\partial z}  _{z_{\text{bio}}^+}$  |
| $z = z_{\text{ox}}$   | continuity          | 4) $\text{ALK}(z_{\text{ox}}^-) = \text{ALK}(z_{\text{ox}}^+)$   |
|                       | flux                | 5) $-D_{\text{ALK}} \cdot \frac{\partial \text{ALK}}{\partial z}  _{z_{\text{ox}}^-} + F_{\text{ALK}}(z_{\text{ox}}) = -D_{\text{ALK}} \cdot \frac{\partial \text{ALK}}{\partial z}  _{z_{\text{ox}}^+}$<br>$F_{\text{ALK}}(z_{\text{ox}}) = \frac{1-\phi}{\phi} \cdot \left( \text{ALK}^{\text{H}_2\text{S}} \cdot \gamma_{\text{H}_2\text{S}} \int_{z_{\text{NO}_3}}^{\text{SO}_4} \sum_i \text{SO}_4 \text{C} \cdot k_i \cdot \text{POC}_i dz \right) + \frac{1-\phi}{\phi} \cdot \left( \text{ALK}^{\text{NIT}} \frac{\gamma_{\text{NH}_4}}{1+k_{\text{NH}_4}} \int_{z_{\text{NO}_3}}^{\infty} \sum_i \text{NC}_i \cdot k_i \cdot \text{POC}_i dz \right)$ |
|                       | where:              |  |
| $z = z_{\text{NO}_3}$ | continuity          | 6) $\text{ALK}(z_{\text{NO}_3}^-) = \text{ALK}(z_{\text{NO}_3}^+)$   |
|                       | flux                | 7) $-D_{\text{ALK}} \cdot \frac{\partial \text{ALK}}{\partial z}  _{z_{\text{NO}_3}^-} = -D_{\text{ALK}} \cdot \frac{\partial \text{ALK}}{\partial z}  _{z_{\text{NO}_3}^+}$   |
| $z = z_{\text{SO}_4}$ | continuity          | 8) $\text{ALK}(z_{\text{SO}_4}^-) = \text{ALK}(z_{\text{SO}_4}^+)$   |
|                       | flux (with AOM)     | 9) $-D_{\text{ALK}} \cdot \frac{\partial \text{ALK}}{\partial z}  _{z_{\text{SO}_4}^-} + F_{\text{ALK}}(z_{\text{SO}_4}) = -D_{\text{ALK}} \cdot \frac{\partial \text{ALK}}{\partial z}  _{z_{\text{SO}_4}^+}$<br>$F_{\text{ALK}}(z_{\text{SO}_4}) = \frac{1-\phi}{\phi} \cdot \left( \text{ALK}^{\text{AOM}} \gamma_{\text{CH}_4} \cdot \int_{z_{\text{SO}_4}}^{\infty} \sum_i k_i \cdot \text{POC}_i dz \right)$   |
|                       | where:              |  |
| $z = z_\infty$        | zero ALK flux       | 10) $\frac{\partial \text{ALK}}{\partial z}  _{z_\infty} = 0$  |

## 2.3 Determination of Integration Constants

- 630 The integration constants of all general analytical solutions derived above change in response to changing boundary conditions. Thus, OMEN-SED has to re-determine integration constants for each dynamic zone (i.e.  $z_{\text{ox}}$ ,  $z_{\text{bio}}$ ,  $z_{\text{NO}_3}$  and  $z_{\text{SO}_4}$ ) at every time step for all biogeochemical tracers. The bioturbation boundary poses a particular challenge as it can theoretically occur in any of the dynamic geochemical zones (Fig. 3). Therefore, in order to generalise and simplify this recurring boundary  
635 matching problem, an independent, generic algorithm is implemented (rather than using multiple fully-worked-out algebraic solutions for each possible case and every biogeochemical tracer). The algorithm only has to solve a two-simultaneous-equation problem.

### 2.3.1 Generic Boundary Condition Matching (GBCM)

- As discussed in Section 2.1, the solution of the general steady-state transport-reaction equation (Eq.  
640 (2)) for a generic tracer  $C$  is of the general form:

$$C(z) = A \exp(az) + B \exp(bz) + \sum_j \frac{\alpha_j}{D\beta_j^2 - w\beta_j - k} \cdot \exp(-\beta_j z) + \frac{Q}{k} \quad (34)$$

and can therefore be expressed as:

$$645 \quad C(z) = A \cdot E(z) + B \cdot F(z) + G(z) \quad (35)$$

where  $E(z)$ ,  $F(z)$  are the homogeneous solutions of the ODE,  $G(z)$  the particular integral (collectively called the basis functions), and  $A$ ,  $B$  are the integration constants that must be determined with the boundary conditions (shown in Fig. 3 for the whole sediment column).

Each internal boundary matching problem (i.e. excluding  $z = 0$  and  $z = z_\infty$ ) involves matching  
650 continuity and flux for the two solutions of the respective reaction-transport equation above,  $C_U(z)$  ( $=$  'upper'), and below,  $C_L(z)$  ( $=$  'lower'), the dynamic boundary at  $z = z_b$ :

$$C_U(z) = A_U \cdot E_U(z) + B_U \cdot F_U(z) + G_U(z) \quad (36)$$

$$C_L(z) = A_L \cdot E_L(z) + B_L \cdot F_L(z) + G_L(z). \quad (37)$$

655 OMEN-SED generally applies concentration continuity and flux boundary conditions at its internal, dynamic boundaries:

Continuity (where for generality we allow a discontinuity  $V_b$ )

$$C_U(z_b) = C_L(z_b) + V_b \quad (38)$$

660 Flux

$$D_U C'_U(z_b) + w C_U(z_b) = D_L C'_L(z_b) + w C_L(z_b) + F_b \quad (39)$$

where  $w$  is advection,  $D$  are the diffusion coefficients and  $F_b$  is any flux discontinuity (e.g. resulting from secondary redox reactions).

665 Considering that the advective flux above and below the boundary is equal (i.e.  $w C_U(z_b) = w C_L(z_b)$ ) and substituting the general ODE solutions (36), (37), the boundary conditions can be represented as two equations connecting the four integration constants:

$$\begin{pmatrix} E_U & F_U \\ D_U E'_U & D_U F'_U \end{pmatrix} \begin{pmatrix} A_U \\ B_U \end{pmatrix} = \begin{pmatrix} E_L & F_L \\ D_L E'_L & D_L F'_L \end{pmatrix} \begin{pmatrix} A_L \\ B_L \end{pmatrix} + \begin{pmatrix} G_L - G_U + V_b \\ D_L G'_L - D_U G'_U + F_b - w V_b \end{pmatrix} \quad (40)$$

where the ODE solutions  $E$ ,  $F$ ,  $G$  are all evaluated at  $z_b$ .

670 Equation (40) can now be solved to give  $A_U$  and  $B_U$  as a function of the integration constants from the layer below ( $A_L$  and  $B_L$ ), thereby constructing a piecewise solution for both layers, with just two integration constants (this is implemented in the function **benthic\_utils.matchsoln** of OMEN-SED):

$$\begin{pmatrix} A_U \\ B_U \end{pmatrix} = \begin{pmatrix} c_1 & c_2 \\ c_3 & c_4 \end{pmatrix} \begin{pmatrix} A_L \\ B_L \end{pmatrix} + \begin{pmatrix} d_1 \\ d_2 \end{pmatrix}. \quad (41)$$

675 Using Eq. (41),  $C_U(z)$  in (36) can now be rewritten as a function of  $A_L$  and  $B_L$  (implemented in **benthic\_utils.xformsoln**):

$$C_U(z) = (c_1 A_L + c_2 B_L + d_1) \cdot E_U(z) + (c_3 A_L + c_4 B_L + d_2) \cdot F_U(z) + G_U(z) \quad (42)$$

and hence define the “transformed” basis functions  $E_U^*(z)$ ,  $F_U^*(z)$ ,  $G_U^*(z)$  such that:

$$C_U(z) = A_L \cdot E_U^*(z) + B_L \cdot F_U^*(z) + G_U^*(z) \quad (43)$$

680 where

$$E_U^*(z) = c_1 E_U(z) + c_3 F_U(z)$$

$$F_U^*(z) = c_2 E_U(z) + c_4 F_U(z) \quad (44)$$

$$G_U^*(z) = G_U(z) + d_1 E_U(z) + d_2 F_U(z)$$

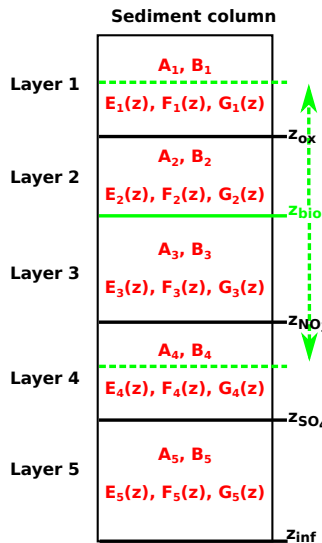


**Figure 3.** Schematic of the generic boundary condition matching (GBCM) problem. Showing the resulting integration constants ( $A_i, B_i$ ) and ODE solutions ( $E_i, F_i, G_i$ ) for the different sediment layers and the variable bioturbation boundary.

685 Equations (41), (43) and (44) can now be consecutively applied for each of the dynamic biogeochemical zone boundaries, starting at the bottom of the sediment column. The net result is a piecewise solution of the whole sediment column with just two integration constants (coming from the lowest layer), which can then be solved for by applying the boundary conditions at the sediment-water interface and the bottom of the sediments.

### 690 2.3.2 Abstracting out the bioturbation boundary

The bioturbation boundary affects the diffusion coefficient of the modelled solutes, as well as the conservation equation of organic matter (and thereby the exact form of each reaction-transport equation). This boundary is particularly inconvenient as it can, in principle, occur in the middle of any of the dynamically shifting biogeochemical zones and therefore generate multiple cases (Fig. 3). The

695 GBCM algorithm described above is thus not only used to construct a piecewise solution of the whole  
 sediment column, but also to abstract out the bioturbation boundary. For each biogeochemical zone  
 the "bioturbation-status" is initially tested (i.e. fully bioturbated, fully non-bioturbated, or crossing  
 the bioturbation boundary). Therefore, the upper and lower boundaries for the different zones (e.g.  
 for the nitrogenous zone:  $z_U = z_{\text{ox}}$ ,  $z_L = z_{\text{NO}_3}$ ), as well as the respective reactive terms and diffu-  
 700 sion coefficients (bioturbated and non-bioturbated) are passed over to the routine **zTOC.prepfg\_I12**  
 where the bioturbation-status is determined. In case the bioturbation depth is located within this zone  
 (i.e.  $z_U < z_{\text{bio}} < z_L$ ) a piecewise solution for this layer is constructed. Therefore, the reactive terms  
 and diffusion coefficients are handed over to the routines **zTOC.calcfg\_I1** and **zTOC.calcfg\_I2**  
 which calculate the basis functions ( $E_U, F_U, G_U$  and  $E_L, F_L, G_L$ ) and their derivatives for the bio-  
 705 turbated and the non-bioturbated part of this specific geochemical zone. The concentration and flux  
 for both solutions at  $z_{\text{bio}}$  are matched and the coefficients  $c_1, c_2, c_3, c_4, d_1, d_2$  (as in Eq. (41)) are cal-  
 culated by the routine **benthic\_utils.matchsoln**. These coefficients and the "bioturbation-status"  
 of the layer are passed back to the main GBCM algorithm where they can be used by the routine  
**benthic\_utils.xformsoln** to calculate the "transformed" basis functions ( $E_U^*(z)$ ,  $F_U^*(z)$ ,  $G_U^*(z)$ )  
 710 such that both layers are expressed in the same basis (compare Eq. (42 - 44)).

For instance, in the case of sulfate, **zTOC.prepfg\_I12** is called three times before the actual  
 profile is calculated (once per zone: oxic, nitrogenous, sulfidic) and hands back the information  
 about the "bioturbation-status" of the three layers and the coefficients  $c_1, c_2, c_3, c_4, d_1, d_2$  for the  
 715 biogeochemical zone including the bioturbation depth. When calculating the complete piecewise  
 solution for the sediment column, this information is passed to the function **zTOC.calcfg\_I12** which  
 sorts out the correct solution type to use. The main GBCM algorithm therefore never needs to know  
 whether it is dealing with a piecewise solution (i.e. matched across the bioturbation boundary) or a  
 "simple" solution (i.e. the layer is fully bioturbated or fully non-bioturbated).

## 2.4 Model Parameters

720 The following section provides a summary of global relationships used to constrain reaction and  
 transport parameters in OMEN-SED. Table 9 synthesises sediment and transport parameters, while  
 table 10 provides an overview of all biogeochemical parameters used in OMEN-SED.

### 2.4.1 Transport Parameters

The burial of sediments and pore water is directly related to the accumulation of new material on  
 725 the seafloor (i.e. sedimentation, Burdige, 2006). This results in a downward advective flux of older  
 sediment material and pore water in relation to the sediment-water interface. When coupled to an  
 ocean model, its sedimentation flux can be readily used in OMEN-SED. The stand-alone version of  
 OMEN-SED uses the empirical global relationship between sediment accumulation rate ( $\text{cm yr}^{-1}$ )

and seafloor depth (m) of Middelburg et al. (1997):

$$730 \quad w = 3.3 \cdot 10^{-0.87478367 - 0.00043512 \cdot \text{depth}}, \quad (45)$$

As mentioned before (Section 2.1), the diffusion coefficient of species  $i$  is calculated as  $D_i = D_{i,0} + D_{\text{bio}} = D_{\text{mol},i} \cdot f_{ir} + D_{\text{bio}}$  for dissolved species and  $D_i = D_{\text{bio}}$  for solid species. The bioturbation coefficient  $D_{\text{bio}}$  ( $\text{cm}^2 \text{ yr}^{-1}$ ) is constant in the bioturbated zone and also follows the empirical relationship by Middelburg et al. (1997):

$$735 \quad D_{\text{bio}} = 5.2 \cdot 10^{0.76241122 - 0.00039724 \cdot \text{depth}} \quad (46)$$

Observations indicate that bioturbation is largely restricted to the upper 10 cm of the sediments and is only marginally related to seafloor depth (e.g. Boudreau, 1998; Teal et al., 2010). Therefore, OMEN-SED imposes a globally invariant bioturbation depth  $z_{\text{bio}}$  of 10 cm. In case the bottom water oxygen concentration is below  $5 \text{ nmol cm}^{-3}$  infaunal activity is assumed to cease and  $z_{\text{bio}} = 0.01$  cm. We choose a low value unequal to zero in order to simplify the implementation of the model. This approach ensures that the sediment column always consists of a bioturbated (even though very small for the low oxygen condition) and a non-bioturbated zone, thus the same GBCM algorithm can be used to solve the conservation equations. Furthermore, when OMEN-SED is coupled to an Earth system model the same method can be used to convert the POC depositional flux into a SWI concentration (i.e. the flux needs to be converted assuming bioturbation, see Section 4.1).

Bioirrigation (i.e the pumping activity by burrow-dwelling animals) exchanges burrow water with overlying water and may enhance the SWI-flux of solutes (Aller, 1984, 1988). Several approaches exist to incorporate this into a 1-D diagenetic model, for instance as a non-local transport/exchange process (Boudreau, 1984; Emerson et al., 1984) or as an enhancement factor of the molecular diffusion coefficient (Devol and Christensen, 1993; Soetaert et al., 1996). In OMEN-SED the latter approach is applied and the apparent “bio-diffusion” coefficient is calculated as  $D_{i,0} = D_{\text{mol},i} \cdot f_{ir}$ . Soetaert et al. (1996) derived an empirical relationship between  $f_{ir}$  and seafloor depth ( $f_{ir} = \text{Min}\{1; 15.9 \cdot \text{depth}^{-0.43}\}$ ) based on observations from Archer and Devol (1992) and Devol and Christensen (1993). As this relationship just varies for depth below  $\sim 623$  m (with a maximum value of 3 at  $\sim 50$  m) a constant value of  $f_{ir} = 1$  is used in the default OMEN-SED configuration. The specific molecular diffusion coefficients  $D_{\text{mol},i}$  are corrected for sediment porosity  $\phi$ , tortuosity  $F$  and are linearly interpolated for an ambient temperature  $T$  using zero-degree coefficients  $D_i^0$  and temperature-dependent diffusion coefficients  $D_i^T$  (Soetaert et al., 1996):

$$D_{\text{mol},i} = (D_i^0 + D_i^T \cdot T) \cdot \frac{1}{\phi \cdot F}.$$

760 Tortuosity can be expressed in terms of porosity as  $F = \frac{1}{\phi^m}$  (Ullman and Aller, 1982) with the exponent  $m$  varying according to the type of sediment (here  $m=3$  is used). Values for  $D_i^T$  and  $D_i^0$  are summarised in Table 9 and are adapted from Li and Gregory (1974), Schulz (2006) and Gypens et al. (2008).

**SA:** need to explain why not 0; **DH:** Decent explanation?

**Table 9.** Sediment characteristics and transport parameters.

| Parameter   | Unit  | Value                                 | Description/Source  |
|---|---|---------------------------------------|---|
| $\rho_{\text{sed}}$   | $\text{g cm}^{-3}$                          | 2.6                                   | Sediment density  |
| $w$   | $\text{cm yr}^{-1}$                         | Fct. of seafloor<br>depth or from ESM | Advection/Sediment accumulation rate<br>(Middelburg et al., 1997) |
| $z_{\text{bio}}$  | cm  | 10 or 0.01                            | Bioturbation depth<br>(Boudreau, 1998; Teal et al., 2010)         |
| $D_{\text{bio}}$  | $\text{cm}^2 \text{yr}^{-1}$                | Fct. of seafloor<br>depth             | Bioturbation coefficient<br>(Middelburg et al., 1997)             |
| $\phi$  | -   | 0.85                                  | Porosity  |
| F   | -   | $\frac{1}{\phi^m}$                    | Tortuosity, here m=3  |
| $f_{ir}$  | -   | 1                                     | Irrigation factor   |
| <b>Diffusion coefficients</b> (Li and Gregory, 1974; Schulz, 2006; Gypens et al., 2008) |   |                                       |   |
| $D_{\text{O}_2}^0$  | $\text{cm}^2 \text{yr}^{-1}$                | 348.62                                | Molecular diffusion coefficient of oxygen at 0°C                  |
| $D_{\text{O}_2}^T$  | $\text{cm}^2 \text{yr}^{-1} \text{°C}^{-1}$ | 14.09                                 | Diffusion coefficient for linear temp. dependence of oxygen       |
| $D_{\text{NO}_3}^0$   | $\text{cm}^2 \text{yr}^{-1}$                | 308.42                                | Molecular diffusion coefficient of nitrate at 0°C                 |
| $D_{\text{NO}_3}^T$   | $\text{cm}^2 \text{yr}^{-1} \text{°C}^{-1}$ | 12.26                                 | Diffusion coefficient for linear temp. dependence of nitrate      |
| $D_{\text{NH}_4}^0$   | $\text{cm}^2 \text{yr}^{-1}$                | 309.05                                | Molecular diffusion coefficient of ammonium at 0°C                |
| $D_{\text{NH}_4}^T$   | $\text{cm}^2 \text{yr}^{-1} \text{°C}^{-1}$ | 12.26                                 | Diffusion coefficient for linear temp. dependence of ammonium     |
| $D_{\text{SO}_4}^0$   | $\text{cm}^2 \text{yr}^{-1}$                | 157.68                                | Molecular diffusion coefficient of sulfate at 0°C                 |
| $D_{\text{SO}_4}^T$   | $\text{cm}^2 \text{yr}^{-1} \text{°C}^{-1}$ | 7.88                                  | Diffusion coefficient for linear temp. dependence of sulfate      |
| $D_{\text{H}_2\text{S}}^0$  | $\text{cm}^2 \text{yr}^{-1}$                | 307.48                                | Molecular diffusion coefficient of sulfide at 0°C                 |
| $D_{\text{H}_2\text{S}}^T$  | $\text{cm}^2 \text{yr}^{-1} \text{°C}^{-1}$ | 9.64                                  | Diffusion coefficient for linear temp. dependence of sulfide      |
| $D_{\text{PO}_4}^0$   | $\text{cm}^2 \text{yr}^{-1}$                | 112.91                                | Molecular diffusion coefficient of phosphate at 0°C               |
| $D_{\text{PO}_4}^T$   | $\text{cm}^2 \text{yr}^{-1} \text{°C}^{-1}$ | 5.59                                  | Diffusion coefficient for linear temp. dependence of phosphate    |
| $D_{\text{DIC}}^0$  | $\text{cm}^2 \text{yr}^{-1}$                | 151.69                                | Molecular diffusion coefficient of DIC at 0°C                     |
| $D_{\text{DIC}}^T$  | $\text{cm}^2 \text{yr}^{-1} \text{°C}^{-1}$ | 7.93                                  | Diffusion coefficient for linear temp. dependence of DIC          |
| $D_{\text{ALK}}^0$  | $\text{cm}^2 \text{yr}^{-1}$                | 151.69                                | Molecular diffusion coefficient of ALK at 0°C                     |
| $D_{\text{ALK}}^T$  | $\text{cm}^2 \text{yr}^{-1} \text{°C}^{-1}$ | 7.93                                  | Diffusion coefficient for linear temp. dependence of ALK          |
| Note: DIC and ALK coefficients are the values of $\text{HCO}_3^-$ from Schulz (2006).   |   |                                       |   |

## 2.4.2 Stoichiometries and reaction parameters

765 The first-order organic matter degradation constants of compound class  $i$ ,  $k_i$  ( $\text{yr}^{-1}$ ), are assumed invariant along the sediment column and therefore independent of the nature of the terminal electron acceptor. The rate constants can be altered manually to fit observed sediment profiles (compare Section 3.2) or related to a master variable provided by a coupled Earth system model (e.g. sedimentation rate, compare Section 4.2). The partitioning of the bulk OM pool into reactivity classes  
770 ( $f_i$ ) is also done manually in the stand-alone version or is provided by the ESM. Organic matter degradation releases N, P and DIC to the pore water using Redfield molar ratios (Redfield, 1963) and consumes TEA with specific stoichiometries ( $\text{O}_2\text{C}$ ,  $\text{NO}_3\text{C}$ ,  $\text{SO}_4\text{C}$ ) as summarised in Table 10. Table 15 in the appendix provides a list of reactions and their stoichiometries as implemented in OMEN-SED. The effect of OM degradation and secondary redox reactions on total alkalinity is  
775 also accounted for via reaction specific stoichiometries representing the release of  $\text{NH}_4$ ,  $\text{H}_2\text{S}$  and P and is based on Jourabchi et al. (2005). The secondary redox parameters (i.e.  $\gamma_{\text{NH}_4}$ ,  $\gamma_{\text{H}_2\text{S}}$ ,  $\gamma_{\text{CH}_4}$ ), accounting for the fraction of reduced substances that are reoxidised, would be ideally parameterised for instance in relation to bottom water oxygen concentration or oxygen penetration depth ( $z_{\text{ox}}$ ). Gypens et al. (2008) for example expressed  $\gamma_{\text{NH}_4}$  as a function of oxygen penetration depth  
780 ( $\gamma_{\text{NH}_4} = 0.243 \cdot \ln(z_{\text{ox}}) + 1.8479$ ) based on a fitting exercises to a numerical model and showed that the fraction varies between 0.2 for  $z_{\text{ox}} = 0.1\text{cm}$  and 1.0 for  $z_{\text{ox}} > 3\text{cm}$ . Due to mathematical constraints for finding an analytical solution to the model equations these fractions take constant values generally representing oxygenated deep sea conditions. The instantaneous equilibrium adsorption coefficients of  $\text{NH}_4$  and  $\text{PO}_4$  ( $K_{\text{NH}_4}$ ,  $K_{\text{PO}_4}^{\text{ox}}$ ,  $K_{\text{PO}_4}^{\text{anox}}$ ) are based on Wang and Van Cappellen (1996)  
785 and Slomp et al. (1998), respectively. The first order rate constants for sorption of  $\text{PO}_4$  to Fe oxides ( $k_s$ ), release of  $\text{PO}_4$  from Fe-bound P due to Fe-oxide reduction ( $k_m$ ) and authigenic CFA precipitation ( $k_a$ ), as well as the pore water equilibrium concentrations for P sorption and CFA precipitation ( $\text{PO}_4^s$ ,  $\text{PO}_4^a$ ) and the asymptotic concentration for Fe-bound P ( $\text{FeP}^\infty$ ) are taken from Slomp et al. (1996). See Table 10 for a complete summary of the parameters and their values.

## 790 3 Stand-alone sensitivity analysis and case studies

### 3.1 Sensitivity Analysis

#### 3.1.1 Methodology

Model parameters implicitly account for processes that are not explicitly resolved. Therefore, model parameters are notoriously difficult to constrain and a source of uncertainty for numerical and analytical models. A comprehensive sensitivity analysis (SA) can help quantify this uncertainty and identify the most sensitive parameters. More specifically, sensitivity analysis is used to investigate how the variations in the outputs ( $y_1, \dots, y_N$ ) of a model can be attributed to variations in the differ  
795

**Table 10.** Values for biogeochemical parameters used in OMEN-SED. The variables  $x$ ,  $y$  and  $z$  denote the atomic ratio of carbon, nitrogen and phosphorus of the degrading organic matter (here set to  $C : N : P = 106 : 16 : 1$ ).

| Parameter/Variable  | Unit                 | Value                                     | Description   |
|---|----------------------|---|---|
| <b>Stoichiometric factors and molecular ratios</b>                                      |                      |   |   |
| NC <sub>i</sub>   | mol/mol              | $\frac{y}{x} = \frac{16}{106}$            | Nitrogen to carbon ratio                              |
| PC <sub>i</sub>   | mol/mol              | $\frac{z}{x} = \frac{1}{106}$             | Phosphorus to carbon ratio                            |
| MC  | mol/mol              | 0.5                                       | Methane to carbon ratio                               |
|   |                      |   | produced during methanogenesis                        |
| DICC <sup>I</sup>   | mol/mol              | 1.0                                       | DIC to carbon ratio until z <sub>SO<sub>4</sub></sub> |
| DICC <sup>II</sup>  | mol/mol              | 0.5                                       | DIC to carbon ratio below z <sub>SO<sub>4</sub></sub> |
| O <sub>2</sub> C  | mol/mol              | $\frac{x+2y}{x} = \frac{138}{106}$        | Oxygen to carbon ratio                                |
| NO <sub>3</sub> C   | mol/mol              | $\frac{4x+3y}{5x} = \frac{94.4}{106}$     | Nitrate to carbon ratio                               |
| SO <sub>4</sub> C   | mol/mol              | $\frac{1}{2}O_2C = \frac{138}{212}$       | Sulfate to carbon ratio                               |
| ALK <sup>OX</sup>   | mol/mol              | $\frac{y-2z}{x} = \frac{14}{106}$         | ALK from aerobic degradation                          |
| ALK <sup>NIT</sup>  | mol/mol              | -2  | ALK from nitrification                                |
| ALK <sup>DEN</sup>  | mol/mol              | $\frac{4x+3y-10z}{5x} = \frac{92.4}{106}$ | ALK from denitrification                              |
| ALK <sup>SUL</sup>  | mol/mol              | $\frac{x+y-2z}{x} = \frac{120}{106}$      | ALK from sulfate reduction                            |
| ALK <sup>MET</sup>  | mol/mol              | $\frac{y-2z}{x} = \frac{14}{106}$         | ALK from methanogenesis                               |
| ALK <sup>H<sub>2</sub>S</sup>   | mol/mol              | -2  | ALK from H <sub>2</sub> S oxidation                   |
| ALK <sup>AOM</sup>  | mol/mol              | 2   | ALK from AOM  |
| <b>Secondary reaction parameters</b>  |                      |   |   |
| γ <sub>NH<sub>4</sub></sub>   | -                    | 0.9                                       | Fraction of NH <sub>4</sub> that is nitrified         |
| γ <sub>H<sub>2</sub>S</sub>   | -                    | 0.95                                      | Fraction of H <sub>2</sub> S that is oxidised         |
| γ <sub>CH<sub>4</sub></sub>   | -                    | 0.99                                      | Fraction of CH <sub>4</sub> that is oxidised          |
| <b>Adsorption coefficients</b> (Wang and Van Cappellen, 1996; Slomp et al., 1998)       |                      |   |   |
| K <sub>NH<sub>4</sub></sub>   | -                    | 1.4                                       | NH <sub>4</sub> adsorption coefficient                |
| K <sub>PO<sub>4</sub></sub> <sup>OX</sup> , K <sub>PO<sub>4</sub></sub> <sup>ANOX</sup> | -                    | 200.0, 2.0                                | PO <sub>4</sub> adsorption coefficient (oxic, anoxic) |
| <b>P related parameters</b> (Slomp et al., 1996)  |                      |   |   |
| k <sub>s</sub>  | yr <sup>-1</sup>     | 94.9                                      | Rate constant for PO <sub>4</sub> sorption            |
| k <sub>m</sub>  | yr <sup>-1</sup>     | 0.193                                     | Rate constant for Fe-bound P release                  |
| k <sub>a</sub>  | yr <sup>-1</sup>     | 0.365                                     | Rate constant for authigenic CFA precipitation        |
| PO <sub>4</sub> <sup>s</sup>  | mol cm <sup>-3</sup> | $1 \cdot 10^{-9}$                         | Equilibrium conc. for P sorption                      |
| FeP <sup>∞</sup>  | mol cm <sup>-3</sup> | $1.99 \cdot 10^{-10}$                     | Asymptotic concentration for Fe-bound P               |
| PO <sub>4</sub> <sup>a</sup>  | mol cm <sup>-3</sup> | $3.7 \cdot 10^{-9}$                       | Equilibrium conc. for authigenic P precipitation      |

**DH:** ALK<sup>OX</sup> correct?  
y=NH<sub>4</sub> prod.; -2z=P release

ent input parameters ( $x_1, \dots, x_M$ , Pianosi et al., 2016). Different types of sensitivity indices, which quantify the relative influence of parameter  $x_i$  on output  $y_j$  with a scalar  $S_{i,j}$  (for  $i \in \{1, \dots, M\}$  and  $j \in \{1, \dots, N\}$ ), can be calculated, ranging from simple one-at-a-time methods to statistical evaluations of the output distribution (e.g. variance-based or density-based approaches Pianosi et al., 2016). The latter indices take values between zero and one ( $S_{i,j} \in [0, 1]$ ), where zero indicates a non-influential parameter and a higher value a more influential parameter. Here, SA is used mainly to identify which parameters have the largest impact on the different model outputs and therefore require careful calibration. As the probability density functions of our model outputs (i.e. the resulting SWI-fluxes) are generally highly-skewed towards extreme organic matter degradation rates (not shown) variance-based sensitivity indices may not be a suitable proxy for output uncertainty (Pianosi et al., 2016). Hence the novel density-based PAWN method by Pianosi and Wagener (2015) is employed which considers the entire conditional and unconditional Cumulative Distribution Function (CDF) of the model output rather than its variance only. The unconditional CDF,  $F_y(y)$ , of output  $y$  is obtained when all uncertain parameters ( $x_1, \dots, x_M$ ) are varied simultaneously, and the conditional CDFs,  $F_{y|x_i}(y)$ , are obtained when all inputs but the  $i$ -th parameter are varied (i.e.  $x_i$  is fixed to a so-called conditioning value). The sensitivity index of parameter  $i$  is measured by the distance between the two CDFs using the Kolmogorov-Smirnov statistic (Kolmogorov, 1933; Smirnov, 1939), i.e.:

$$S_i = \max_{x_i} \max_y |F_y(y) - F_{y|x_i}(y)|. \quad (47)$$

Since  $F_{y|x_i}(y)$  accounts for what happens when the variability due to  $x_i$  is removed, the distance between the two CDFs provides a measure of the effects of  $x_i$  on the output  $y$ . Due to the model complexity it is impossible to compute the sensitivity indices analytically. Therefore, they are approximated from a Latin-Hypercube sampling of parameter inputs and calculated outputs. For a brief description of the methodology see Fig. 4. For more details we refer the interested reader to Pianosi and Wagener (2015).

The PAWN method, as implemented within the Sensitivity Analysis for Everyone (SAFE) matlab toolbox (Pianosi et al., 2015), is used to investigate  $M = 11$  model parameters for ranges as specified in Table 11. Sensitivity indices for all resulting SWI-fluxes for two idealised sediment conditions (i.e. anoxic at 400 m and oxic at 4000 m, see Table 12) are calculated. We use  $NU = 200$  samples to estimate the unconditional CDF,  $NC = 100$  samples to estimate the conditional CDFs and  $n = 10$  conditioning points. Thus as  $N_{eval} = 200 + 100 \cdot 10 \cdot 11$ , 11200 model evaluations are performed for each sediment condition. The resulting indices are then translated into a color code and summarised in a pattern plot to simplify comparison (Fig. 5).

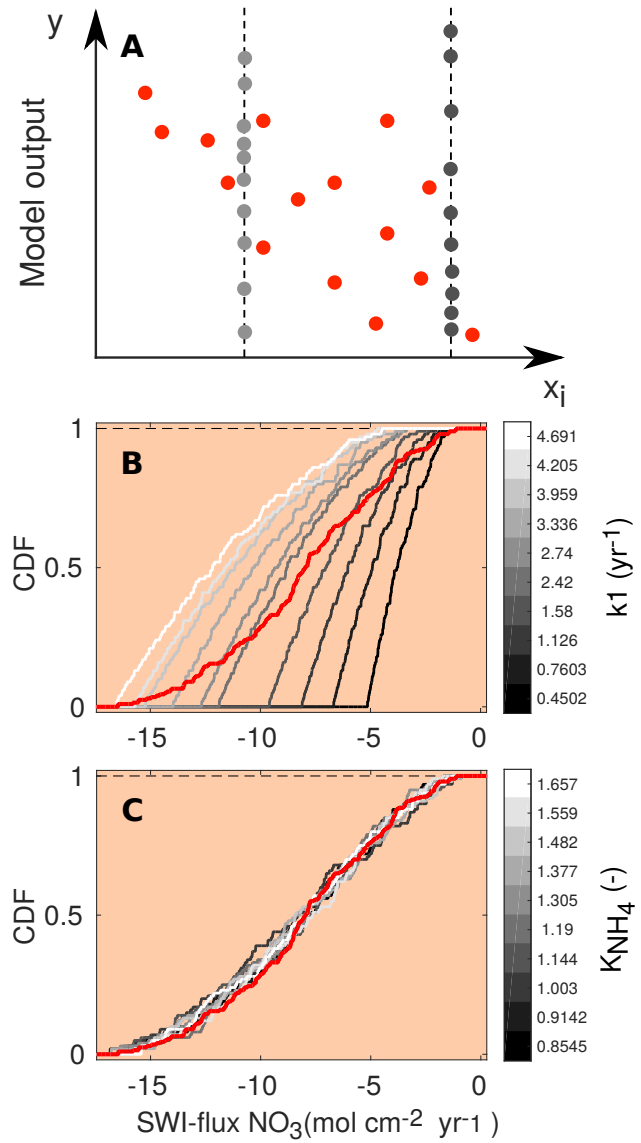


**Figure 4.** A: Schematic of the PAWN method, plotting an uncertain parameter ( $x_i$ ) against a generic model output ( $y$ ). Red dots represent points for calculating the unconditional CDF (NU, here 15), grey dots are points for calculating each conditional CDF (NC, here 10) with  $n = 2$  conditioning points as an example. The user can change the values of NU, NC and  $n$ . The number of model evaluations equals  $N_{\text{eval}} = \text{NU} + n \cdot \text{NC} \cdot M$ , where  $M$  is the number of uncertain input parameters. B + C: Two examples of CDFs of the model calculated SWI-flux of  $\text{NO}_3$  using NU = 200, NC = 100 and  $n = 10$ . The red lines are the unconditional distribution functions  $F_y(\text{NO}_3)$  and the grey lines are the conditional distribution functions  $F_{y|x_i}(\text{NO}_3)$  at different fixed values of the input parameters  $k_1$  (B) and  $K_{\text{NH}_4}$  (C). As the maximal distance between conditional CDFs and unconditional CDF is greater for  $k_1$ , this parameter is more influential for the model output (here SWI-flux of  $\text{NO}_3$ , compare Fig. 5).

**Table 11.** Range of model parameters used for sensitivity analysis of model predicted output.

| Parameter                       | Description   | Units            | Minimum   | Maximum   | Source |
|---------------------------------|---|------------------|-----------|-----------|--------|
| $k_1$                           | labile OM degradation constant  | $\text{yr}^{-1}$ | $1e^{-4}$ | 5.0       | (1)    |
| $\tilde{k}_2$                   | order of refractory OM degradation<br>$(k_2 = \tilde{k}_2 \cdot k_1)$ | -                | $1e^{-4}$ | $1e^{-1}$ | (1)    |
| $f_1$                           | fraction of labile OM   | -                | 0.02      | 0.98      | -      |
| $K_{\text{NH}_4}$               | Adsorption coefficient  | -                | 0.8       | 1.7       | (2)    |
| $\gamma_{\text{NH}_4}$          | $\text{NH}_4$ fraction oxidised                                       |                  | 0.5       | 1.0       | -      |
| $\gamma_{\text{H}_2\text{S}}$   | $\text{H}_2\text{S}$ fraction oxidised                                |                  | 0.5       | 1.0       | -      |
| $K_{\text{PO}_4}^{\text{ox}}$   | Adsorption coeff. oxic  | -                | 100.0     | 400.0     | (3)    |
| $K_{\text{PO}_4}^{\text{anox}}$ | Adsorption coeff. anoxic  | -                | 1.3       | 2.0       | (3)    |
| $k_s$                           | kinetic P sorption  | $\text{yr}^{-1}$ | 0.1       | 100.0     | (4, 5) |
| $k_m$                           | Fe-bound P release  | $\text{yr}^{-1}$ | 0.015     | 0.02      | (4, 5) |
| $k_a$                           | authigenic P formation  | $\text{yr}^{-1}$ | 0.001     | 10.0      | (4, 6) |

Sources: (1) Arndt et al. (2013); (2): Van Cappellen and Wang (1996); (3): Krom and Berner (1980)  
(4): Gypens et al. (2008); (5): Slomp et al. (1996); (6): Van Cappellen and Berner (1988)

**Table 12.** Model boundary conditions for the two idealised sediment conditions used for the sensitivity analysis (Fig. 5 and 6). All solute concentrations are in  $\text{nmol cm}^{-3}$ .

| Depth (m) | Temp. ( $^{\circ}\text{C}$ ) | OC (wt%) | $\text{O}_2$ | $\text{NO}_3$ | $\text{SO}_4$ | $\text{PO}_4$ | $z_{\text{bio}}$ (cm) |
|-----------|------------------------------|----------|--------------|---------------|---------------|---------------|-----------------------|
| 400       | 8.0                          | 2.0      | 0.0          | 40.0          | 28,000        | 40.0          | 0.001                 |
| 4000      | 1.5                          | 1.0      | 300.0        | 20.0          | 28,000        | 40.0          | 10.0                  |

### 3.1.2 Results

Fig. 5 summarises results of the sensitivity analysis as a colour map. Results indicate that generally the most significant parameters for all model outputs are the degradation rate constant for the labile OM pool ( $k_1$ ) and the fraction of this pool to the total OM stock ( $f_1$ ). Other parameters play a minor role for the SWI-fluxes, with the exception of the secondary redox parameters (i.e.  $\gamma_{\text{NH}_4}$ ,  $\gamma_{\text{H}_2\text{S}}$ ) in the oxic scenario. Here,  $\text{NH}_4$ ,  $\text{SO}_4$  and  $\text{H}_2\text{S}$  are very sensitive to changes in  $\gamma_{\text{NH}_4}$  and  $\gamma_{\text{H}_2\text{S}}$ , as these parameters determine how much of the respective TEA is produced in situ via reoxidation, thus affecting the resulting SWI-fluxes. For the oxic scenario, the reoxidation of  $\text{H}_2\text{S}$  produced in the sulfidic layer ( $\gamma_{\text{H}_2\text{S}}$ , Table 8 Eq. 5) also has a strong influence on alkalinity as it decreases alkalinity by 2 moles per mole of S oxidized ( $\text{ALK}_{\text{H}_2\text{S}}$ , Table 10). For the anoxic scenario the secondary redox parameters are essentially non-influential as no  $\text{O}_2$  is available for the reoxidation of reduced substances. Especially for the oxic condition the  $\text{PO}_4$  SWI-flux appears to be insensitive to P-related parameters (i.e.  $K_{\text{PO}_4}^{\text{ox}}$ ,  $K_{\text{PO}_4}^{\text{anox}}$ ,  $k_s$ ,  $k_m$ ,  $k_a$ ) as the majority is absorbed to Fe-oxides. The sensitivities change if other  $\text{PO}_4$  related equilibrium concentrations  $\text{PO}_4^s$ ,  $\text{PO}_4^a$  and  $\text{FeP}^\infty$  are used

845 (not shown). Overall the results of the sensitivity analysis are in line with what one would expect from a diagenetic model and thus provide ground to confirm that OMEN-SED provides sensible results.

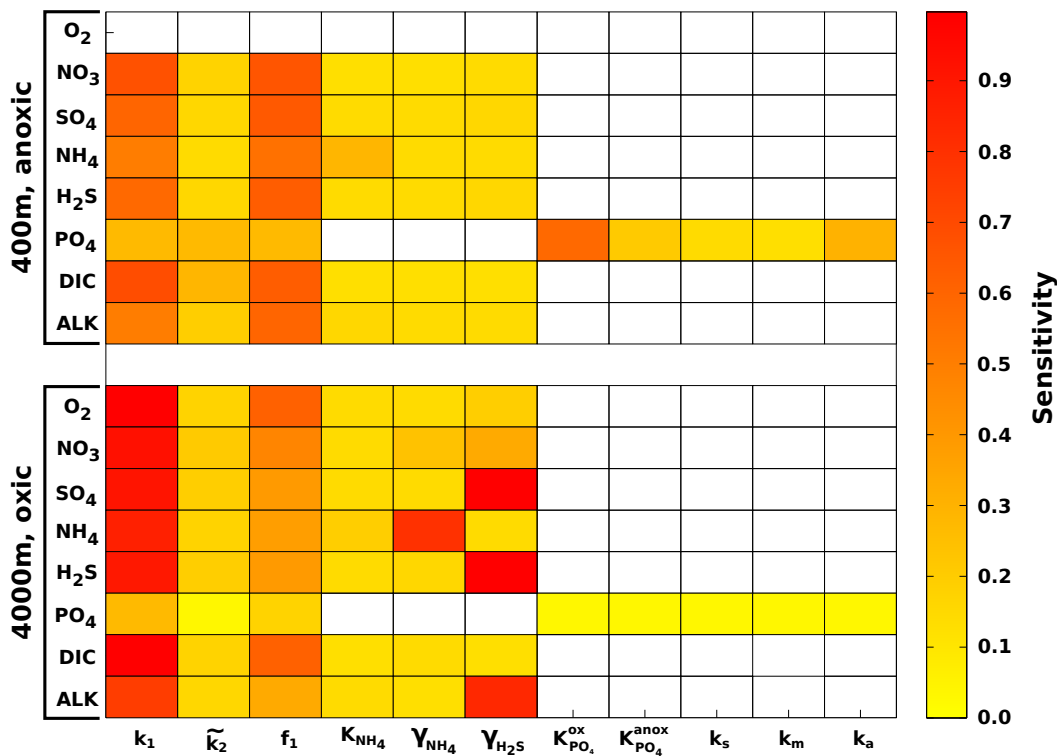


**Figure 5.** Pattern plot, showing the output sensitivity for each SWI flux (i.e. the chemical compounds on the vertical axis) and each input factor (i.e. the model parameters on the horizontal axis) for two idealised sediment cores. White patterns are assigned where the SWI flux is independent of the specific parameter.

**DH:** Rather low PO<sub>4</sub> sensitivity - bc of Equil. concn.?

We further explore the sensitivity of simulated sediment-water exchange fluxes to variations in organic matter degradation parameters by varying k<sub>1</sub>, f<sub>1</sub> and k̃<sub>2</sub> while all other model parameters are set to their default values (Tables 9 and 10). Minimum and maximum values for k<sub>1</sub>, k̃<sub>2</sub> and f<sub>1</sub> in the shallow ocean are as in Table 11. For the deep sea condition we account for the presence of more refractory OM by sampling f<sub>1</sub> ∈ [0.02, 0.3], whereas the variation of k<sub>1</sub> and k̃<sub>2</sub> is as in the shallow ocean. The parameter space is sampled using another Latin-Hypercube approach with sample sizes of N = 3500 for each idealised sediment condition. Figure 6 summarises the results of the sensitivity study and the ranges of observed O<sub>2</sub> and NO<sub>3</sub> sediment-water interface fluxes extracted from a global database (Stolpovsky et al., 2015) are indicated on the colour scale. Figure 6 shows that the ranges of SWI-fluxes simulated with OMEN-SED are comparable to the observed ranges reported by Stolpovsky et al. (2015). The colour patterns in Figure 6 A and B also reveal the complex interplay

between the amount of labile OM  $f_1$  and its degradation rate  $k_1$  for the resulting SWI-fluxes of NO<sub>3</sub> in anoxic sediments and O<sub>2</sub> in aerobic sediments. In general, a higher degradation rate in combination with more labile OM available leads to a higher SWI-flux. However, higher fluxes extend over a larger range of  $k_1$ -values when the amount of labile OM  $f_1$  is high. The absence of a colour pattern in Figure 6 C highlights the limited interaction of the two model parameters for NO<sub>3</sub> SWI-fluxes under oxic conditions.

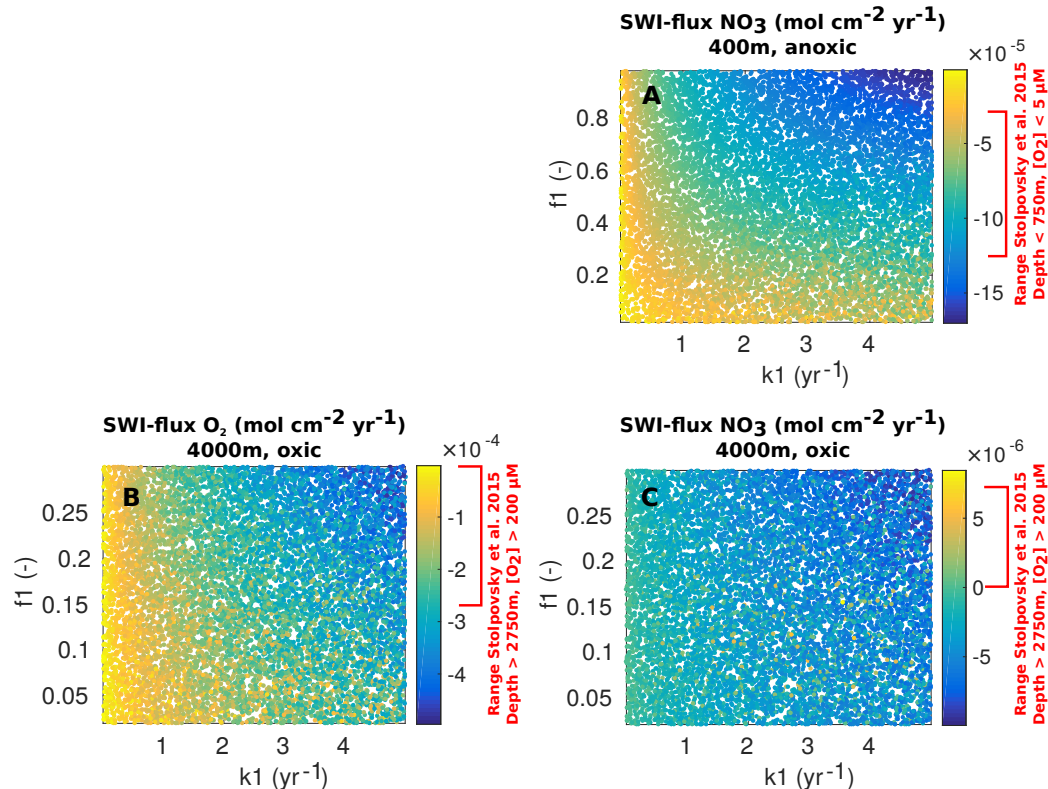


**Figure 6.** Scatter plots ( $k_1$  vs  $f_1$ ) of resulting OMEN-SED SWI-fluxes for the 400m anoxic (A: NO<sub>3</sub>) and 4000m oxic (B: O<sub>2</sub>, C: NO<sub>3</sub>) scenario. Negative values represent a flux from the water column into the sediments. Ranges indicated in red on the colour scale correspond to observed benthic fluxes as reported in the global database of Stolpovsky et al. (2015).

### 865 3.2 Case study: Simulations of sediment cores

#### 3.2.1 Methodology

In order to illustrate the capabilities of OMEN-SED, comprehensive datasets from the Santa Barbara Basin (Reimers et al., 1996), as well as from the Iberian margin and the Nazaré Canyon (Epping et al., 2002) are modelled. Modelled profiles are compared with measured pore water data from

870 different depths including the continental shelf (108 m) and the lower slope (2213 m) located at the Iberian margin, the upper slope (585 m) from the Santa Barbara Basin, and a deep sea site (4298 m) in the Nazaré Canyon. The Santa Barbara Basin is characterised by anoxic bottom waters, high POC concentrations and varved sediments (Reimers et al., 1990), therefore the depth of bioturbation in OMEN-SED is restricted to the upper 0.01 cm. In the uppermost sediments iron(III) hydroxides are  
875 reduced, releasing  $\text{Fe}^{2+}$  which reacts with sulfide to form iron sulfides. Thus, the Fe cycle exerts a strong control on sulfide concentrations in the sediments of this basin (Reimers et al., 1996). In addition, the sediments are generally supersaturated with respect to carbonate fluorapatite by and below 2 cm (Reimers et al., 1996). The Iberian margin, situated in the northeastern Atlantic, generally belongs to the more productive regions of the global ocean (Longhurst et al., 1995), however, sea-  
880 sonal changes in upwelling creates a strong temporal variability in primary productivity and organic carbon deposition. Submarine canyons in this area (like the Nazaré Canyon) may deliver organic carbon from the shelf to the ocean interior (van Weering et al., 2002; Epping et al., 2002). For a more detailed description of the study areas and the experimental work, the interested reader is referred to the publications by Reimers et al. (1996) and Epping et al. (2002).

885 In OMEN-SED sediment characteristics and boundary conditions are set to the observed values where available (Table 13). Other sediment characteristics (e.g. sedimentation rate, porosity, density), stoichiometric factors and secondary reaction parameters are set to the default value (see Tables 9 and 10). Organic matter is modelled as two fractions, with different first-order degradation rate constants. The POC and pore water profiles were fitted by optimizing the POC partitioning into  
890 the fast and slow degrading pool and their respective first-order degradation rate constants (priority is given to reproduce the POC and  $\text{O}_2$  profiles). For phosphorus the equilibrium concentration for authigenic P formation ( $\text{PO}_4^{\text{a}}$ ) was adjusted to fit the  $\text{PO}_4$  concentration at  $z_\infty$ .

### 3.2.2 Results

Fig. 7 compares modelled and observed sediment profiles for the Santa Barbara Basin and the Iberian  
895 margin. Results show that OMEN-SED is able to capture the main diagenetic features across a range of different environments without changing model parameters (e.g. stoichiometric ratios or secondary reaction parameters) to site specific conditions. For the two open Iberian margin stations (108 and 2213 m) OMEN-SED fits all observations well. OMEN-SED does especially well at seafloor depth (SFD) 2213 m by reproducing the deep  $\text{O}_2$  penetration and the subsurface maximum  
900 in  $\text{NO}_3^-$  concentration due to the nitrification of  $\text{NH}_4^+$  (note, that  $\text{NH}_4^+$  is overestimated at this SFD). For the anoxic Santa Barbara Basin (585 m) the decrease in  $\text{SO}_4^{2-}$  and the increase in ALK concentration with sediment depth is well represented, indicating the importance of sulfate reduction as the primary pathway of OM degradation at this site (compare with Meysman et al., 2003). However, a misfit is observed for  $\text{H}_2\text{S}$  and  $\text{PO}_4^{2-}$  in the upper 20 cm of this sediment core. The discrepancy  
905 for  $\text{H}_2\text{S}$  can be explained by high iron(III) hydroxide concentrations, which is reduced to degrade

**Table 13.** Model boundary conditions for the simulated sediment profiles in the Santa Barbara basin (108 and 2213 m) and Iberian margin (585 and 4298 m) reported in Figure 7. For all sites a DIC bottom water concentration of 2,400 nmols cm<sup>-3</sup> is assumed.

| <b>Sediment characteristics:</b> |               |                          |   |                           |                           |                                       |                                       |
|----------------------------------|---------------|--------------------------|---|---------------------------|---------------------------|---------------------------------------|---------------------------------------|
| Depth<br>(m)                     | Temp.<br>(°C) | $z_{\text{bio}}$<br>(cm) | $D_{\text{bio}}$<br>(cm <sup>2</sup> yr <sup>-1</sup> ) | POC <sub>1</sub><br>(wt%) | POC <sub>2</sub><br>(wt%) | k <sub>1</sub><br>(yr <sup>-1</sup> ) | k <sub>2</sub><br>(yr <sup>-1</sup> ) |
| 108                              | 12.5          | 1.0                      | 0.02  | 2.64                      | 1.8                       | 0.65                                  | $1.0e^{-5}$                           |
| 585                              | 5.85          | 0.01                     | 0.02  | 2.0                       | 3.5                       | 0.2                                   | $8.0e^{-4}$                           |
| 2213                             | 3.2           | 10.0                     | 0.17  | 0.45                      | 0.5                       | 0.1                                   | $4.0e^{-4}$                           |
| 4298                             | 2.5           | 4.2                      | 0.18  | 0.83                      | 1.2                       | 0.052                                 | $1e^{-5}$                             |

| <b>Bottom water concentrations of solutes (all in nmol cm<sup>-3</sup>):</b> |                |                 |                 |                 |                  |                 |                              |            |
|--|----------------|-----------------|-----------------|-----------------|------------------|-----------------|------------------------------|------------|
| Depth  | O <sub>2</sub> | NO <sub>3</sub> | SO <sub>4</sub> | NH <sub>4</sub> | H <sub>2</sub> S | PO <sub>4</sub> | PO <sub>4</sub> <sup>a</sup> | Alkalinity |
| 108  | 210            | 9.6             | 28,000          | 0.4             | 0.0              | 0.0             | 15.0                         | 2,400      |
| 585  | 10             | 25.0            | 28,000          | 0.0             | 0.0              | 50.0            | 90.0                         | 2,480      |
| 2213   | 250            | 25.0            | 28,000          | 0.6             | 0.0              | 0.0             | 5.0                          | 2,400      |
| 4298   | 243            | 30.1            | 28,000          | 0.22            | 0.0              | 0.0             | 5.0                          | 2,400      |

organic matter (especially in the 2 – 4 cm depth interval), therefore placing the beginning of the sulfate reduction zone and the production of H<sub>2</sub>S to the deeper sediments (Reimers et al., 1996). Iron processes are currently not dynamically represented in OMEN-SED. In addition, produced dissolved Fe reacts with H<sub>2</sub>S to form iron sulfides (e.g. pyrite, FeS<sub>2</sub>) and thus further inhibits the rise 910 of H<sub>2</sub>S (Reimers et al., 1990). The iron cycle also plays a critical role for phosphorus, as the reduction of iron(III) hydroxides in the surface sediments releases sorbed phosphate, leading to pore waters around and below 2 cm which are supersaturated with respect to fluorapatite, thus initiating CFA precipitation. Reimers et al. (1996) could even show that the accumulation of CFA is mainly restricted to the near-surface sediments (~ 5 cm) instead of throughout the sediment column. As 915 OMEN-SED does not include an iron-cycle, and Fe-bound P and CFA processes are highly parameterised, the model is not able to capture these complex, non-steady state phosphorus dynamics at this specific site. For the Nazaré Canyon station (4298 m) satisfactory fits could be realised apart from NH<sub>4</sub>. However, also Epping et al. (2002) could not obtain a better fit using a more complex diagenetic model. They suggested non-local solute exchange resulting from bioirrigation being 920 responsible for the higher NH<sub>4</sub> concentrations at this site which is neglected in their model, as well as in OMEN-SED. Furthermore, the fractured POC profile (indicating episodic depositional events through the canyon) could have been approximated using a different partitioning of the bulk POC into labile and refractory pool with different degradation rate constants, thus potentially leading to a better fit of the NH<sub>4</sub> profile. In general, better approximations of the data could have potentially been 925 acquired by applying a sensitivity study using different NC-ratios (e.g. Epping et al., 2002, report

different ratios from Redfield stoichiometry) and exploring the parameter space for the secondary reaction parameters ( $\gamma_{NH_4}$ ,  $\gamma_{H_2S}$ ). However, considering these generalisations and our assumption of steady-state, which might not be valid, particularly for the complex Santa Barbara basin, the shallow core and the Nazaré Canyon, which are affected by seasonality and biology, OMEN-SED performs  
930 well in capturing the main diagenetic processes.

### 3.3 Case study: Stand-alone simulations of global ocean transect

#### 3.3.1 Methodology

In this section it is tested to which degree OMEN-SED is capable of capturing the dynamics of organic matter degradation pathways and related TEA-fluxes as simulated with a complete, numerical  
935 diagenetic model. Therefore, we reproduce the simulations of typical conditions along a global ocean hypsometry of Thullner et al. (2009) and compare our modelled TEA-fluxes with the results of the complete model as well as with observations from Middelburg et al. (1996). To explore the global degradation of OM in the seafloor Thullner et al. (2009) quantified various diagenetic processes using the Biogeochemical Reaction Network Simulator (BRNS, Aguilera et al., 2005), a flexible  
940 simulation environment suitable for reactive transport simulations of complex biogeochemical problems (e.g. Jourabchi et al., 2005; Thullner et al., 2005). Thullner et al. (2009) used seafloor depth (SFD) as the master variable and calculated model parameters, such as  $w$ ,  $D_{bio}$  and  $\phi$ , from existing empirical relationships (e.g. Van Cappellen and Wang, 1995; Middelburg et al., 1997). Organic matter degradation was described with a 1-G approach, thus assuming a single pool of organic matter  
945 of uniform reactivity. The first order rate constant was related to the burial velocity,  $w$  (cm year<sup>-1</sup>), following the empirical relationship of Boudreau (1997):

$$k = 0.38 \cdot w^{0.59}. \quad (48)$$

This rate constant can be assumed as the mean reactivity of the organic matter fractions which are degraded in the upper, bioturbated 10 – 20 cm of the sediments. Thus, more reactive fractions  
950 (degraded during days/weeks close to the SWI) and more refractory fractions (degraded on longer time scales deeper in the sediments) are not captured by this relationship (Boudreau, 1997). BRNS simulations were performed using boundary conditions and parameters for depths representative for shelf, slope and deep sea sediments (i.e. SFD of 100m, 200m, 500m, 1000m, 2000m, 3500m and 5000m). In order to reproduce these results, OMEN-SED is configured here as a 1-G model and  
955 boundary conditions and model parameters are defined as in Thullner et al. (2009, see Table 14). As OMEN-SED assumes a fixed fraction of reduced substances to be reoxidised, which exerts a large impact on the resulting SWI-fluxes (compare Section 3.1), two sets of simulations are performed in order to show the range of possible model outputs. In the first setup 95% of the reduced substances are reoxidised (i.e.  $\gamma_{NH_4} = \gamma_{H_2S} = 0.95$ ) and in the second only 5% are reoxidised (all other model  
960 parameters and boundary conditions are equal).

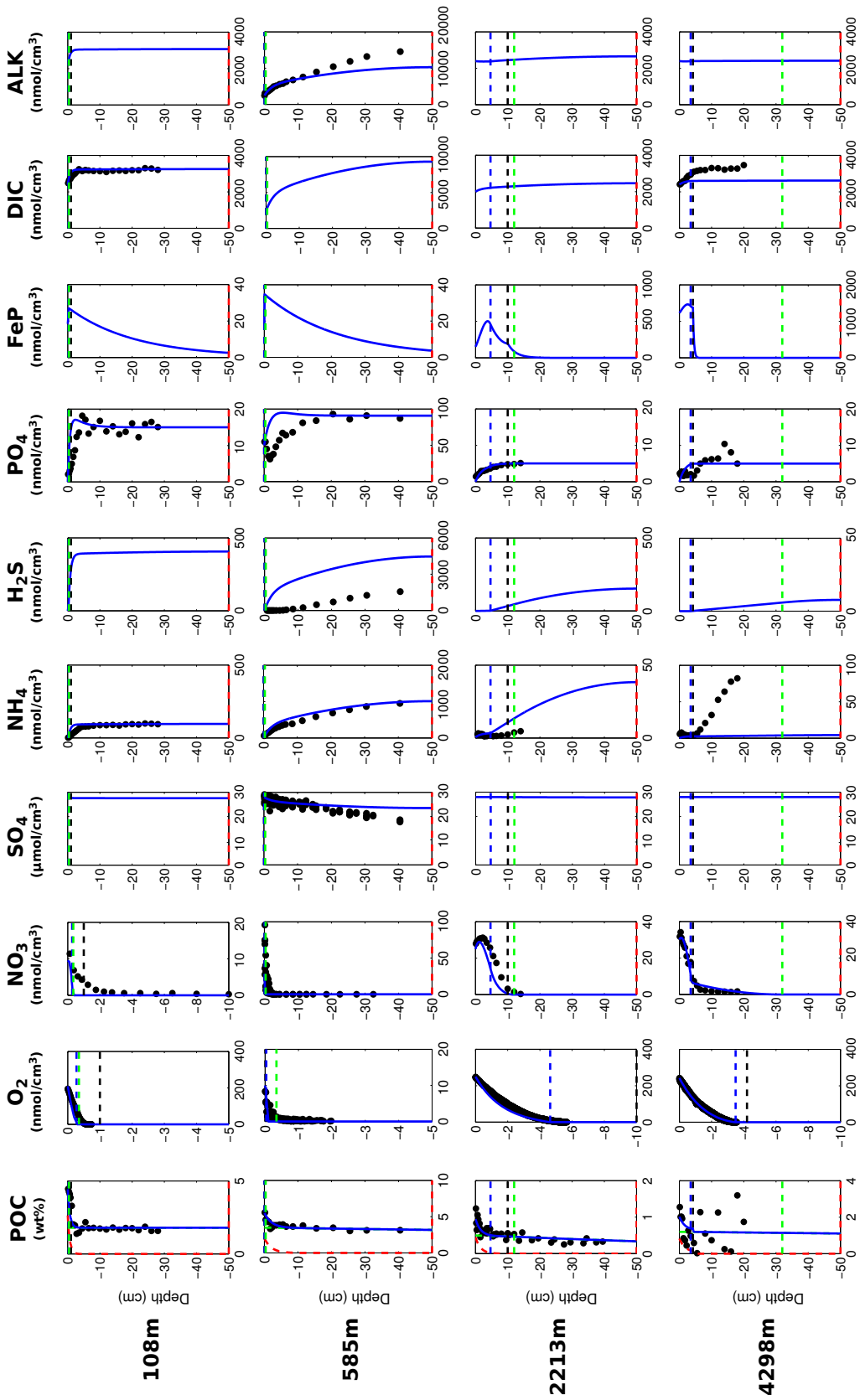


**Figure 7.** Modelled (curves) and measured (filled dots) solid phase and dissolved pore water profiles for four different sediment cores. Note that different scales are used for different stations. The blue POC curve represents the sum of the refractory (green) and labile (red) POC fraction. The horizontal dashed lines in each panel indicate the bioturbation depth (black) and the penetration depths of oxygen (blue), nitrate (green) and sulfate (red) as calculated by OMEN-SED.

**Table 14.** Seafloor depth dependency of key model parameters and boundary conditions (adapted from Thullner et al., 2009).

|  | Seafloor depth        |                       |                       |                       |                       |                       |                       |
|--|-----------------------|-----------------------|-----------------------|-----------------------|-----------------------|-----------------------|-----------------------|
|  | 100 m                 | 200 m                 | 500 m                 | 1000 m                | 2000 m                | 3500 m                | 5000 m                |
| <b>Model parameters</b>  |                       |                       |                       |                       |                       |                       |                       |
| $w^a$ (cm yr <sup>-1</sup> )   | $3.98 \times 10^{-1}$ | $3.60 \times 10^{-1}$ | $2.67 \times 10^{-1}$ | $1.62 \times 10^{-1}$ | $5.94 \times 10^{-2}$ | $1.32 \times 10^{-2}$ | $2.94 \times 10^{-3}$ |
| $D_{\text{bio}}^a$ (cm <sup>2</sup> yr <sup>-1</sup> )                     | 27.5                  | 25.1                  | 19.0                  | 12.1                  | 4.83                  | 1.23                  | 0.310                 |
| $\phi^b$   | 0.85                  | 0.85                  | 0.80                  | 0.80                  | 0.80                  | 0.80                  | 0.80                  |
| T <sup>c</sup> (°C)  | 10.3                  | 9.7                   | 8.1                   | 5.8                   | 3.0                   | 1.5                   | 1.4                   |
| $\rho_{\text{sed}}^c$ (g cm <sup>-3</sup> )                                | 2.5                   | 2.5                   | 2.5                   | 2.5                   | 2.5                   | 2.5                   | 2.5                   |
| $k^d$ (yr <sup>-1</sup> )  | 0.221                 | 0.208                 | 0.174                 | 0.130                 | 0.0718                | 0.0296                | 0.0122                |
| <b>Upper boundary conditions</b>   |                       |                       |                       |                       |                       |                       |                       |
| POC <sub>flux</sub> <sup>a</sup> (μmol cm <sup>-2</sup> yr <sup>-1</sup> ) | 510                   | 467                   | 357                   | 228                   | 93.0                  | 24.3                  | 6.33                  |
| POC <sup>e</sup> (wt%)   | 0.79                  | 0.78                  | 0.55                  | 0.50                  | 0.42                  | 0.32                  | 0.25                  |
| O <sub>2,0</sub> <sup>c</sup> (nmol cm <sup>-3</sup> )                     | 132                   | 129                   | 121                   | 114                   | 116                   | 135                   | 141                   |
| NO <sub>3,0</sub> <sup>c</sup> (nmol cm <sup>-3</sup> )                    | 17.3                  | 18.6                  | 22.1                  | 26.5                  | 31.0                  | 31.6                  | 31.6                  |
| SO <sub>4,0</sub> <sup>b</sup> (nmol cm <sup>-3</sup> )                    | 28,000                | 28,000                | 28,000                | 28,000                | 28,000                | 28,000                | 28,000                |

<sup>a</sup> Derived from Middelburg et al. (1997).

<sup>b</sup> Derived from Van Cappellen and Wang (1995).

<sup>c</sup> Derived from Conkright et al. (2002).

<sup>d</sup> Derived from Boudreau (1997).

<sup>e</sup> Calculated with OMEN-SED from POC<sub>flux</sub>.

### 3.3.2 Results

Figure 8 compares simulated SWI-fluxes of TEAs (i.e. O<sub>2</sub>, NO<sub>3</sub> and SO<sub>4</sub>) along the global hypsometry using OMEN-SED (black lines) with the results of Thullner et al. (2009) (red lines). Observations for O<sub>2</sub> and NO<sub>3</sub> fluxes are taken from Middelburg et al. (1996). Due to the applied empirical

965 relations organic matter flux to the seafloor decreases by 2 orders of magnitude from 100 to 5000 m and its degradation rate constant by 1 order of magnitude (Table 14). Therefore, the rate of organic matter degradation is about 50 times greater at 100 m than at 5000 m (compare Thullner et al., 2009), thus resulting in a decrease of TEA-fluxes along the hypsometry (Figure 8). The 95%-reoxidation ex-

periments (dots) show proportionally higher O<sub>2</sub> in-fluxes than the 5%-reoxidation experiments 970 (triangles) because more O<sub>2</sub> is utilised for in situ production of NO<sub>3</sub> and SO<sub>4</sub> in the sediments. This is also mirrored by the increased NO<sub>3</sub> out-flux and decreased SO<sub>4</sub> in-flux for shallower SFDs.

This is in line with the results of Thullner et al. (2009) which showed that in situ production is an important pathway of SO<sub>4</sub> supply in the sediment, which is responsible for ~80% of the total OM degradation at depths between 100 and 2000 m (SO<sub>4</sub> is not used for OM degradation in OMEN-SED 975 below 2000m). In general, Figure 8 shows that OMEN-SED captures the main trends in observed

TEA fluxes well and fluxes calculated with BRNS fall within the range of possible OMEN-SED results.

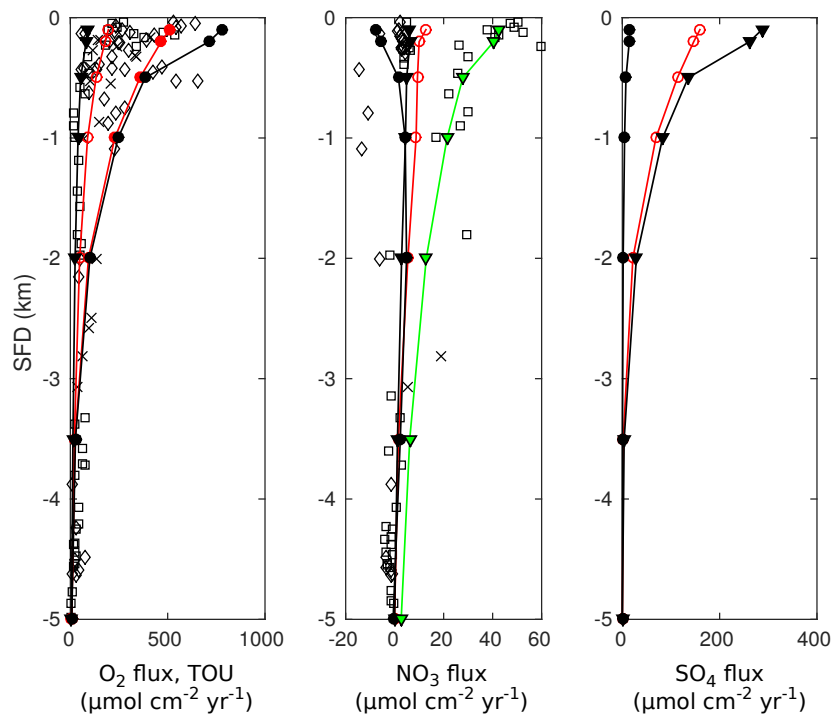


**Figure 8.** Fluxes of  $O_2$ ,  $NO_3$  and  $SO_4$  to the sediment along the global hypsometry. Red lines (with open symbols) are modelled fluxes from Thullner et al. (2009) using BRNS; black lines are results from OMEN-SED ( $\bullet$ :  $\gamma_{NH_4} = \gamma_{H_2S} = 0.95$ ;  $\blacktriangledown$ :  $\gamma_{NH_4} = \gamma_{H_2S} = 0.05$ ). Observations of TEA fluxes are taken from Middelburg et al. (1996) ( $\diamond$ : Atlantic,  $\square$ : Pacific,  $\times$ : Arctic/Indian Ocean). Also plotted in Figure (A) are the total oxygen uptake (TOU) estimates of Thullner et al. (2009) (filled red symbols). The green line indicates OMEN-SED results for low oxygen/high nitrate levels and the lower NC-ratio. Negative values are directed out of the sediments.

In particular, the observed  $O_2$  fluxes in the upper 2000m are well predicted by the two OMEN-SED simulations. Oxygen fluxes for the deep-sea sediments, however, are slightly underestimated.

980 These deviations can presumably be related to the assumed 1-G description of organic matter degradation, which neglects the more labile OM pool. This highly reactive pool is degraded close to the sediment surface, thus promoting higher aerobic degradation rates and higher  $O_2$  fluxes. Nitrate fluxes in the upper 500m of the Atlantic Ocean are well predicted. However, as in Middelburg et al. (1996) the direction of calculated nitrate fluxes in the upper 1000m of the Pacific Ocean differ from 985 the observations. Middelburg et al. (1996) related these discrepancies to the globally averaged model parameters and the applied boundary conditions. They could reduce the disagreements significantly by using more representative bottom water concentrations for the eastern Pacific and a higher flux of

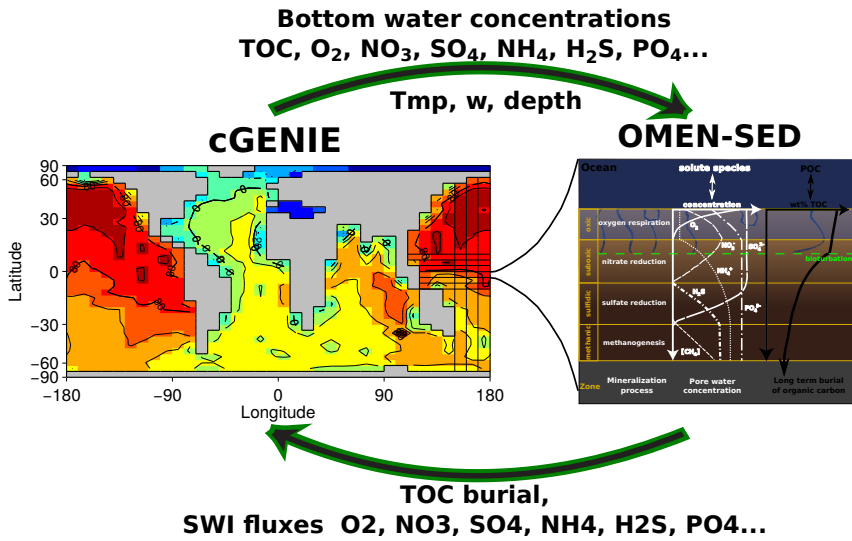


**Figure 9.** Schematic of the relationship between OMEN-SED and cGENIE. Arrows represent the information transferred between models.

labile organic matter for their 2-G model. By changing the boundary conditions and the NC-atomic ratio of organic matter for the whole hypsometry, it is possible to obtain a better model-data fit with  
 990 OMEN-SED for the shallow Pacific Ocean (green line in Fig. 8B). Bohlen et al. (2012) report that the atomic NC-ratio strongly deviates from Redfield stoichiometry (0.151) with specifically lower values for the East Pacific Ocean. The use of their globally averaged value of 0.067 allows reconciling modelled and observed values provided that bottom water conditions are also changed to the low oxygen/high nitrate levels more likely to be found in the shallow Pacific Ocean ( $O_2 = 10 \text{ nmol cm}^{-3}$  and  $NO_3 = 80 \text{ nmol cm}^{-3}$ ).  
 995

#### 4 Coupled pre-industrial Earth system model simulations

##### 4.1 Coupling to the cGENIE Earth system model

OMEN-SED is coupled to the carbon-centric version of the “GENIE” Earth system model (cGENIE, Ridgwell et al., 2007) to illustrate the abilities of the newly developed model. The following section  
 1000 provides a brief description of cGENIE and the coupling procedure (Fig. 9). cGENIE is a model of Intermediate Complexity based on the efficient climate model “C-GOLDSTEIN” of Edwards and Marsh (2005), featuring a frictional-geostrophic 3D-ocean circulation model coupled to a fast Energy-Moisture Balance 2D-atmosphere together with a dynamic-thermodynamic sea-ice component. The version of cGENIE used here includes the marine geochemical cycling of carbon, oxygen,  
 1005 phosphorus and sulfur (Ridgwell et al., 2007), preservation of carbonates in deep-sea sediments (SEDGEM, Ridgwell and Hargreaves, 2007) and terrestrial weathering (Colbourn et al., 2013). The

ocean model is implemented on a  $36 \times 36$  equal-area horizontal grid with 16 vertical levels using the pre-industrial continental configuration and bathymetry as in Archer et al. (2009). A finer grid ( $72 \times 72$ ) is used for the sediments (see Fig. 11C) and OMEN-SED is called by SEDGEM for each  
 1010 wet ocean grid point. Depending on the overlying biogeochemical ocean model, processes can be included or excluded in OMEN-SED and stoichiometric factors need to be adjusted to ensure preservation of mass. As nitrogen is not modelled explicitly in the employed cGENIE configuration,  $NC_i$ ,  $ALK^{NIT}$  and  $ALK^{DEN}$  in OMEN-SED are set to zero. cGENIE, however, implicitly includes the effects of  $NH_4$  release and its complete nitrification on alkalinity but neglects the impact of P release.  
 1015 Therefore, alkalinity stoichiometries for aerobic degradation and sulfate reduction are changed to  $ALK^{OX} = -16/106$  and  $ALK^{SUL} = 122/106$ , respectively (compare to default in Table 10).

Several biogeochemical tracers and parameters are transferred from SEDGEM to OMEN-SED and have to be converted into the required units. Bottom water concentrations of solutes are converted from  $mol\ kg^{-1}$  to  $mol\ cm^{-3}$  and the depositional flux of POC ( $POC_{flux}$ ) is converted from  
 1020  $cm^3\ cm^{-2}\ yr^{-1}$  to  $mol\ cm^{-2}\ yr^{-1}$  assuming an average density of POC of  $1.0\ cm^3\ g^{-1}$ . Within the water column in cGENIE, POC is partitioned into two fractions with different degradation length scales. The labile pool degrades while sinking through the water column, whereas the refractory pool is unreactive (Ridgwell et al., 2007). Thus, depending on seafloor depth, the partitioning of bulk POC reaching the sediments is different (Fig. 10A+B). This information is used by OMEN-  
 1025 SED to define the parameters  $f_1$  and  $f_2$ . Other parameters used from cGENIE are seafloor depth and local temperature. The advection/burial rate ( $w$ ) is generally taken from cGENIE from the previous time-step, however, it is assured that  $w$  is not smaller than the detrital flux ( $Det_{flux}$ ) to the sediments (e.g.  $w < 0$  can occur if the sediments are being eroded during the spin-up of cGENIE). In case  $w \leq Det_{flux} = 0.0$  all POC is remineralised at the ocean floor. Furthermore, a minimum value  
 1030 of  $w = 0.4\ cm\ kyr^{-1}$  is imposed as OMEN-SED tends to be unstable for lower values. The bulk POC<sub>flux</sub> is separated into the labile and refractory component and the routine to find the steady-state solution for POC is called. Here, the two POC depositional fluxes are first converted into SWI concentrations ( $POC_i(z=0)$ , in  $mol\ cm^{-3}$ ) by solving the flux divergence equation:

$$\frac{\partial F}{\partial z} = -\frac{\partial}{\partial z} \left( -\xi D_i \frac{\partial POC_i}{\partial z} + \xi w POC_i \right) \quad (49)$$

1035 for  $z=0$ . OMEN-SED then computes the fraction of POC preserved in the sediment ( $f_{POC}$ , see Eq. (5)) and subsequently calls the routines to find the steady-state solutions for the solute substances. Note, that the calculated benthic uptake/return fluxes  $F_{C_i}$  of dissolved species  $C_i$  (compare Eq. (6)) have to be adjusted for the advective loss at the lower sediment boundary ( $w \cdot C_i(z_\infty)$ ) to assure the preservations of mass in the coupled model:  
 1040

$$F_{C_i} = \phi(0) \left( D_i \frac{\partial C_i(z)}{\partial z} \Big|_{z=0} - w [C_i(0) - C_i(z_\infty)] \right). \quad (50)$$

In case OMEN-SED computes unrealistic results for POC preservation (i.e.  $f_{POC} < 0.0$  or  $f_{POC} > 1.0$ ) we discard the results of OMEN-SED and all POC is remineralised at the ocean floor. Finally,

$f_{POC}$  and the SWI-fluxes of solutes ( $F_{Ci}$ , in  $\text{mol cm}^{-2} \text{yr}^{-1}$ ) are returned to cGENIE. In case no POC is deposited on the seafloor (i.e.  $POC_{flux} = 0$ ), OMEN-SED is not executed and  $f_{POC}$  and  $F_{Ci}$  for all  $i$  are set to zero. In order to reduce memory requirements the sediment profiles (e.g. as shown in Fig. 7) are not calculated in the FORTRAN version of OMEN-SED, however, the boundary conditions are saved at the end of the experiment and sediment profiles for specific grid-cells, ocean basins and ocean transects can be plotted using the stand-alone MATLAB version of OMEN-SED.

## 4.2 Parameterising the OM degradation rate constants in a global model

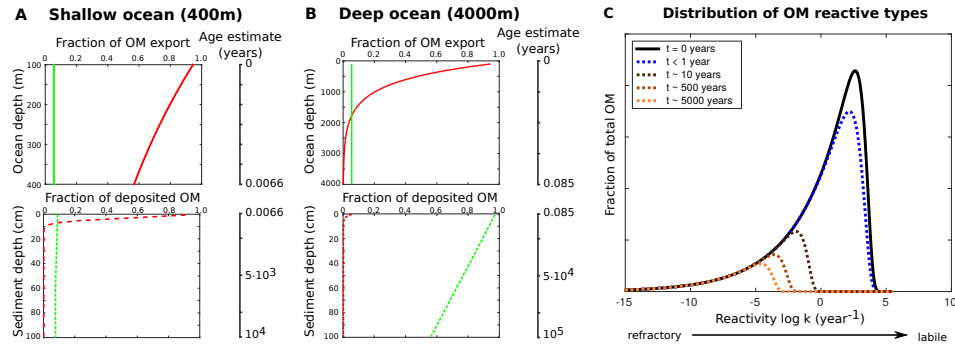


**Figure 10.** Idealised relationship of organic matter decomposition during remineralisation in the water column and the sediments. **A+B - Upper panels:** Water column development of the two organic matter fractions as represented in cGENIE for two ocean depths (red: labile OM with degradation length scale of 589m; green: refractory OM which is unreactive in the water column). The values are normalised to OM export at 100m. Age estimates for the OM since its export from the euphotic zone are calculated using a sinking velocity of 125m/day. **A+B - Lower panels:** Schematic representation of the development of the two OM fractions in the sediments (normalised to OM deposited on the seafloor). For the age estimates in the sediment column an advection rate of 0.01 and 0.001cm/yr is assumed, respectively. **C:** Idealised distribution functions of OM reactive types during remineralisation for different OM ages assuming a reactive continuum model for OM degradation. The initial distribution (at  $t = 0$ ) represents fresh OM when it is exported from the euphotic zone (characterised by  $a = 3e^{-4} \text{ yr}^{-1}$  and  $\nu = 0.125$  Boudreau et al., 2008).

As shown in our sensitivity analysis (Section 3.1) and discussed by Arndt et al. (2013) the degradation rate constants for OM ( $k_i$ ) are the most influential parameters and strongly determine the SWI-flux of redox-sensitive elements as well as the preservation of organic matter. Yet, their spatial variability is unknown at the global scale and reported rate constants in the sediments can vary by about 10 orders of magnitude or more (Middelburg et al., 1993; Arndt et al., 2013). Furthermore, when OMEN-SED is coupled to cGENIE very different timescales have to be considered for OM degradation in the sediments compared to the water column (Fig. 10A+B), thus rate constants cannot be easily adapted from cGENIE. Also, microbes tend to degrade the more reactive organic matter

compounds first (Emerson and Hedges, 1988; Wakeham et al., 1997; Lee et al., 2000), thus depending on the age of OM (or depth in the sediment and water column) the reactivity distribution of its compounds changes significantly (Fig. 10). For instance, in the water column, represented by the reactivity distribution  $t < 1$  year in Fig. 10C, only the most reactive OM compounds are remineralised. This explains why the POC flux in the ocean can be represented with a 1G or pseudo 2G degradation model. In the sediments much longer timescales have to be considered, thus also more reactive compounds are degraded and the reactivity distribution changes significantly already in the upper mm of the sediments ( $t \sim 10$  years, Fig. 10C). Therefore, a broader range of OM reactive types must be represented by the degradation model to capture the reactivity spectrum of OM in surface sediments, explaining why at least a pseudo 3G model is required (including two degradable and one refractory fraction Soetaert et al., 1996; Boudreau, 1997; Stolpovsky et al., 2015). In addition, the advection rate in the sediments determines the age of OM at a specific sediment depth and thus its reactivity. For instance, assuming an advection rate of 0.01 cm/yr for the shallow ocean, OM at 5cm depth is about 500 years old, whereas it is one order of magnitude older for an advection rate of 0.001 cm/year in the deep ocean and thus covers a broader range of reactive types (Fig. 10C).

Thus defining appropriate OM degradation rate constants is a major challenge and source of uncertainty for diagenetic models. The rate constants in models are either determined through profile fitting for a specific site or, for global applications, they are related to a single, readily available characteristic (or master variable) of the local environmental conditions. For instance, considerable effort has been expended to relate the apparent rate constant for oxic and anoxic OM degradation to sedimentation rate ( $w$ ) and various empirical relations have been proposed (Toth and Lerman, 1977; Tromp et al., 1995; Boudreau, 1997; Stolpovsky et al., 2015). Nevertheless, these relationships are generally based on limited data sets and their global applicability is questionable (Arndt et al., 2013).

#### 4.2.1 Methodology

Our objective is not to perform and discuss a detailed calibration of the two models, as this is beyond the scope of this sediment model development paper. We rather want to showcase, that a coupling is possible and that the results show main sediment features one would expect to see on a global scale. Section 4.2.2 compares modelled mean POC weight percentages (wt%) in the upper 5cm of the sediments ( $\text{POC}_{5\text{cm}}$ ) to the global distribution pattern of POC content in surface sediments (< 5cm sediment depth) of Seiter et al. (2004) using different parameterisations for the degradation rate constants  $k_1$  and  $k_2$ . To this end, the original POC distribution pattern in  $1^\circ \times 1^\circ$  grid resolution (interpolated from  $> 5500$  measurements, compare Seiter et al., 2004) has been transformed onto the  $72 \times 72$  SEDGEM grid (Figure 11). The regridding of the original POC distribution obviously affects the resolution of the data, especially for the continental margin, as some sites with higher POC wt% are lost due to the restricted SEDGEM grid-resolution (compare e.g. maximum values for the East Pacific and upwelling waters of the Namibian shelf, Figure 11A + B). The colour of the points in

Figures 12 - 14, which compare modelled and observed POC concentrations, represents SFD of the  
 1095 respective cGENIE grid-cell. As the individual data-points are highly scattered and in order to see if a certain relation between  $k_1$  and  $k_2$  performs better for specific ocean depths, the data-points are binned into 6 uniform depth-classes of 1000m each (respective mean POC wt% and SFD are represented by the triangles). The regression line (and the corresponding  $R^2$ -value) is calculated for the 6 bin-classes and included in the figures.

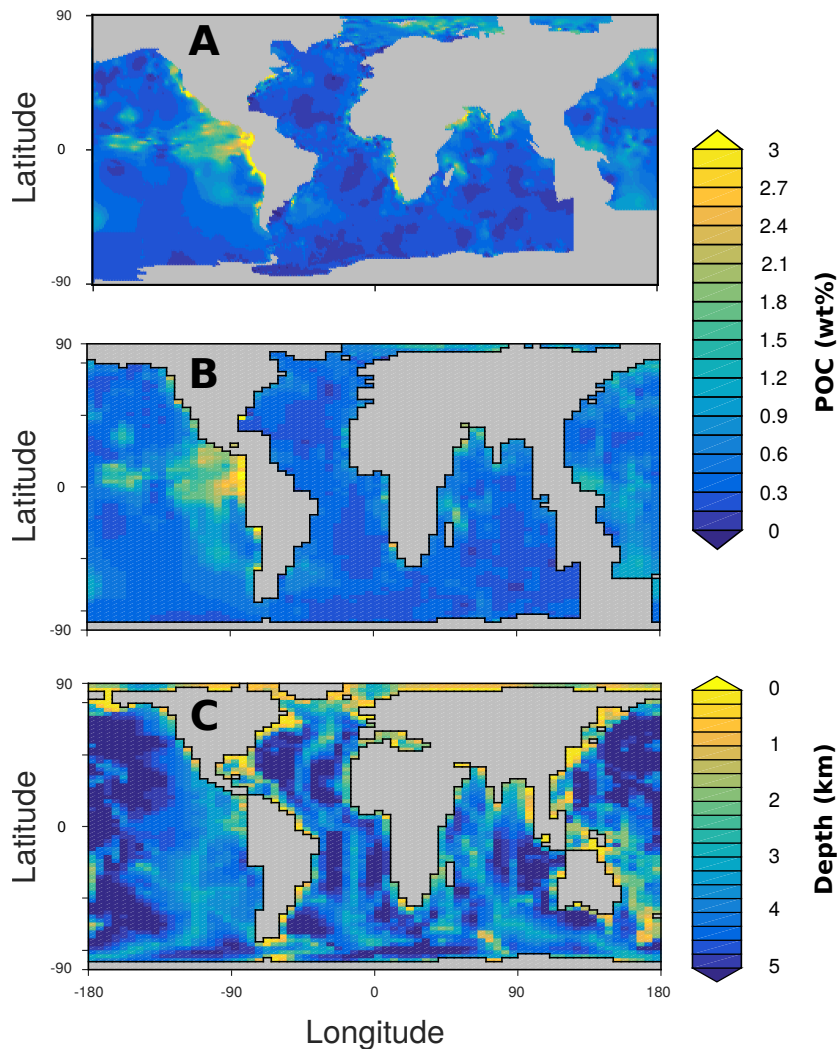


**Figure 11.** Observed distribution of sediment surface (< 5cm) POC wt% (A, B) and cGENIE bathymetry (C).  
 (A) Original global distribution of POC wt% interpolated on a  $1^\circ \times 1^\circ$  grid from more than 5500 individual data points (compare Seiter et al., 2004, for the interpolation procedure). (B) Observed POC wt% data transformed onto the  $72 \times 72$  SEDGEM grid. Grid points without any observations are left blank (grey). (C) Gridded continental configuration and ocean bathymetry of the 16-level,  $72 \times 72$  equal-area cGENIE grid.

1100 TODO Andy: Section describing the prescribed fields of solids (i.e. detrital, opal,  $\text{CaCO}_3$ ) to the sediments!

To parameterise the reactivity of organic matter in OMEN-SED two different approaches are compared. First, globally invariant degradation rate constants  $k_1$  and  $k_2$  are assumed. By providing two pools of POC from the water-column characterised by different degradation rate constants, cGENIE 1105 accounts for the decrease in mean POC reactivity with water-depth. The rate constants for the more refractory OM pool,  $k_2$ , is systematically varied between 0.004 and 0.006 year<sup>-1</sup> and the more labile OM component, described by  $k_1$ , is assumed to degrade  $x \in \{1.1, 1.2, 1.3, 1.5, 2\}$  times faster, respectively. However, although accounting for the decrease in mean POC reactivity with seafloor depth, this approach does not take into account the change in organic matter reactivity types caused 1110 by different burial velocities and thus time scales in the sediments (Fig. 10). Therefore, the second approach uses the empirical relationship proposed by Boudreau (1997), which relates the apparent OM degradation rate constant in the upper sediments to the burial velocity,  $w$  (cm year<sup>-1</sup>, see also Section 3.3):

$$k_{\text{app}} = 0.38 \cdot w^{0.59}. \quad (51)$$

1115 Following Boudreau (1997) and Stolpovsky et al. (2015) it can be assumed that  $k_{\text{app}}$  represents the mean OM reactivity within the upper 10-20cm of the sediments. The following assumptions are made in order to calculate the two degradation rate constants for OMEN-SED:

$$k_{\text{app}} = f_1 \cdot k_1 + f_2 \cdot k_2 \quad (52)$$

$$1120 k_1 = x \cdot k_2 \quad (53)$$

where  $x$  describes the relation between  $k_1$  and  $k_2$  and is subject to sensitivity experiments (with values of  $x \in \{2, 5, 8, 10, 12, 15, 20, 25\}$ ). Note that the differences between  $k_1$  and  $k_2$  using this approach is significantly larger as in the invariant approach. As the fractions of labile and refractory OM reaching the sediments ( $f_1, f_2$ ) is known from cGENIE,  $k_1$  and  $k_2$  can be calculated independently for each grid-cell. All simulations presented here are run for 10,000 years to steady-state from 1125 a 20,000 year cGENIE spin-up without OMEN-SED. The new model OMEN-SED is called for each grid-cell in every time step, feeding back the resulting SWI-fluxes and the fraction of POC preserved in the sediments to cGENIE.

#### 4.2.2 Results

1130 Figure 12 presents results for the globally invariant degradation rate experiments. In general, using globally invariant degradation rate constants 5 of the 6 bin-classes are located closer to the 1:1 line as in the experiments using the Boudreau (1997) relation (Fig. 13). Also the slope of some regression lines is close to 1.0 (e.g.  $(k_2, x) \in \{(0.004, 1.5), (0.0045, 1.3), (0.005, 1.2), (0.005, 1.3), (0.0055, 1.1), (0.0055, 1.2), (0.006, 1.1)\}$ ), indicating that the simpler parameterisation adequately captures the relationship between

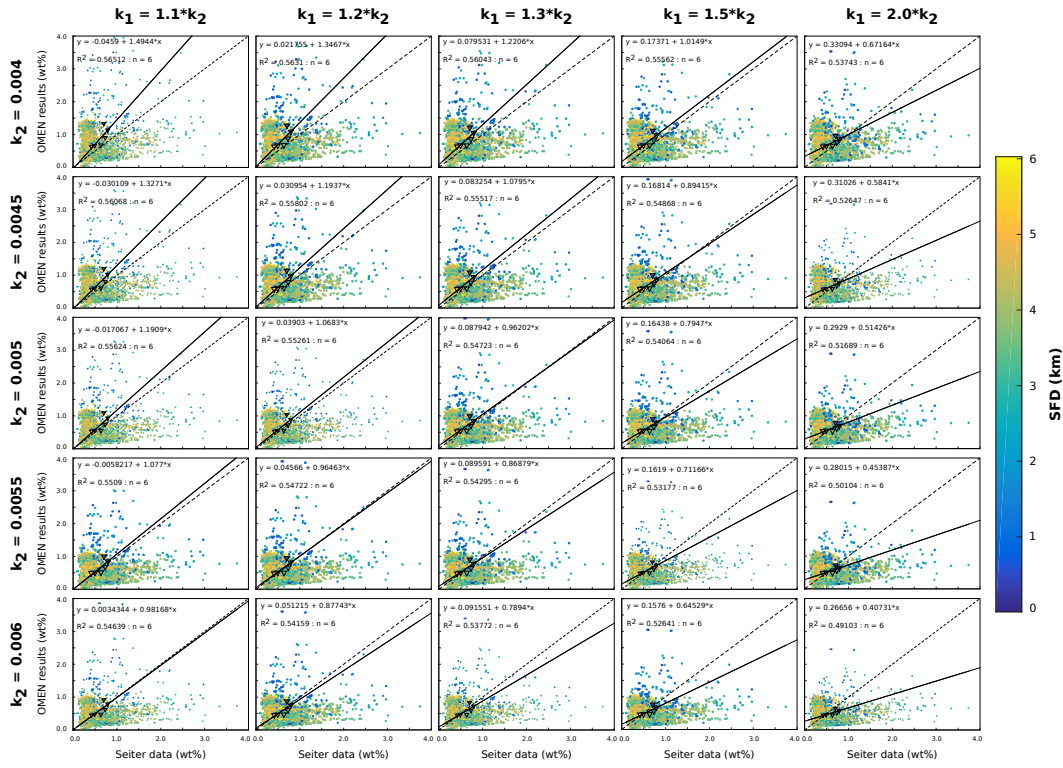


**Figure 12.** Crossplots comparing modelled and observed mean POC wt% in the upper 5 cm of the sediments using globally invariant degradation rate constants  $k_1$  and  $k_2$ . Data-points are binned into 6 uniform depth-classes of 1000m as in Fig. 13, each class is represented by a triangle. Grid-points with more than 4.0 POC wt% are not shown.

1135 depth and observed POC wt% by bin-class. The shallowest bin-class (between 0 and 1000m) represents an exception, as OMEN-SED tends to overestimate POC preservation for this depth class. However, this could also be related to the regridding of the original POC distribution pattern of (Seiter et al., 2004) on to the SEDGEM grid, as some data grid-cells with higher POC wt% on the continental margin are lost due to the restricted SEDGEM resolution (compare Section 4.2). Overall, 1140 using this parameterisation a relationship where the labile POC fraction degrades not more than 1.5 times faster than the refractory fraction fits the Seiter et al. (2004) data better than a larger spread between both POC pools (i.e.  $x > 2.0$ ).

Next the relationship of Boudreau (1997) and the assumptions of Eq. (52) and (53) are used to calculate  $k_1$  and  $k_2$ . In Figure 13 (A-H) the relation between the two degradation rate constants 1145 (Eq. (53)) is changed globally, thus independent of the seafloor depth. The crossplots show that it is not possible to achieve a solution where all bin-classes fall onto, or close to, the 1:1 line. Also, the slope of the regression lines are generally much larger or smaller than 1.0 (with the exception of Figure 13C), indicating that the relationship between depth and observed POC wt% by bin-class

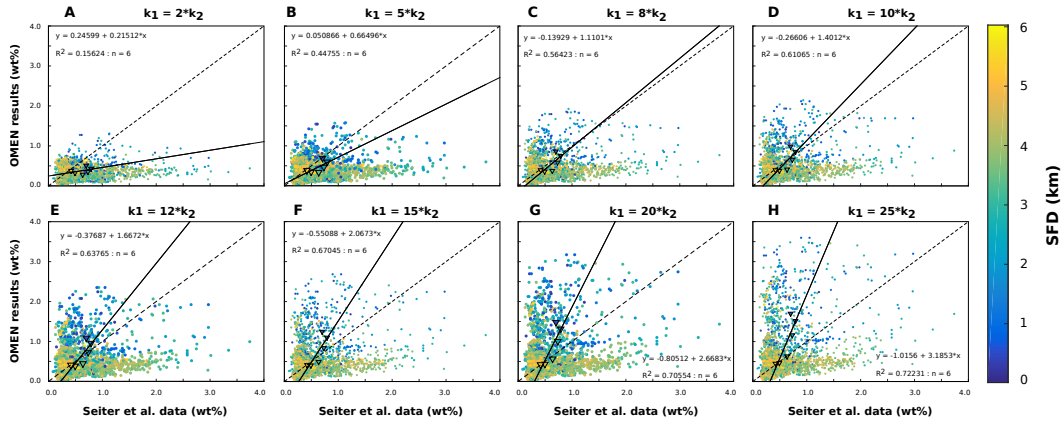


**Figure 13.** Crossplots comparing modelled and observed mean POC wt% in the upper 5 cm of the sediments using the relationship of Boudreau (1997) and the assumptions of Eq. (52) and (53) to calculate  $k_1$  and  $k_2$ . Data-points are binned into 6 uniform depth-classes of 1000m, each class is represented by a triangle. Grid-points with more than 4.0 POC wt% are not shown.

is not adequately represented by the model. The  $R^2$  values are strictly monotonically increasing for  
1150 increasing  $x$  because a depth-dependency is artificially imposed for the modelled POC wt% through  
the relation between  $k_1$  and  $k_2$ . When looking at the individual bin-classes it can be seen that shallow  
ocean depths are better represented by smaller differences between  $k_1$  and  $k_2$  (e.g.  $k_1 = 5 \cdot k_2$  for SFD  
< 1000m, Figure 13B), and the deep ocean by a larger spread (e.g.  $k_1 = 25 \cdot k_2$  for SFD > 3000m,  
Figure 13H). These results reflect the preferential degradation of more reactive organic matter types  
1155 (Wakeham et al., 1997; Lee et al., 2000) and thus the change in the distribution functions of OM  
reactive types for different OM ages (Fig. 10C). In the shallow ocean bulk POC consists of fresher  
organic matter types and is therefore generally more reactive (i.e. higher  $k_{app}$  due to higher  $w$  in the  
model) as in the deep ocean. In addition, OM at 5cm sediment depth in the deep ocean is generally  
older as in the shallow ocean due to lower burial rates, therefore more reactive types are affected by  
1160 degradation and a larger spread between  $k$ -values is needed to capture these dynamics (compare Fig.  
10C).

We use these observations to create a depth dependent relationship between the two degradation  
rate constants, where  $x$  in Eq. (53) is a function of SFD and takes values of  $x = 5$  for SFD < 1000m,  
 $x = 8$  for  $1000m \leq SFD < 2000m$ ,  $x = 12$  for  $2000m \leq SFD < 3000m$  and  $x = 25$  for  $SFD \geq$   
1165 3000m for the 6 SFD bin-classes, respectively. In this depth dependent approach all bin-classes are  
close to the 1:1 line and the resulting regression model accounts for 92.6% of the variance of the  
modeled POC wt% around the observed mean of the bin-classes (Figure 14A). Furthermore, the  
slope of the regression line (0.9662) indicates that the relationship between depth and observed POC  
wt% for the bin-classes is well represented by the model. The histograms (Fig. 14C+D) visualize  
1170 the difference between modelled and observed mean POC concentrations and demonstrate the high

density of data points close to the 1:1 line. For the depth dependent approach, 92.5% of the cGENIE grid-cells show a difference between modelled and observed POC concentration of less than 1.0 POC wt%; in 79.9% of the grid-cells, the difference is less than 0.5 POC wt% (for the invariant approach the percentages are 95.37% and 70.95%, respectively). Both experiments reproduce minimal POC concentrations in the subtropical gyres and generally higher concentrations along the continental margins (Fig. 14E+F). Both experiments, however, underestimate mean POC wt% in the surface sediments of the equatorial east Pacific and overestimate POC concentrations in the North Pacific and Southern Oceans (Fig. 14G+H). The depth dependent approach of Boudreau (1997) shows more spatial variability in POC preservation than the other parameterisation. In general, implementing lower, anaerobic degradation rate constants when bottom water oxygen concentrations fall below a threshold value could potentially improve the simulation of higher POC concentrations in areas with high POC input to the sediments (Palastanga et al., 2011).

#### 4.3 Modelled fluxes and sediment characteristics

For the globally invariant experiment A ( $(k_2, x) = (0.005, 1.3)$ ) modelled SWI-fluxes and sediment characteristics are shown in Figure 15. Modelled total POC degradation ( $\text{POC}_{\text{degr}}$ ) rates in the upper sediments decrease from the shelves to the deep sea by up to 2 orders of magnitude (Fig. 15B). This is in agreement with data from the literature (e.g. Middelburg et al., 1993, 1997) and other model results (e.g. Thullner et al., 2009) which indicate that the highest degradation rates in marine sediments are found in the coastal ocean ( $\text{SFD} < 200\text{m}$ ). Oxygen fluxes into the sediments (Fig. 15C) range from 0.0 for the deep ocean and sites without OM deposition to values of about  $300 \mu\text{mol cm}^{-2}\text{yr}^{-1}$  for the shallow ocean with the highest POC degradation rates. Influx of  $\text{SO}_4$  into the sediments is rather low (between 0.0 and  $23.9 \mu\text{mol cm}^{-2}\text{yr}^{-1}$ ) because in OMEN-SED 95% of produced  $\text{H}_2\text{S}$  is reoxidised to  $\text{SO}_4$ , therefore sulfate reduction is mainly driven by in situ sulfide oxidation. However, in general the coupled model fluxes fall well within the ranges predicted by the stand-alone global hypsometry experiments ( $\text{O}_2$  between 0.0 and  $800 \mu\text{mol cm}^{-2}\text{yr}^{-1}$  and  $\text{SO}_4$  between 0.0 and about  $300 \mu\text{mol cm}^{-2}\text{yr}^{-1}$ , compare Section 3.3). In accordance with the total POC degradation rates the release of  $\text{PO}_4$  shows a maximum value of  $8.12 \text{ nmol cm}^{-2}\text{yr}^{-1}$  on the shelves (Fig. 15D). The relative contribution of aerobic POC degradation in the upper sediments increases from the shelves to the deep sea (Fig. 15G) which is also consistent with estimates from Thullner et al. (2009) who found that oxygen is responsible for less than 10% of  $\text{POC}_{\text{degr}}$  at 100m SFD and for more than 80% in the deep sea. The oxygen penetration depth in OMEN-SED increases from below 1cm at the shelves to more than 10cm in the deep ocean (Fig. 15H). Small oxygen penetration depths of a few millimetres are typical for bioturbated sediments in the coastal ocean (e.g. Wenzhöfer and Glud, 2002) and the oxygen penetration depth has been shown to increase exponentially with SFD to more than 10cm in the deep sea (Meile and Cappellen, 2003; Glud, 2008).

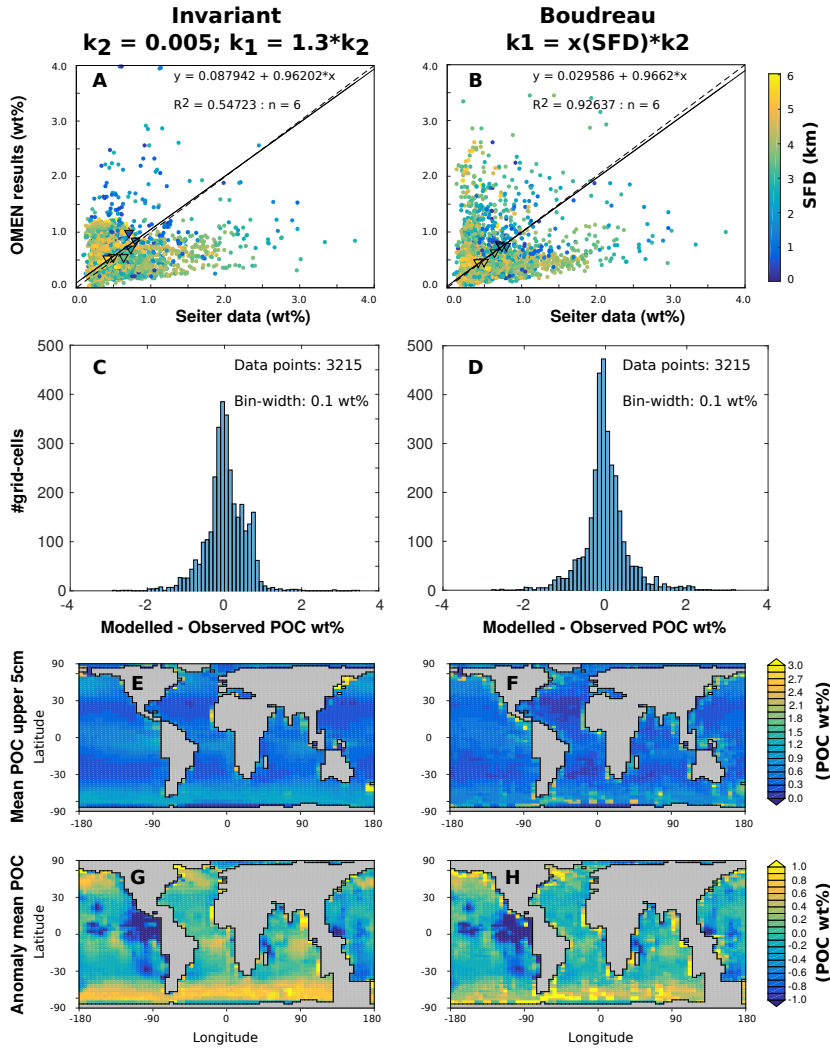


**Figure 14.** Mean POC concentrations in the upper 5cm of the sediments ( $\text{POC}_{5\text{cm}}$ ) using the invariant model ( $k_2 = 0.005$ ,  $k_1 = 1.3 \cdot k_2$ ) and the depth dependent parameterisation  $k_1 = x(\text{SFD}) \cdot k_2$  adapted from Boudreau (1997). A+B: Crossplots as shown before in Fig. 12 and 13. C+D: Histograms of the residuals of modelled minus observed  $\text{POC}_{5\text{cm}}$ . E+F:  $\text{POC}_{5\text{cm}}$  as calculated with OMEN-SED. G+H: Difference map of  $\text{POC}_{5\text{cm}}$  as calculated with OMEN-SED and interpolated data from Seiter et al. (2004).

$$\text{Boudreau } k_1 = x(\text{SFD}) \cdot k_2$$

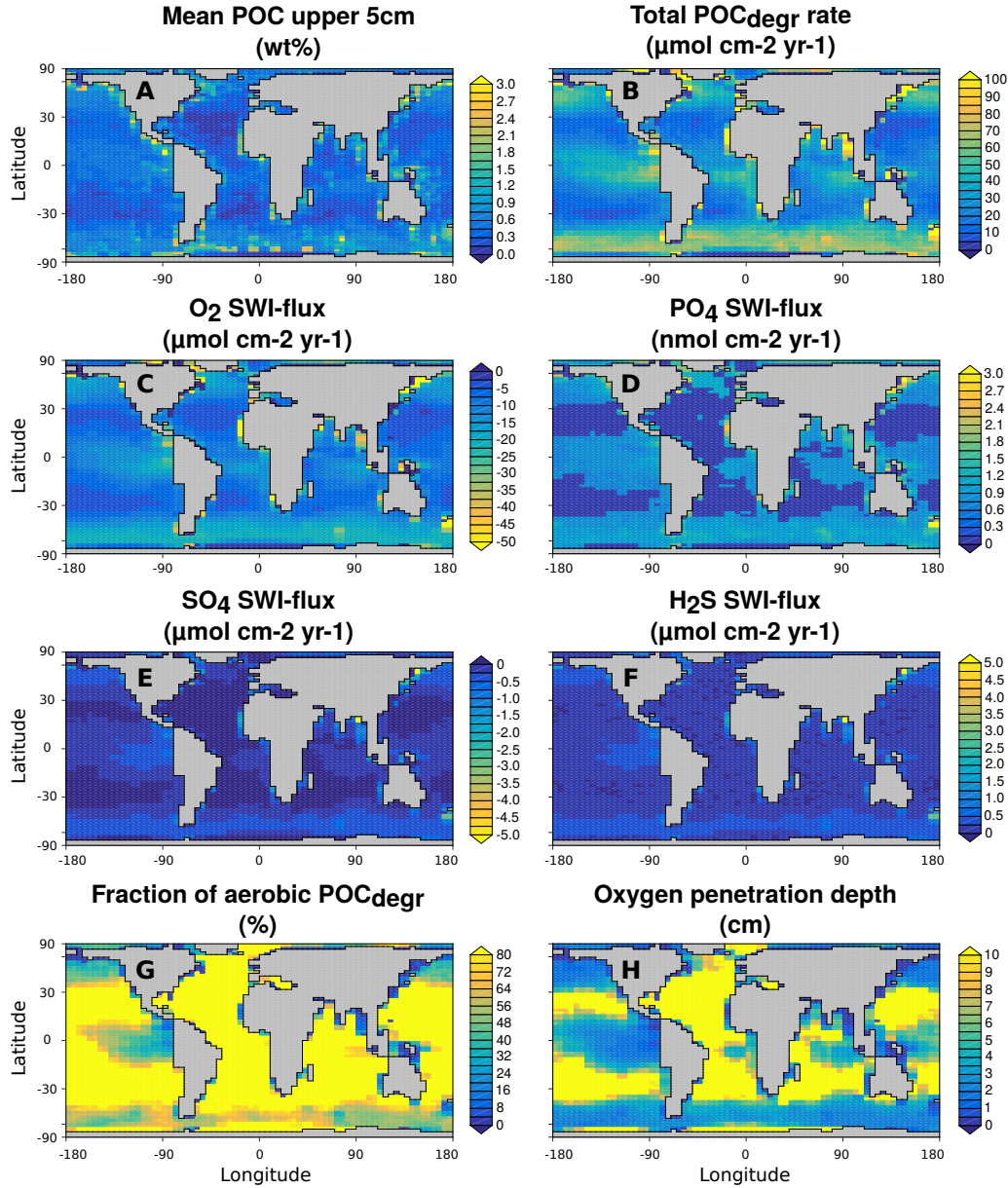


**Figure 15.** Sediment characteristics related to POC degradation and oxygen consumption for the depth dependent parameterisation after Boudreau (1997) with  $k_1 = x(\text{SFD}) \cdot k_2$ . Total POC<sub>degr</sub> rate and fraction of aerobic POC<sub>degr</sub> are the respective values for the first 5cm in the sediments.

## 5 Scope of applicability and model limitations

**Dominik: Needs polishing!?** This is my first draft State-of-the art numerical models representing the full complexity of the diagenetic processes typically perform adequately at reproducing site-specific biogeochemical dynamics, however, tuning model parameters is laborious, the computational demand is high and, thus, their transferability to the global scale is limited. On the other hand, analytical models are very efficient, but existing approaches coupled to global models generally use highly simplified reaction networks, often restricted to oxic degradation with a limited number of explicit pore water tracers. However, our ability to assess the role of organic matter dynamics for global biogeochemical cycles and climate requires tools that resolve the most important biogeochemical processes and tracers explicitly, while at the same time are computationally efficient and have a degree of predictive capability to extrapolate knowledge to data poor areas. The new model OMEN-SED presented here is a legitimate compromise between complexity of biogeochemical processes and computational efficiency. Its scope of applicability covers the entire range from regional to global scales. OMEN-SED's computational efficiency facilitates its use in two very different ways. Firstly, it can be coupled to global Earth system models and therefore allows the investigation of coupled global biogeochemical dynamics over different timescales. Secondly, it can be used to calculate quantitative sensitivity indices requiring large sample sizes such as variance- or density-based approaches. Therefore, OMEN-SED can help to quantitatively investigate how systematic variations in model parameters impact the model output, for instance when the model has been tuned to a site-specific problem. Due to the represented anaerobic processes and secondary-redox reactions, OMEN-SED is also useful to investigate the role of benthic-pelagic coupling on the development of ocean anoxia and euxinia for instance during extreme climate events such as OAEs. On more regional scales it can be applied to systems like continental margins or estuaries which are characterised by complex interactions between different pathways of organic matter degradation and redox reactions. Here, the model can help to disentangle the complex process interplay that drives the biogeochemical dynamics and give quantifications for upper and lower constraints of carbon and nutrient budgets for these dynamic systems. In addition, OMEN-SED can be used to model eutrophication processes in shallow coastal waters as sediment-water oxygen and nutrient exchange fluxes are explicitly modelled and depend on reoxidation of reduced substances which causes a substantial part of oxygen consumption in these environments.

However, the model presented here, despite being more complete than previous analytical models, is still associated with a certain degree of simplifications. In order to solve the diagenetic equation analytically important assumptions have been made, which limit the general applicability of the model. One of the most important simplifications is assuming steady-state. When coupled to an Earth system model this assumption is only valid if the relevant variability in boundary conditions and fluxes is generally longer than the characteristic timescales of the reaction-transport processes. In that case the sediment column can be described by a series of pseudo steady-states as it is done in OMEN-

SED. Consequently, the model can be used for investigating the long term effects of changes in boundary conditions such as input of OM or bottom water oxidation state on degradation and burial dynamics, for instance during OAEs. Yet, OMEN-SED is not able to predict the system response to short-term or seasonal variations of boundary conditions. Furthermore, the separation of the sediment column into distinct biogeochemical zones and the resulting lack of overlap in degradation pathways may cause distorted organic matter degradation rates for the different TEAs. For instance, in OMEN-SED denitrification does not occur in the oxic zone, while in reality, although inhibited by the presence of oxygen, denitrification can still occur in the oxic zone, even at shallow sediments depths with high OM contents. Manganese and iron are not represented and as such OMEN-SED is not able to model all processes important in coastal marine environments and highly accumulating upwelling regions. Furthermore, it limits the scope of applicability of the model, especially in systems characterized by high Fe oxide inputs and anoxic conditions, where redox driven iron dissolution-precipitation reactions induce a high internal recycling of the sedimentary Fe pool. This can cause problems when modelling H<sub>2</sub>S and PO<sub>4</sub> profiles in anoxic environments as their concentrations are affected by these metal ions (compare Section 3.2). The model also simulates DIC and alkalinity production and, thus, has the potential to predict pH profiles within the sediment. A major limitation at this stage is the lack of representation of CaCO<sub>3</sub> precipitation/dissolution coupled to OM decomposition, which also controls the inorganic carbon system (Krumins et al., 2013). In addition the depth invariant porosity limits the correct calculation of the sediment-water interface flux of dissolved species as in reality porosity decreases with sediment depth.

## 6 Conclusions

In this paper we have described and tested a new, analytical early diagenetic model resolving organic matter cycling and associated biogeochemical dynamics called OMEN-SED. Our new model is the first analytical model to explicitly represent oxic degradation, denitrification, sulfate reduction and implicitly methanogenesis, as well as the reoxidation of reduced substances produced during organic matter degradation. Pore water tracers include O<sub>2</sub>, NO<sub>3</sub>, NH<sub>4</sub>, SO<sub>4</sub>, H<sub>2</sub>S, DIC and ALK and the solid phase includes two degradable fractions of organic matter, Fe-bound P and authigenic Ca-P minerals. We have shown that the new analytical model is able to reproduce observed pore water profiles from different ocean depths when organic matter partitioning and degradation rate constants are tuned to site specific conditions. An extensive sensitive analysis, based on the novel density-based PAWN method (Pianosi and Wagener, 2015), has been performed to asses the importance of 11 internal model parameters for all resulting SWI-fluxes. The results reveal that the degradation rate constant for labile organic matter is the most influential parameter for all model outputs. Under anoxic conditions secondary redox parameters exert an important control on related SWI-fluxes of SO<sub>4</sub>, H<sub>2</sub>S, NH<sub>4</sub> and alkalinity. In addition, the sensitivity analysis showed that produced model re-

sults fall well into the range of globally observed benthic O<sub>2</sub> and NO<sub>3</sub> fluxes. OMEN-SED is also used to quantify terminal electron acceptor fluxes across the sediment-water interface associated with  
1280 organic matter degradation along a global ocean hysometry. The results demonstrate that OMEN-  
SED is capable of capturing most of the dynamics simulated with a complex, numerical diagenetic model and our model results fall well within the range of observed fluxes. Furthermore, the coupling of OMEN-SED to the Earth system model cGENIE is described and globally invariant degradation rate constants as well as the empirical relationship of Boudreau (1997) for the apparent first order  
1285 degradation rate constant are tested to fit modelled to observed global organic matter concentrations. Generally, large scale patterns of modelled surface sediment organic matter concentrations are in agreement with observations of Seiter et al. (2004) and calculated SWI-fluxes and sediment characteristics are consistent with estimates from the literature. However, results also show that smaller scale OM degradation dynamics in the sediments are too complex in time and space to be adequately  
1290 represented using globally invariant or depth-independent OM rate constant parameterisations. More work is needed to develop and test mechanistic parameterisations relating degradation rate constants to available environmental parameters (e.g. bottom water oxygenation, burial rate, seafloor depth) in order to model the heterogeneous reactivity distribution of OM types due to preferential degradation and different time scales in the sediments. Due to its computational efficiency the coupled model  
1295 presented here can be used to explore these questions using large simulation ensembles and objective statistical methods for sensitivity analysis. Furthermore, as the major parts of the global carbon cycle are included in the new model it is well suited to examine the role of sediments for global biogeochemical cycles and climate and for exploring feedbacks within the Earth system in response to a wide range of perturbations and over various timescales.

## 1300 7 Code Availability

The OMEN-SED source code (Fortran and Matlab) related to this article is provided as a supplementary package together with a ReadMe file, where hardware and software requirements, source code files and model output file management are fully described.

## Appendix A: Reaction Network

## 1305 Appendix B: Sensitivity Analysis

### B1

*Acknowledgements.* We thank Claire Reimers and Filip Meysman for supplying the dataset from the Santa Barbara Basin, as well as Martin Thullner and Jack Middelburg for making the BRNS results and observations included in Section 3.3 available. We are also grateful to Andy Dale for providing the global flux database used in

**Table 15.** Primary pathways of organic matter degradation, secondary redox reactions and stoichiometries implemented in the reaction network.

| Pathway  | Stoichiometry  |
|--|--|
| Primary Redox reactions                        |  |
|  |  |
| Aerobic degradation                            | $(\text{CH}_2\text{O})_x(\text{NH}_3)_y(\text{H}_3\text{PO}_4)_z + (\text{x}+2\text{y})\text{O}_2 + (\text{y}+2\text{z})\text{HCO}_3^- \rightarrow (\text{x}+\text{y}+2\text{z})\text{CO}_2 + \text{yNO}_3^- + \text{zHPO}_4^{2-} + (\text{x}+2\text{y}+2\text{z})\text{H}_2\text{O}$  |
| Denitrification                                | $(\text{CH}_2\text{O})_x(\text{NH}_3)_y(\text{H}_3\text{PO}_4)_z + \frac{(\text{4x}+3\text{y})}{5}\text{NO}_3^- \rightarrow \frac{(\text{2x}+\text{3y})}{5}\text{N}_2 + \frac{(\text{x}-3\text{y}+10\text{z})}{5}\text{CO}_2 + \frac{(\text{4x}+3\text{y}-10\text{z})}{5}\text{HCO}_3^- + \text{zHPO}_4^{2-} + \frac{(\text{3x}+6\text{y}+10\text{z})}{5}\text{H}_2\text{O}$ |
| Sulfate reduction                              | $(\text{CH}_2\text{O})_x(\text{NH}_3)_y(\text{H}_3\text{PO}_4)_z + \frac{\text{x}}{2}\text{SO}_4^{2-} + (\text{y}-2\text{z})\text{CO}_2 + (\text{y}-2\text{z})\text{H}_2\text{O} \rightarrow \frac{\text{x}}{2}\text{H}_2\text{S} + (\text{x}+\text{y}-2\text{z})\text{HCO}_3^- + \text{yNH}_4^+ + \text{zHPO}_4^{2-}$   |
| Methanogenesis                                 | $(\text{CH}_2\text{O})_x(\text{NH}_3)_y(\text{H}_3\text{PO}_4)_z + (\text{y}-2\text{z})\text{H}_2\text{O} \rightarrow \frac{\text{x}}{2}\text{CH}_4 + \frac{\text{x}-2\text{y}+4\text{z}}{2}\text{CO}_2 + (\text{x}-2\text{z})\text{HCO}_3^- + \text{yNH}_4^+ + \text{zHPO}_4^{2-}$  |
| Secondary Redox reactions                      |  |
|  |  |
| Nitrification                                  | $\text{NH}_4^+ + 2\text{O}_2 + 2\text{HCO}_3^- \rightarrow \text{NO}_3^- + 2\text{CO}_2 + 3\text{H}_2\text{O}$   |
| Sulfide oxidation                              | $\text{H}_2\text{S} + 2\text{O}_2 + 2\text{HCO}_3^- \rightarrow \text{SO}_4^{2-} + 2\text{CO}_2 + 2\text{H}_2\text{O}$   |
| AOM  | $\text{CH}_4 + \text{CO}_2 + \text{SO}_4^{2-} \rightarrow 2\text{HCO}_3^- + \text{H}_2\text{S}$  |
| Adsorption reactions and mineral precipitation |  |
|  |  |
| $\text{NH}_4$ adsorption                       | $\text{NH}_4^+ \xrightarrow{\text{K}_{\text{NH}_4}} \text{NH}_4^+(\text{ads})$   |
| P ad-/desorption ???                           | $\text{PO}_4^{2-} \xrightarrow{\text{K}_{\text{PO}_4}^{\text{I},\text{II}}} \text{PO}_4^{2-}(\text{ads}); \quad \text{PO}_4^{2-} \xrightarrow{\text{k}_s} \text{Fe-bound P} \xrightarrow{\text{k}_m} \text{PO}_4^{2-}$   |
| CFA precipitation                              | $\text{PO}_4^{2-} \xrightarrow{\text{k}_a} \text{CFA}$   |

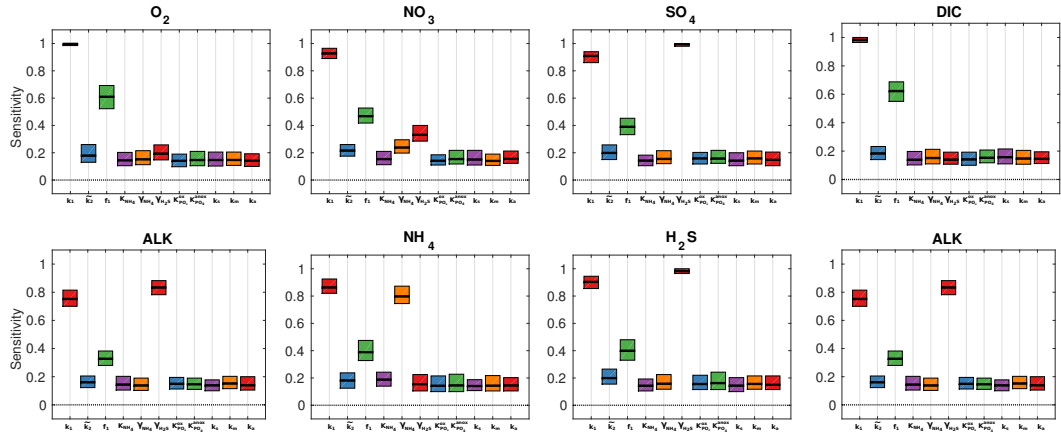


**Figure 16. Move to Appendix** Box plot of parameter sensitivities for the calculated SWI-fluxes for the 4000m oxic condition. Average sensitivities (black lines) and 90% confidence intervals using  $N = 11200$  model evaluations and  $Nboot = 100$  bootstrap resamples.

- 1310 Section 3.1 and acknowledge BODC for the OMEXDIA dataset (check CD!). We are also grateful to Francesca Pianosi for helpful insights into sensitivity analysis. DH is supported by a graduate teaching studentship by the University of Bristol. SA is supported by funding from the European Unions Horizon 2020 research and innovation programme under the Marie Skłodowska-Curie grant agreement no. 643052 (C-CASCADES). AR acknowledge funding from the EU grant ERC-2013-CoG-617313.

1315 **References**

- Aguilera, D. R., Jourabchi, P., Spiteri, C., and Regnier, P. (2005). A knowledge-based reactive transport approach for the simulation of biogeochemical dynamics in Earth systems. *Geochemistry, Geophysics, Geosystems*, 6(7).
- Aller, R. C. (1984). The importance of relict burrow structures and burrow irrigation in controlling sedimentary solute distributions. *Geochimica et Cosmochimica Acta*, 48(10):1929–1934.
- Aller, R. C. (1988). Benthic fauna and biogeochemical processes in marine sediments: the role of burrow structures. In Blackburn, T. and Sorensen, J., editors, *Nitrogen cycling in coastal marine environments*, pages 301–338. Scope, Chichester.
- Archer, D. and Devol, A. (1992). Benthic oxygen fluxes on the Washington shelf and slope: A comparison of in situ microelectrode and chamber flux measurements. *Limnology and Oceanography*, 37(3):614–629.
- Archer, D., Eby, M., Brovkin, V., Ridgwell, A., Cao, L., Mikolajewicz, U., Caldeira, K., Matsumoto, K., Munhoven, G., Montenegro, A., and Tokos, K. (2009). Atmospheric Lifetime of Fossil Fuel Carbon Dioxide. *Annual Review of Earth and Planetary Sciences*, 37(1):117–134.
- Archer, D. and Maier-Reimer, E. (1994). Effect of Deep-Sea Sedimentary Calcite Preservation on Atmospheric Co<sub>2</sub> Concentration. *Nature*, 367(6460):260–263. 00506 WOS:A1994MR49400052.
- Archer, D., Winguth, A., Lea, D., and Mahowald, N. (2000). What caused the glacial/interglacial atmospheric pCO<sub>2</sub> cycles? *Reviews of Geophysics*, 38(2):159–189. 00414.
- Archer, D. E., Morford, J. L., and Emerson, S. R. (2002). A model of suboxic sedimentary diagenesis suitable for automatic tuning and gridded global domains. *Global Biogeochemical Cycles*, 16(1):17–1.
- 1335 Arndt, S., Jørgensen, B., LaRowe, D., Middelburg, J., Pancost, R., and Regnier, P. (2013). Quantifying the degradation of organic matter in marine sediments: A review and synthesis. *Earth-Science Reviews*, 123:53–86.
- Arthur, M. A., Dean, W. E., and Pratt, L. M. (1988). Geochemical and climatic effects of increased marine organic carbon burial at the Cenomanian/Turonian boundary. *Nature*, 335(6192):714–717.
- 1340 Berner, R. A. (1980). *Early Diagenesis: A Theoretical Approach*. Princeton University Press.
- Berner, R. A. (1991). A model for atmospheric CO<sub>2</sub> over Phanerozoic time. 291(4):339–376.
- Berner, R. A. (2004). *The Phanerozoic Carbon Cycle: CO<sub>2</sub> and O<sub>2</sub>*. Oxford University Press. 00000.
- Billen, G. (1982). An idealized model of nitrogen recycling in marine sediments. *American Journal of Science*, 282(4):512–541.
- 1345 Bohlen, L., Dale, A. W., and Wallmann, K. (2012). Simple transfer functions for calculating benthic fixed nitrogen losses and C:N:P regeneration ratios in global biogeochemical models. *Global Biogeochemical Cycles*, 26(3):GB3029.
- Boudreau, B. P. (1984). On the equivalence of nonlocal and radial-diffusion models for porewater irrigation. *Journal of Marine Research*, 42(3):731–735.
- 1350 Boudreau, B. P. (1986). Mathematics of tracer mixing in sediments; I, Spatially-dependent, diffusive mixing. *American Journal of Science*, 286(3):161–198.
- Boudreau, B. P. (1996). A method-of-lines code for carbon and nutrient diagenesis in aquatic sediments. *Computers & Geosciences*, 22(5):479–496.
- Boudreau, B. P. (1997). *Diagenetic models and their implementation*, volume 505. Springer Berlin.

- 1355 Boudreau, B. P. (1998). Mean mixed depth of sediments: The wherefore and the why. *Limnology and Oceanography*, 43(3):524–526.
- Boudreau, B. P., Arnosti, C., Jørgensen, B. B., and Canfield, D. E. (2008). Comment on "Physical Model for the Decay and Preservation of Marine Organic Carbon". *Science*, 319(5870):1616–1616.
- Boudreau, B. P., Mucci, A., Sundby, B., Luther, G. W., and Silverberg, N. (1998). Comparative diagenesis at 1360 three sites on the Canadian continental margin. *Journal of Marine Research*, 56(6):1259–1284.
- Boudreau, B. P. and Ruddick, B. R. (1991). On a reactive continuum representation of organic matter diagenesis. *American Journal of Science*, 291(5):507–538.
- Broecker, W. S. (1982). Ocean chemistry during glacial time. *Geochimica et Cosmochimica Acta*, 46(10):1689–1705.
- 1365 Burdige, D. J. (2006). *Geochemistry of marine sediments*, volume 398. Princeton University Press Princeton.
- Canfield, D. E., Kristensen, E., and Thamdrup, B. (2005). *Aquatic Geomicrobiology*. Gulf Professional Publishing.
- Colbourn, G., Ridgwell, A., and Lenton, T. M. (2013). The Rock Geochemical Model (RokGeM) v0.9. *Geosci. Model Dev.*, 6(5):1543–1573.
- 1370 Conkright, M. E., Locarnini, R. A., Garcia, H. E., O'Brien, T. D., Boyer, T. P., Stephens, C., and Antonov, J. I. (2002). *World Ocean Atlas 2001: Objective analyses, data statistics, and figures: CD-ROM documentation*. US Department of Commerce, National Oceanic and Atmospheric Administration, National Oceanographic Data Center, Ocean Climate Laboratory.
- Devol, A. H. and Christensen, J. P. (1993). Benthic fluxes and nitrogen cycling in sediments of the continental 1375 margin of the eastern North Pacific. *Journal of Marine Research*, 51(2):345–372.
- Edwards, N. R. and Marsh, R. (2005). Uncertainties due to transport-parameter sensitivity in an efficient 3-D ocean-climate model. *Climate Dynamics*, 24(4):415–433.
- Emerson, S. and Bender, M. L. (1981). Carbon fluxes at the sediment-water interface of the deep-sea: calcium carbonate preservation. *Journal of Marine Research*, 39:139–162.
- 1380 Emerson, S. and Hedges, J. I. (1988). Processes controlling the organic carbon content of open ocean sediments. *Paleoceanography*, 3(5):621–634.
- Emerson, S., Jahnke, R., and Heggie, D. (1984). Sediment-water exchange in shallow water estuarine sediments. *Journal of Marine Research*, 42(3):709–730.
- Epping, E., van der Zee, C., Soetaert, K., and Helder, W. (2002). On the oxidation and burial of organic 1385 carbon in sediments of the Iberian margin and Nazaré Canyon (NE Atlantic). *Progress in Oceanography*, 52(2–4):399–431.
- Glud, R. N. (2008). Oxygen dynamics of marine sediments. *Marine Biology Research*, 4(4):243–289.
- Goloway, F. and Bender, M. (1982). Diagenetic models of interstitial nitrate profiles in deep sea suboxic sediments1. *Limnology and Oceanography*, 27(4):624–638.
- 1390 Goosse, H., Brovkin, V., Fichefet, T., Haarsma, R., Huybrechts, P., Jongma, J., Mouchet, A., Selten, F., Barriat, P.-Y., Campin, J.-M., Deleersnijder, E., Driesschaert, E., Goelzer, H., Janssens, I., Loutre, M.-F., Morales Maqueda, M. A., Opsteegh, T., Mathieu, P.-P., Munhoven, G., Pettersson, E. J., Renssen, H., Roche, D. M., Schaeffer, M., Tartineville, B., Timmermann, A., and Weber, S. L. (2010). Description of the earth system model of intermediate complexity LOVECLIM version 1.2. *Geosci. Model Dev.*, 3(2):603–633.

- 1395 Gypens, N., Lancelot, C., and Soetaert, K. (2008). Simple parameterisations for describing n and p diagenetic processes: Application in the north sea. *Progress in Oceanography*, 76(1):89–110.
- Heinze, C., Maier-Reimer, E., Winguth, A. M. E., and Archer, D. (1999). A global oceanic sediment model for long-term climate studies. *Global Biogeochemical Cycles*, 13(1):221–250.
- Hensen, C., Zabel, M., and Schulz, H. N. (2006). Benthic Cycling of Oxygen, Nitrogen and Phosphorus. In Schulz, H. D. and Zabel, M., editors, *Marine Geochemistry*, pages 207–240. Springer Berlin Heidelberg.
- 1400 Hulse, D., Arndt, S., Wilson, J. D., Munhoven, G., and Ridgwell, A. (2017). Understanding the causes and consequences of past marine carbon cycling variability through models. *Earth-Science Reviews*, 171:349–382.
- Ilyina, T., Six, K. D., Segschneider, J., Maier-Reimer, E., Li, H., and Núñez-Riboni, I. (2013). Global ocean biogeochemistry model HAMOCC: Model architecture and performance as component of the MPI-Earth system model in different CMIP5 experimental realizations. *Journal of Advances in Modeling Earth Systems*, 5(2):287–315.
- 1405 Ingall, E. and Jahnke, R. (1994). Evidence for enhanced phosphorus regeneration from marine sediments overlain by oxygen depleted waters. *Geochimica et Cosmochimica Acta*, 58(11):2571–2575. 00302.
- Jarvis, I., Lignum, J. S., Gröcke, D. R., Jenkyns, H. C., and Pearce, M. A. (2011). Black shale deposition, atmospheric CO<sub>2</sub> drawdown, and cooling during the Cenomanian-Turonian Oceanic Anoxic Event. *Paleoceanography*, 26(3):n/a–n/a.
- Jenkyns, H. C. (2010). Geochemistry of oceanic anoxic events. *Geochemistry, Geophysics, Geosystems*, 11(3).
- Jørgensen, B. B. (1978). A comparison of methods for the quantification of bacterial sulfate reduction in coastal 1415 marine sediments: II Calculation from mathematical models. *Geomicrobiology Journal*, 1:29–47.
- Jourabchi, P., Cappellen, P. V., and Regnier, P. (2005). Quantitative interpretation of pH distributions in aquatic sediments: A reaction-transport modeling approach. *American Journal of Science*, 305(9):919–956.
- Jørgensen, B. B. and Kasten, S. (2006). Sulfur Cycling and Methane Oxidation. In Schulz, P. D. H. D. and Zabel, D. M., editors, *Marine Geochemistry*, pages 271–309. Springer Berlin Heidelberg.
- 1420 Kolmogorov, A. (1933). Sulla determinazione empirica di una leggi di distribuzione. *Giorn. Ist Ital. Attuari*, 4, 91.
- Krom, M. D. and Berner, R. A. (1980). Adsorption of phosphate in anoxic marine sediments1. *Limnology and Oceanography*, 25(5):797–806.
- Krumins, V., Gehlen, M., Arndt, S., Van Cappellen, P., and Regnier, P. (2013). Dissolved inorganic carbon 1425 and alkalinity fluxes from coastal marine sediments: Model estimates for different shelf environments and sensitivity to global change. *Biogeosciences*.
- Lee, C., Wakeham, S. G., and I. Hedges, J. (2000). Composition and flux of particulate amino acids and chloropigments in equatorial Pacific seawater and sediments. *Deep Sea Research Part I: Oceanographic Research Papers*, 47(8):1535–1568.
- 1430 Lenton, T. M. and Watson, A. J. (2000). Redfield revisited: 1. Regulation of nitrate, phosphate, and oxygen in the ocean. *Global Biogeochemical Cycles*, 14(1):225–248.
- Li, Y.-H. and Gregory, S. (1974). Diffusion of ions in sea water and in deep-sea sediments. *Geochimica et Cosmochimica Acta*, 38(5):703–714.

- Longhurst, A., Sathyendranath, S., Platt, T., and Caverhill, C. (1995). An estimate of global primary production in the ocean from satellite radiometer data. *Journal of Plankton Research*, 17(6):1245–1271.
- 1435 Mackenzie, F. T. (2005). *Sediments, Diagenesis, and Sedimentary Rocks: Treatise on Geochemistry, Second Edition*. Elsevier. 00000.
- Meile, C. and Cappellen, P. V. (2003). Global estimates of enhanced solute transport in marine sediments. *Limnology and Oceanography*, 48(2):777–786.
- 1440 Meysman, F. J. R., Middelburg, J. J., Herman, P. M. J., and Heip, C. H. R. (2003). Reactive transport in surface sediments. II. Media: an object-oriented problem-solving environment for early diagenesis. *Computers & Geosciences*, 29(3):301–318. 00067.
- Middelburg, J. J., Soetaert, K., and Herman, P. M. (1997). Empirical relationships for use in global diagenetic models. *Deep Sea Research Part I: Oceanographic Research Papers*, 44(2):327–344.
- 1445 Middelburg, J. J., Soetaert, K., Herman, P. M. J., and Heip, C. H. R. (1996). Denitrification in marine sediments: A model study. *Global Biogeochemical Cycles*, 10(4):661–673.
- Middelburg, J. J., Vlug, T., Jaco, F., and van der Nat, W. A. (1993). Organic matter mineralization in marine systems. *Global and Planetary Change*, 8(1):47–58.
- Mort, H. P., Adatte, T., Föllmi, K. B., Keller, G., Steinmann, P., Matera, V., Berner, Z., and Stüben, D. (2007).
- 1450 Phosphorus and the roles of productivity and nutrient recycling during oceanic anoxic event 2. *Geology*, 35(6):483–486. 00135.
- Munhoven, G. (2007). Glacial-interglacial rain ratio changes: Implications for atmospheric and ocean-sediment interaction. *Deep Sea Research Part II: Topical Studies in Oceanography*, 54(5–7):722–746.
- 1455 Najjar, R. G., Jin, X., Louanchi, F., Aumont, O., Caldeira, K., Doney, S. C., Dutay, J.-C., Follows, M., Gruber, N., Joos, F., Lindsay, K., Maier-Reimer, E., Matear, R. J., Matsumoto, K., Monfray, P., Mouchet, A., Orr, J. C., Plattner, G.-K., Sarmiento, J. L., Schlitzer, R., Slater, R. D., Weirig, M.-F., Yamanaka, Y., and Yool, A. (2007). Impact of circulation on export production, dissolved organic matter, and dissolved oxygen in the ocean: Results from Phase II of the Ocean Carbon-cycle Model Intercomparison Project (OCMIP-2). *Global Biogeochemical Cycles*, 21(3):GB3007.
- 1460 Palastanga, V., Slomp, C. P., and Heinze, C. (2011). Long-term controls on ocean phosphorus and oxygen in a global biogeochemical model. *Global Biogeochemical Cycles*, 25(3):GB3024.
- Pianosi, F., Beven, K., Freer, J., Hall, J. W., Rougier, J., Stephenson, D. B., and Wagener, T. (2016). Sensitivity analysis of environmental models: A systematic review with practical workflow. *Environmental Modelling & Software*, 79:214–232.
- 1465 Pianosi, F., Sarrazin, F., and Wagener, T. (2015). A Matlab toolbox for Global Sensitivity Analysis. *Environmental Modelling & Software*, 70:80–85.
- Pianosi, F. and Wagener, T. (2015). A simple and efficient method for global sensitivity analysis based on cumulative distribution functions. *Environmental Modelling & Software*, 67:1–11.
- 1470 Redfield, A. C. (1963). The influence of organisms on the composition of seawater. *The sea*, 2:26–77.
- Regnier, P., Dale, A. W., Arndt, S., LaRowe, D. E., Mogollon, J., and Van Cappellen, P. (2011). Quantitative analysis of anaerobic oxidation of methane (AOM) in marine sediments: A modeling perspective. *Earth-Science Reviews*, 106(1):105–130.

- Reimers, C. E., Lange, C. B., Tabak, M., and Bernhard, J. M. (1990). Seasonal spillover and varve formation  
1475 in the Santa Barbara Basin, California. *Limnology and Oceanography*, 35(7):1577–1585.
- Reimers, C. E., Ruttenberg, K. C., Canfield, D. E., Christiansen, M. B., and Martin, J. B. (1996). Porewater  
pH and authigenic phases formed in the uppermost sediments of the Santa Barbara Basin. *Geochimica et  
Cosmochimica Acta*, 60(21):4037–4057.
- Ridgwell, A. and Hargreaves, J. C. (2007). Regulation of atmospheric CO<sub>2</sub> by deep-sea sediments in an Earth  
1480 system model. *Global Biogeochemical Cycles*, 21(2):n/a–n/a.
- Ridgwell, A., Hargreaves, J. C., Edwards, N. R., Annan, J. D., Lenton, T. M., Marsh, R., Yool, A., and Watson,  
A. (2007). Marine geochemical data assimilation in an efficient Earth System Model of global biogeochemical  
cycling. *Biogeosciences*, 4(1):87–104. 00090.
- Ridgwell, A. and Zeebe, R. E. (2005). The role of the global carbonate cycle in the regulation and evolution of  
1485 the Earth system. *Earth and Planetary Science Letters*, 234(3–4):299–315. 00172.
- Ruardij, P. and Van Raaphorst, W. (1995). Benthic nutrient regeneration in the ERSEM ecosystem model of the  
North Sea. *Netherlands Journal of Sea Research*, 33(3):453–483.
- Ruttenberg, K. C. (1993). Reassessment of the oceanic residence time of phosphorus. *Chemical Geology*,  
107(3):405–409.
- 1490 Schulz, H. D. (2006). Quantification of Early Diagenesis: Dissolved Constituents in Pore Water and Signals  
in the Solid Phase. In Schulz, P. D. H. D. and Zabel, D. M., editors, *Marine Geochemistry*, pages 73–124.  
Springer Berlin Heidelberg.
- Seiter, K., Hensen, C., Schröter, J., and Zabel, M. (2004). Organic carbon content in surface sediments—defining regional provinces. *Deep Sea Research Part I: Oceanographic Research Papers*,  
1495 51(12):2001–2026.
- Shaffer, G., Malskær Olsen, S., and Pepke Pedersen, J. O. (2008). Presentation, calibration and validation of  
the low-order, DCESS Earth System Model (Version 1). *Geosci. Model Dev.*, 1(1):17–51. 00007.
- Slomp, C., Malschaert, J., and Van Raaphorst, W. (1998). The role of adsorption in sediment-water exchange  
of phosphate in north sea continental margin sediments. *Limnology and Oceanography*, 43(5):832–846.
- 1500 Slomp, C. P., Epping, E. H., Helder, W., and Van Raaphorst, W. (1996). A key role for iron-bound phosphorus  
in authigenic apatite formation in north atlantic continental platform sediments. *Journal of Marine Research*,  
54(6):1179–1205.
- Smirnov, N. V. (1939). On the estimation of the discrepancy between empirical curves of distribution for two  
independent samples. *Bull. Math. Univ. Moscou*, 2(2).
- 1505 Soetaert, K., Herman, P. M. J., and Middelburg, J. J. (1996). A model of early diagenetic processes from the  
shelf to abyssal depths. *Geochimica et Cosmochimica Acta*, 60(6):1019–1040.
- Soetaert, K., Middelburg, J. J., Herman, P. M. J., and Buis, K. (2000). On the coupling of benthic and pelagic  
biogeochemical models. *Earth-Science Reviews*, 51(1–4):173–201.
- Stein, R., Rulkötter, J., and Welte, D. H. (1986). Accumulation of organic-carbon-rich sediments in the Late  
1510 Jurassic and Cretaceous Atlantic Ocean — A synthesis. *Chemical Geology*, 56(1–2):1–32.
- Stolpovsky, K., Dale, A. W., and Wallmann, K. (2015). Toward a parameterization of global-scale or-  
ganic carbon mineralization kinetics in surface marine sediments. *Global Biogeochemical Cycles*,  
29(6):2015GB005087.

- Stumm, W. and Morgan, J. J. (2012). *Aquatic Chemistry: Chemical Equilibria and Rates in Natural Waters*.  
1515 John Wiley & Sons.
- Teal, L., Bulling, M., Parker, E., and Solan, M. (2010). Global patterns of bioturbation intensity and mixed depth of marine soft sediments. *Aquatic Biology*, 2(3):207–218.
- Thullner, M., Dale, A. W., and Regnier, P. (2009). Global-scale quantification of mineralization pathways in marine sediments: A reaction-transport modeling approach. *Geochemistry, Geophysics, Geosystems*, 10(10).
- 1520 Thullner, M., Van Cappellen, P., and Regnier, P. (2005). Modeling the impact of microbial activity on redox dynamics in porous media. *Geochimica et Cosmochimica Acta*, 69(21):5005–5019.
- Tjiputra, J. F., Roelandt, C., Bentsen, M., Lawrence, D. M., Lorentzen, T., Schwinger, J., Seland, Ø., and Heinze, C. (2013). Evaluation of the carbon cycle components in the Norwegian Earth System Model (NorESM). *Geosci. Model Dev.*, 6(2):301–325. 00057.
- 1525 Toth, D. J. and Lerman, A. (1977). Organic matter reactivity and sedimentation rates in the ocean. *American Journal of Science*, 277(4):465–485.
- Tromp, T. K., Van Cappellen, P., and Key, R. M. (1995). A global model for the early diagenesis of organic carbon and organic phosphorus in marine sediments. *Geochimica et Cosmochimica Acta*, 59(7):1259–1284. 00164.
- 1530 Tsandev, I. and Slomp, C. (2009). Modeling phosphorus cycling and carbon burial during Cretaceous Oceanic Anoxic Events. *Earth and Planetary Science Letters*, 286(1–2):71–79.
- Ullman, W. J. and Aller, R. C. (1982). Diffusion coefficients in nearshore marine sediments. *Limnology and Oceanography*, 27(3):552–556.
- Van Cappellen, P. and Berner, R. A. (1988). A mathematical model for the early diagenesis of phosphorus and 1535 fluorine in marine sediments; apatite precipitation. *American Journal of Science*, 288(4):289–333.
- Van Cappellen, P. and Ingall, E. D. (1994). Benthic phosphorus regeneration, net primary production, and ocean anoxia: A model of the coupled marine biogeochemical cycles of carbon and phosphorus. *Paleoceanography*, 9(5):677–692.
- Van Cappellen, P. and Wang, Y. (1995). Metal cycling in surface sediments: modeling the interplay of transport 1540 and reaction. *Metal contaminated aquatic sediments*, pages 21–64.
- Van Cappellen, P. and Wang, Y. (1996). Cycling of iron and manganese in surface sediments; a general theory for the coupled transport and reaction of carbon, oxygen, nitrogen, sulfur, iron, and manganese. *American Journal of Science*, 296(3):197–243.
- van Weering, T. C. E., de Stigter, H. C., Boer, W., and de Haas, H. (2002). Recent sediment transport and 1545 accumulation on the NW Iberian margin. *Progress in Oceanography*, 52(2):349–371.
- Vanderborght, J.-P. and Billen, G. (1975). Vertical distribution of nitrate concentration in interstitial water of marine sediments with nitrification and denitrification. *Limnology and Oceanography*, 20(6):953–961.
- Vanderborght, J.-P., Wollas, R., and Bitten, G. (1977). Kinetic models of diagenesis in disturbed sediments. Part 2. Nitrogen diagenesis. *Limnology and Oceanography*, 22(5):794–803.
- 1550 Wakeham, S. G., Hedges, J. I., Lee, C., Peterson, M. L., and Hernes, P. J. (1997). Compositions and transport of lipid biomarkers through the water column and surficial sediments of the equatorial Pacific Ocean. *Deep Sea Research Part II: Topical Studies in Oceanography*, 44(9):2131–2162.

- Wang, Y. and Van Cappellen, P. (1996). A multicomponent reactive transport model of early diagenesis: Application to redox cycling in coastal marine sediments. *Geochimica et Cosmochimica Acta*, 60(16):2993–3014.
- 1555 00283.
- Wenzhöfer, F. and Glud, R. N. (2002). Benthic carbon mineralization in the Atlantic: a synthesis based on in situ data from the last decade. *Deep Sea Research Part I: Oceanographic Research Papers*, 49(7):1255–1279.
- Wolf-Gladrow, D. A., Zeebe, R. E., Klaas, C., Kötzinger, A., and Dickson, A. G. (2007). Total alkalinity: The explicit conservative expression and its application to biogeochemical processes. *Marine Chemistry*, 106(1–2):287–300.
- 1560